Synthesis, Characterization and Application of Organic Dye-Sensitized Silver and Zinc doped NiO Nanoparticles in DSSC

QUAID-I-AZAM UNIVERSITY

ISLAMABAD

Master of Philosophy

In

Physical Chemistry

By

AYESHA RIAZ

Department of Chemistry

Quaid -i-Azam University

Islamabad, Pakistan

2023

Synthesis, Characterization and Application of Organic Dye-Sensitized Silver and Zinc doped NiO Nanoparticles in DSSC

QUAID-I-AZAM UNIVERSITY

ISLAMABAD

A Dissertation Submitted to the Department of Chemistry, Quaid-i-Azam University, Islamabad, for Partial Fulfillment of the Requirements for the Degree

of

Master of Philosophy

In

Physical Chemistry

By

AYESHA RIAZ

Department of Chemistry

Quaid-i-Azam University

Islamabad, Pakistan

2023

بِسْمِ اللهِ الرَّحْمٰنِ الرَّحِيمِ

وَتَخْشَى ٱلنَّاسَ وَٱللَّهُ أَحَقُّ أَن تَخْشَىٰهُ

And you feared the people,
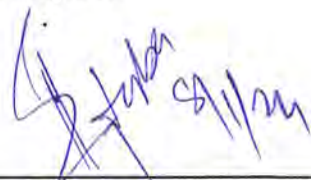while ALLAH has more right
that you fear HIM.

[Qur'an 33:37]

This is to certify that this dissertation entitled **"Synthesis, Characterization and Application of Organic Dye-Sensitized Silver and Zinc doped NiO Nanoparticles in DSSC"** submitted by *Ms. Ayesha Riaz* is accepted in its present form by the Department of Chemistry, Quaid-i-Azam University, Islamabad, as satisfying the dissertation requirements for the degree of Master of Philosophy in *Physical Chemistry*.

External Examiner:

Dr. Hafiz-ur-Rehman
Principal Scientific Officer
Dr. A.Q Khan Research Laboratories
P.O Box. No. 502,
Rawalpindi

Supervisor:

Prof. Dr. Syed Mujtaba Shah
Department of Chemistry
Quaid-i-Azam University
Islamabad

Head of Section:

Prof. Dr. Hazrat Hussain
Department of Chemistry
Quaid-i-Azam University
Islamabad.

Chairman:

Prof. Dr. Aamer Saeed Bhatti
Department of Chemistry
Quaid-i-Azam University
Islamabad

DEDICATION

Dedicated to the people I adore dearly. Especially my devoted and supportive father **Mr. Riaz Hanif Rahi,** my loving mother **Ms. Nusrat Perveen,**

My supervisor **Prof. Dr. Syed Mujtaba Shah,**

My teachers and friends.

Thanks for your endless support,

trust, and prayers.

ACKNOWLEDGEMENTS

Table of Contents

Table of figures

List of tables

List of Abbreviations

AM	Air mass
Ag-NiO	Ag doped NiO
CB	Conduction Band
DSSC	Dye Sensitized Solar Cell
DI	Deionized
eV	Electron volt
FTIR	Fourier Transform Infrared
FF	Fill Factor
HOMO	Highest Occupied Molecular Orbital
ITO	Indium-doped Tin Oxide
LUMO	Lowest Unoccupied Molecular Orbital
M_{pp}	Maximum Power Point
NiO NPs	Nickel Oxide Nanoparticles
Voc	Open Circuit Voltage
P3HT	Poly-3-hexyl thiophene
PEDOT: PSS	Poly (3,4-ethylene dioxythiophene) Polystyrene Sulfonate
SEM	Scanning Electron Microscope
Jsc	Short Circuit Current density
UV-Vis	Ultra Voilet- Visible
XRD	X-Ray Diffraction
Zn-NiO	Zn doped NiO

Abstract

In this research work, the pure and transition metals (Silver and Zinc) doped NiO NPs were successfully synthesized by using the Co-precipitation method. The characterization of as-synthesized nanoparticles was done by UV-Visible spectroscopy, X-ray diffraction (XRD), Fourier Transform Infrared spectroscopy (FTIR), Scanning Electron Microscopy (SEM), Energy Dispersive X-ray spectroscopy (EDX), and I-V characterization. The optical properties of as-synthesized NPs were studied by UV-Visible spectroscopy and resulted absorption spectra thus obtained revealed that with the increase in dopants percentage from 1-5%, a red shift (λ_{max} shifted towards longer wavelength) in the spectra was observed. To find the band gaps of pure and doped nanoparticles, Tauc's plots were used, and it shows tuning in band gaps for all doped nanoparticles. The band gap of pure NiO NPs was observed to be 3.17 eV which was tuned up to about 2.10 eV due to Ag and 2.00 eV due to Zn dopants. To estimate the average crystallite size and the purity of nanomaterial X-ray diffraction analysis was used. XRD analysis confirmed the formation of face centered cubic crystalline structure of NiO and its high degree of crystalline nature. The morphological changes in nanostructured material were analyzed by SEM studies. Some clusters of spherical and somewhat oval nanoparticles are visible in the SEM picture. The elemental composition of nanostructured material was analyzed by EDX studies. EDX studies revealed the presence of Ni, O, Ag and Zn along with some extra peaks of impurities such as C, and Cl. FTIR studies helped in detecting the specific vibrational bands. Three cost effective and commercially available organic dyes (Carminic Acid, Coomassie Violet R200, Arsenazo III) were selected and investigated to be used as photosensitizers for DSSCs (dye-sensitized solar cells). The FTIR peak for the -COOH functionality in the case of Carminic acid and -SO_3H group in the case of Coomassie violet R200 and Aesenazo III get vanished in the nanohybrid spectrum compared to pure dye, demonstrating efficient functionalization (grafting) of the nanoparticles with the corresponding dyes. The nanohybrid materials thus formed were used as semiconducting working electrode in DSSCs. To overcome the problems offered using liquid electrolyte, an organic hole conducting polymer (P3HT) was employed as a solid electrolyte in solid-state DSSCs. The results obtained from above studies revealed that among all the fabricated

devices, the greatest efficiency was acquired for devices sensitized with Arsenazo III in solid-state-DSSCs. For DSSC based on Carminic acid dye sensitized Ag-NiO the efficiency was obtained to be 0.40% with J_{sc} of 3.10 mA/cm^2 and V_{oc} of 0.31 V. For Arsenazo III dye sensitized Ag-NiO based DSSC, the maximum efficiency was observed to be 1.03% with J_{sc} of 7.90 mA/cm^2 and V_{oc} of 0.31 V, as compared to the reference cell (0.07%).

Chapter 1: Introduction

1.1. Outlook for global energy

Global energy consumption is always rising, yet conventional energy sources have limited supplies[1]. Presently, it is estimated that seven billion people worldwide use roughly 13 TW (terawatts) of energy, and in 40 years, that number would likely increase by another 10 TW. Finding and using new conventional energy sources is getting more and more challenging because of the unknowable size of the reserves of coal, oil, and gas, as well as the costly and hazardous methods of extraction[1]. Resources for fossil fuels are few and quickly running out. Finding alternate energy sources is therefore urgently needed to meet our needs. Nuclear power, renewable energy sources like solar, and carbon fuel-based sources are the three options now under consideration. The fundamental argument against carbon-based energy is that it has a negative effect on the environment[2]. Using it will significantly raise atmospheric CO_2 levels, which will result in catastrophic climate changes. The construction of nuclear power plants with a capacity of hundreds of gigawatts (GW) would be necessary to meet the world's energy needs, but there is currently no practical way to get rid of the hazardous nuclear fuel waste. So, the third option, which is renewable energy using the sun as the source, is very appealing and promising for several reasons. Sunshine is a plentiful and unrestricted energy source that is delivered right to our homes. 120,000 TW of solar energy is received by the surface of earth[3].

1.2. Resources of Energy

There are "3" different kinds of energy resources[3].

- Renewable
- Non-renewable
- Secondary

1.2.1. Renewable Energy Resources

Natural resources are the source of renewable energy that are regenerated more quickly than they are used up. There are numerous and accessible sources of renewable energy. It is also called clean energy[4].

1

- Solar energy
- Wind power
- Hydraulic power
- Wave power
- Biofuel

1.2.2. Non-Renewable Energy Resources

Natural resources that cannot be easily replenished by natural processes at a rate rapid enough to keep up with use are considered non-renewable resources[4].

- Oil
- Natural gas
- Coal
- Nuclear energy

1.2.3. Secondary Resources

All energy sources that come from the transformation of primary sources (sources that involve direct extraction of energy from natural resources) should be referred to as secondary energy[5].

- Liquid fuels
- Electricity
- Heat

1.3. Solar Energy

Solar energy provides mankind with a generally well-distributed, clean, climatically friendly, extremely abundant, and unlimited energy source. The sun supplies the surface of the planet with around 120,000 terawatts of energy, or 6000 times more energy than is now being used worldwide. It is still extremely difficult to harness solar power and turn it into cheap electricity or chemical propellants like hydrogen while using widely accessible raw materials[6]. According to the International Energy Agency's Light's Labour's Lost 2018 report's high-renewable scenario version, solar photovoltaic (PV) and solar thermal energy

systems might collectively supply up to 25% of the world's electricity by 2050. After hydropower and wind power, solar photovoltaics is now the third most significant renewable energy source and has experienced a staggering 33.2% rise since the end of 2015. This is because, by the end of 2016, 301 GW worth of solar panels will have been installed globally. Solar energy provided 1.3% of the world's power, a small yet significant contribution given recent and anticipated potential advancements in solar technologies[7].

In many parts of the world, solar radiation is recognized as one of the finest potential energy sources. The two primary techniques for turning solar radiation into energy are passive and active designs of solar energy. The cornerstone of passive solar design, which attempts to do away with the need for artificial lighting and heating, is typically the most effective architecture for gathering solar energy. Solar energy researchers are particularly interested in the design and optimization of solar energy houses for passive solar systems. Globally, increasing building energy efficiency is a top priority. The measures used to reduce energy use can take a variety of forms, and the person making the decision must choose the best option while considering a number of different and frequently conflicting goals, including energy use, expenses, the environment, and other factors. Water heating is the foundation of active solar design, which turns solar radiation into heat by employing photovoltaic panels and solar cells to transform the solar radiation into energy[8].

1.4. Technologies of Harnessing Solar Energy

Based on how solar radiation is captured and dispersed, the following sorts of technology have been employed to harvest energy coming continuously from an unlimited source like the sun[9].

- Passive solar system
- Active solar system

1.4.1. Active Solar System

By considering the application related to solar systems that are termed as active, we become able to perform the transformation of energy obtained from sun into other various beneficial kinds of energy. Normally, energy obtained from sources linked to electricity

and heat will surely have the capability of being transformed in a given manner. In buildings, the relevant energy then further in turn will be available for its utilization for fulfilling certain tasks like that of cooling, heating or to counteract other alternative energy consumption or expenditures. For this process, active solar systems employ mechanical or electrical machinery[10].

Active solar systems do include solar photovoltaics, fuel cells, dye-sensitized solar cells, solar collector and photocatalysis.

1.4.2. Passive Solar System

Whenever we take into consideration passive building designs, or building design or solar system, floors, windows, and walls are constructed to collect, save for future use, and disperse the directly striking solar energy in the certain nature of subsequent heat in the cold times during winter and does result in ultimate drop in solar heat's extent during the hot times in the summer season[11]. Since it doesn't take into careful consideration the corresponding components like that of electrical or mechanical, as contrary to solar heating systems belonging to active category, a passive solar system is also known as climatic design[12]. The type of replacement windows, warm insulating materials, warm masses, and covering are a few factors that need to be considered. While the existing structures can be modified or retrofitted, passive solar system approaches are easier to apply to new construction.

1.5. Solar Energy Converters

The three most common types of solar energy converters are as follows[13]:

- Photovoltaic energy converters
- Photochemical energy converters
- Solar thermal converters

1.5.1. Photovoltaic Energy Converters

Whenever the light from any source does strike at surface of our materials that are semiconductor in nature, a certain part of the photons corresponding to light are in turn able to be getting absorbed through crystal that is semiconductor inherently, and all this

4

phenomenon further results in increasing the availability of electrons, that are free in nature, in the subsequent crystal. A cell photovoltaic in nature is generally believed to own the ability of conversion of energy obtained from light into purposeful electricity and that too with the virtue of an effect known as photovoltaic and thus it serves to be the most valuable part of a system[14]. Generally, light can either be reflected by a certain medium provided or it does pass thoroughly by that medium, furthermore, the left-over light is eventually captured by our material and all these three processes do happen only when a particular beam of light does collide with a certain material.

Photovoltaic is the acronym for solar-generated electricity (or PV). The photovoltaic effect is a process that governs the transformation into electrical form of energy and that from available form of energy which is light. Sunlight is converted to direct current electricity using photovoltaic solar cells. Semiconductor materials are used to create the solar cells in the PV module[15]. Electrons are released when light energy hits the cell. When photons strike a material, absorption of a sufficient amount of photon is carried out, and subsequent photons in turn can serve the purpose of excitation of some of the electrons corresponding to the covalent bond that is present. When this happens, relevant excited electrons are sufficiently energetic, and they can easily perform the task of moving to conduction bond from a band of lower energy that is valence one. The corresponding electrons then deviate from their past identity of having covalent bond and this becomes possible only because conduction band is the only place where the final energy level related to above mentioned electrons does lie, and the result involves the increase in number of leftover holes in each band and that too with the release of respective electrons from that one. Within the crystal structure, these so-called free electrons drift at random. The electrons can be trapped as a D.C current owing to the electrical conductors connecting to the material's positive and negative scales. The resulting electricity generated in this case can and will be utilized to perform efficient functions like that of either storage in a battery or powering a certain load[16].

Interconnected systems and standalone off-grid are generally involved when main categorization of certain photovoltaic systems does take place. In areas without utility grid service, off-grid (stand-alone) systems are frequently employed. This tends to be cheap to a large extent to supply usable forms of such energy to remote locations, more specifically

for hospitals, rural banking, and IT. Obviously, the installation of such systems taking into account PV is far more cheap as well as efficient and durable than conventionally assembling the transformers of step down type and power lines for the purpose of transmission and this is becoming must needed specifically in locations of remote villages. Panels operating on solar energy are generally able to generate purposeful energy without burning, odor, noise, vibration, or other types of pollutants. Unwanted disturbance is thus eradicated to an overall extent. Also, there will be no more extra burden or charges allocated for maintaining special structures or moving and adjusting different components, unlike other systems are source of fruitful energy and they do require training at a professional level for an efficient installation and in competitive range[17].
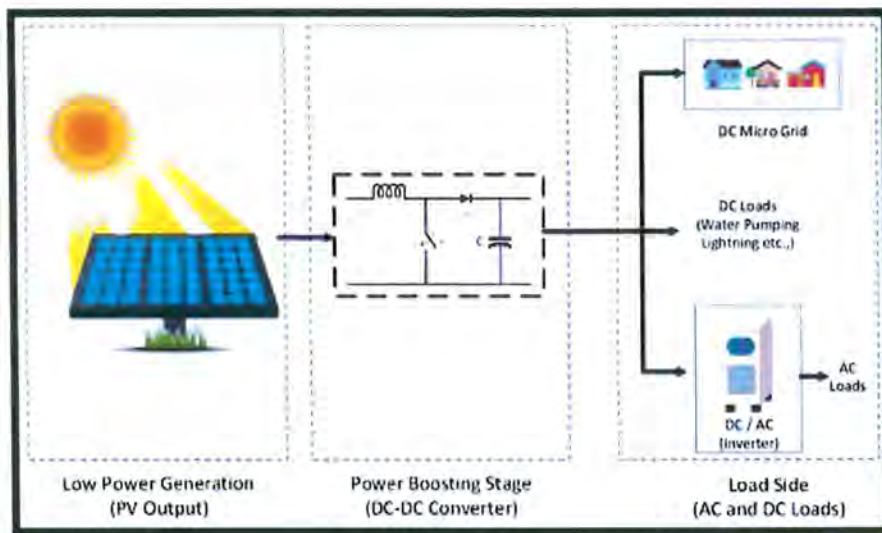
Figure 1.1. Photovoltaic energy conversion[18].

1.5.2. Photochemical Energy Converters

Energy is transformed in the form of an increase in chemical potential using photochemical energy converters. It entails converting sunlight directly into electrical or chemical energy through a photochemical process.

Photosynthesis by plants, algae, and bacteria is a reliable process with reasonable conversion efficiency. These systems already create three times the yearly world energy consumption or 3×10^{21} J of stored energy. In order to create additional products like hydrogen, reduced carbon compounds, ammonia, and power, photosynthesis can be

6

imitated and redirected. Creating artificial systems for the storage and photochemical conversion of solar energy is a rapidly expanding subject.

Photochemical energy conversion takes place by following means:

➢ Natural photosynthesis
➢ Artificial photosynthesis
➢ Hybrid systems
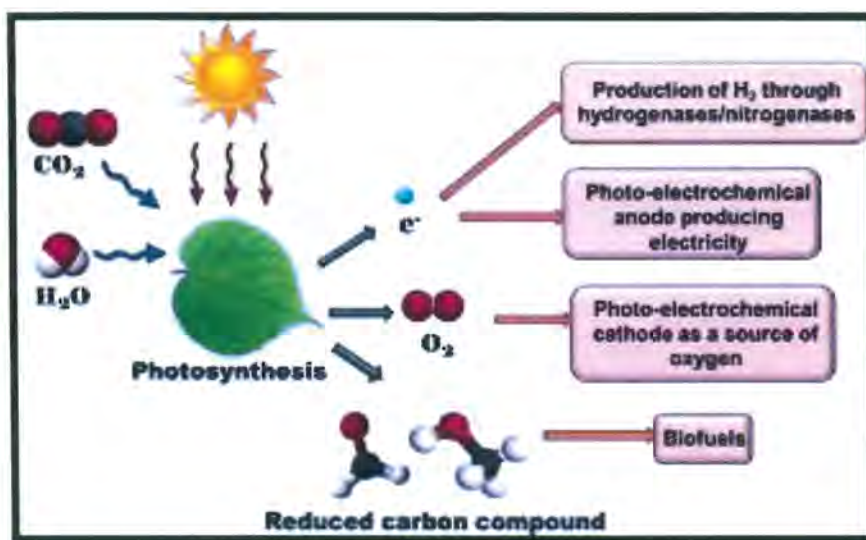
Figure 1.2. photochemical energy conversion[19].

1.5.3. Solar Thermal Converters

These are the devices that harness the sun's energy as intense heat. These devices do follow a certain procedure which can be referred to as concentrating solar power (CSP). The resulting energy in the form of solar is focused by making utilization of lenses and mirrors and lenses and ultimately targeted in direction of a receiver in concentrating solar power (CSP). Inside the receiver, a heat transfer fluid circulates and does absorb all available heat of the solar radiation in concentrated form before transferring it to a thermodynamic power cycle.

CSP needs a lot of direct normal irradiance (DNI). The generation of power as well as electricity by making the use of CSP power is limited to DNI locations that are too high in order to be economically viable, furthermore, corresponding technological advancement is specifically applicable to only power production at utility scale[7].
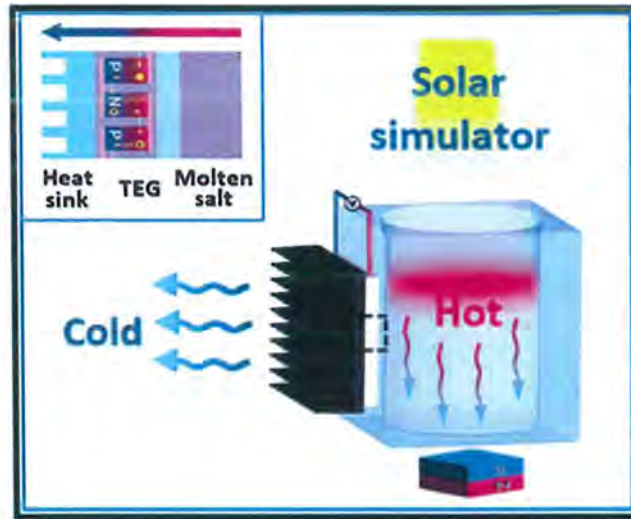
Figure 1.3. Concentrating solar power (CSP)[20].

1.6. Photovoltaic Technology

Photovoltaic cells, which can also be termed as solar cells, are devices of category of electronics which do have ability of turning into electricity, of directly striking sunlight. Edmond Becquerel, a French physicist, made the initial discovery of photovoltaic energy in 1839. In 1882, Charles Fritts created the first functional solar cell. The major benefit of photovoltaic devices is their construction as stand-alone systems, which may and will be a substantial source for provision of values of outputs generally falling in the micro to megawatts. They do demand a very little effort for maintenance and are simple, facile and robust in their adapted design. As a result, they are employed in a variety of applications, including power generation, power plants working on the scale of megawatt, water pumping, reverse osmosis plants, remote buildings, spacecraft, solar home systems, satellites and even communications. Only because of having such a wide range of applications, the subsequent need for photovoltaics is rising each year. Ready availability of solar radiation and efficiency conversion are two factors influencing PV technology. Extraction of solar cell/module parameters is one of the most essential requirements for increasing the capacity of PV systems.

1.6.1. Components of Photovoltaic System

There are in total six components regarding a general photovoltaic system which are as follows.

- An electric grid
- The solar PV array
- A utility meter
- A charge controller
- An inverter
- A battery bank

The precise and accurate installment of each of these components is solemnly responsible for the resulting effectiveness as well influence of the solar panels.
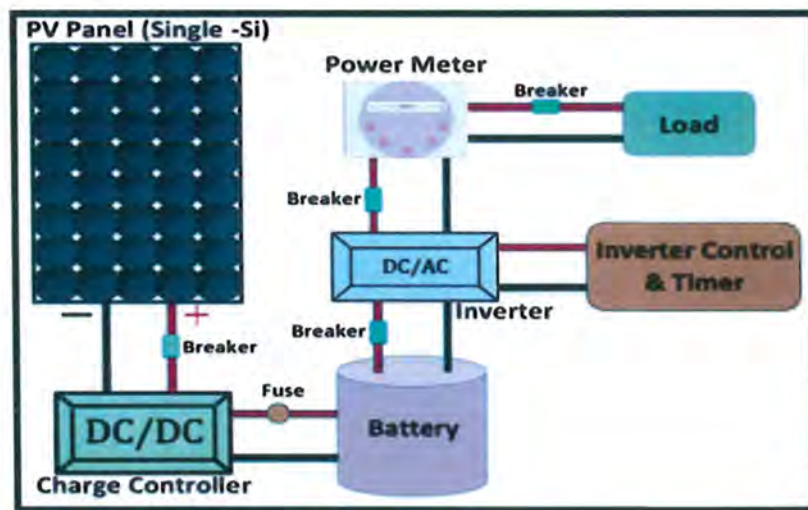
Figure 1.4. Constituents of Photovoltaic Assembly [21].

1.6.2. Working and Principles of Photovoltaic Cell

The most influential as well as direct way to which can be utilized for efficient conversion of energy in solar form to the energy behaving in electrical form which is also termed as electricity and that too without emitting greenhouse gases including carbon dioxide or contributing to global warming is through photovoltaic technology. The photovoltaic effect is the foundation of solar energy. A photovoltaic material is a semiconductor layer. In semiconductors, the valence band is created by the overall sum of

energy of the bound valence type of electrons, while the band of conduction is produced by adding all the subsequent energy of the electrons that are free in nature. The structure related to band describes how energy and motion are interdependent. The so-called bandgap is actually a result of contrast which is present among the conduction band's lowest energy and highest energy which is owned by valence band[22]. A PV device has a semiconductor material with a p-n junction across which solar radiation develops a voltage. The characteristics of the concerned material belonging to n and p type along with their constant related to diffusion determine the voltage produced across the junction. Our current semiconductor material, which is necessary for the construction of a cell that is PV in nature, must demonstrate an extraordinary absorption of the majority of the solar spectrum's radiations in order to achieve high efficiency as regarded with collection.

1.6.3. Carrier (electron-hole) Generation

While considering the interactions linked with a semiconductor material with the irradiation, energy of photon is required to have a value that is far less than bandgap of material, and so in this above-mentioned case the coefficient due to absorption is extremely low and the photon can be absorbed by lattice or free carriers only. On the contrary, if in any case the energy corresponding to photon comes out to be far more in value than the semiconductor's band gap, the coefficient owing to absorption generally tend to rise sharply in value as a function of energy related to photon and furthermore, the process of absorption which is usually limited to band-to-band (inter band) does take place. The band structures and photon energy both affect the absorption coefficient.

In the so-called direct bandgap arrangement, the maximum energy corresponding to the valence band and the lowest energy level in the conductive band have the identical momentum. "Direct" semiconductors include GaAs, CdTe, and CuInSe$_2$. Upon absorption of a photon with energy greater than the bandgap, an electron moves from the valence band to the conductive band. Since the photon momentum is $h/\lambda = 0$, the resulting electron and hole have almost the same momentum. As photon energy grows, so does the kinetic energy of the resultant electrons and holes. The surplus amount of energy that was available is ultimately lost in a type of heat and this happens owing to vibrations due to lattice to achieve thermal equilibrium. Meanwhile all this mess is created only because of dispersing

of holes as well electrons and this dispersing mainly tends to take place by the aid of vibrations due to lattices and these can also be termed as phonons. This process is termed thermalization.

In the so-called indirect band structure, there are unique momentum values for the lowest energy electron in the conductive band and the highest energy electron in the valence band. These "indirect" semiconductors include Si, Ge, and GaP, for instance. In this case, the transition between the valence band maximum and the conductive band minimum is not possible with merely the absorption of photons with energy close to the bandgap. Since the photon momentum is zero, transitions can only be performed by absorbing photons and simultaneously absorbing or emitting phonons. As comparison to "direct" transitions, "indirect transitions" have a comparatively low absorption coefficient due to the necessity of synchronous electron-photon-phonon interaction. With increasing photon energy, the absorption coefficient rises rather slowly. Permissible transitions that are said to be direct do tend to be achieved from the band structure that is referred to as indirect at high enough photon energies. As a result, the absorption coefficient increases more abruptly at higher photon energy. Indirect semiconductors also experience the effects of produced carrier thermalization.

The bandgap and band structure of semiconductors has a significant impact on how many carriers are produced during solar energy conversion. Photons with insufficient energy are not absorbed, and excess carrier production cannot transfer their energy. The excess sufficiently available amount of energy belonging to that of photons while having energies greater than the one that does take place due to bandgap, is converted to heat. Consequently, just a smaller portion of solar energy that is generally directly striking can be transformed into free charge production and, ultimately, into electric power. After photon absorption, some materials have the ability to produce an exciton, which generally corresponds to hole/electron pair that is always constrained by Coulomb forces. Exciton can diffuse through a material and, after gaining an extra energy greater than its bounding energy, it can undergo easy recombination and break itself apart into a subsequent pair of hole-electrons. Excitation production is a significant as well as a substantial and familiar phenomenon taking place in materials that are naturally and inherently organic and it does also occur at the interfaces between materials that are inorganic as well as organic[23].

1.6.4. Carrier (electron-hole) Recombination

Photogeneration generates extra carrier pairs, resulting in a larger carrier concentration than at thermodynamic equilibrium. An electron-hole pair is annihilated when the system strives to approach equilibrium and fall of the excited electrons from the conduction band does take place which in turn recombine with holes in the valence band and thus resulting in their recombination with the corresponding holes. It is called a wasteful recombination process.

Both energy and momentum conservation must be satisfied during the recombination process. The extra energy is either converted to photons (irradiative recombination) or dissipated as heat (non-irradiative recombination).
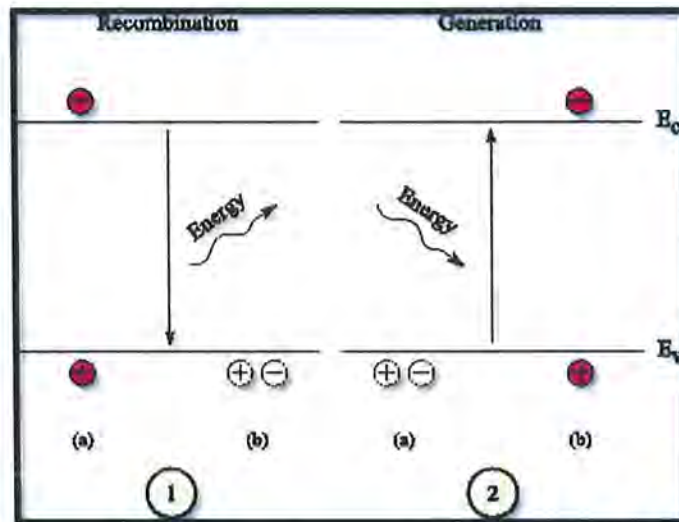
Figure 1.5. Carrier's Generation and Recombination process.

The three most significant recombination mechanisms are listed below.

1.6.4.1. Radiative Recombination (Band-to-Band)

In this process, an electron belonging to the conduction band must undergo a transition into a hole which is generally present in open state within a valence band from a permissible state linked to conduction band. It serves to be the opposite of the process of carrier's generation in which the extra amount of energy is primarily emitted in the shape of photon withholding energy not so far from the bandgap[24]. The number of surplus carriers

as well as doping concentration (donor or acceptor) affect the rate of irradiative recombination. It is mostly present in materials with a direct bandgap semiconductor. Band-to-band recombination is another name for this process.

1.6.4.2. Auger Recombination

It is a general process regarding recombination which is in turn non radiative in nature. The recombination of a hole originally arising of valence band does take place with an electron who is inhabitant of conduction band which can be thought of as a three-particle interaction[25]. The extra energy is then transmitted to another extra particle which can either be a free hole or an electron and that too in the form of kinetic energy while whenever the process of thermalization does happen, it is further transformed into useless heat. In a highly doped semiconductor, where the carrier lifetime significantly relies on the number of free carriers, the Auger recombination may be quite significant[24]. While taking into account the layers who do possess the concentration of specifically used dopant in value much superior to 1019 cm^3, Auger recombination may be the predominant recombination process. Smaller bandgap semiconductors frequently experience this behavior.

1.6.4.3. Trap Assisted Recombination (Non-Radiative)

Discrete energy levels inside the bandgap are produced by defects in semiconductor crystals, which can be caused by impurities or crystallographic flaws like dislocations. Certain energy levels are located deep within the bandgap. These defect levels, often referred to as traps, dramatically enhance the phenomenon of recombination by the aid of special protocol which further does take place in the form of two parts. Firstly, the conduction band's singular free electron does perform relaxation and that too adjacent to the level of defect preceding the forthcoming relaxation further leading to valence band, whereas annihilation of a hole is carried out, in subsequent second step. The center concentration influences the rate of recombination. The carrier lifespan may be controlled by adjusting the concentration of recombination centers. In this process, energy is not emitted in the form of photons but rather transferred in the form of phonons or lattice vibrations. This process is also known as non-radiative recombination[26].

Recombination processes may often be thought of as occurring individually, and the penultimate rate belonging to recombination can only be easily calculated by addition of rates of all individual ones[23].
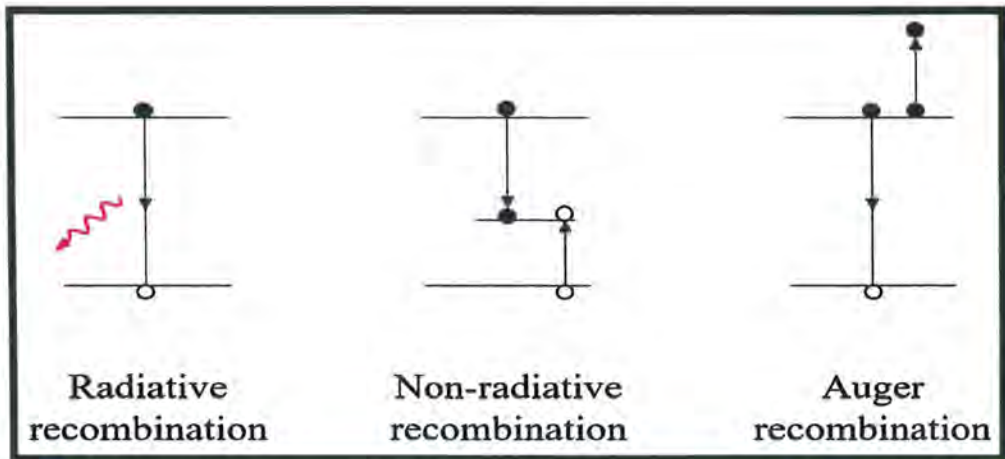
Figure 1.6. Different types of Carrier's Recombination in semiconductors[27].

1.7. P-n junction

After capturing photons, solar cells excite electrons across a semiconductor's bandgap to produce more hole-electron pairs than are required. These pairs are then separated by charges, which occurs more frequently when doping produces a junction of the p-n type. The p-n junction is not a conductor. The space charge region is another name for this non-conducting layer between the p-n junction. A potential difference at the exterior electrodes equal to the bandgap results from the space charges at the interface adjacent to junction of the p-n type which consequently drive holes in one direction along with the electrons in the other[28].

14
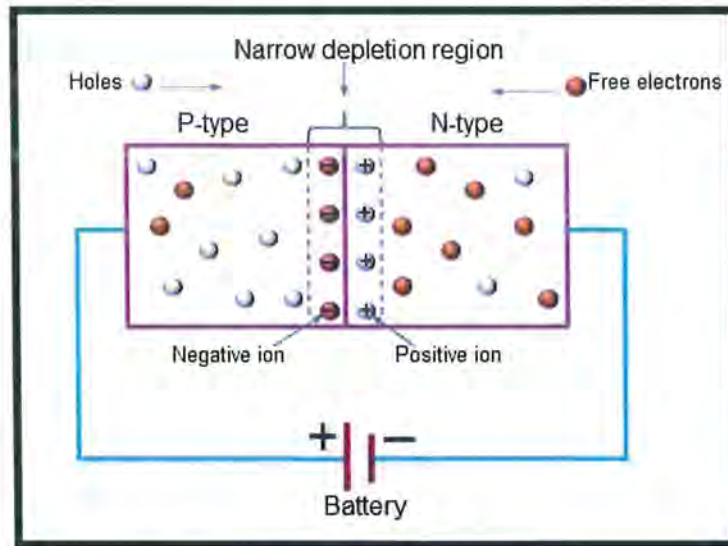
Figure 1.7. P-n junction diode[29].

1.8. Solar Cells

The photovoltaic principle is employed by solar cells to for efficient transformation into purposeful electrical energy from striking sunlight. Employed solar devices do produce voltage as well as current when energy in the form of solar is absorbed. Solar cells are combined to create bigger units known as solar modules since the potential produced in third-generation solar cells is only about 0.5–1 eV, which is extremely low. These modules are connected to even larger units to produce solar panels with greater potential[30].

1.8.1. Solar Cell Working Mechanism

The below mentioned steps are taken into consideration while accounting for working of solar cells.

➤ In a solar cell, the conversion begins with light induced charge carriers' generation.

➤ It is followed by transport regarding certain charge carriers that have already been produced.

➤ The above-mentioned carriers of charges are accurately captured by their respective electrodes.

➤ The movement of electrons as they go through an external circuit.

➤ And subsequent dissipation of power generated in form of load.

15
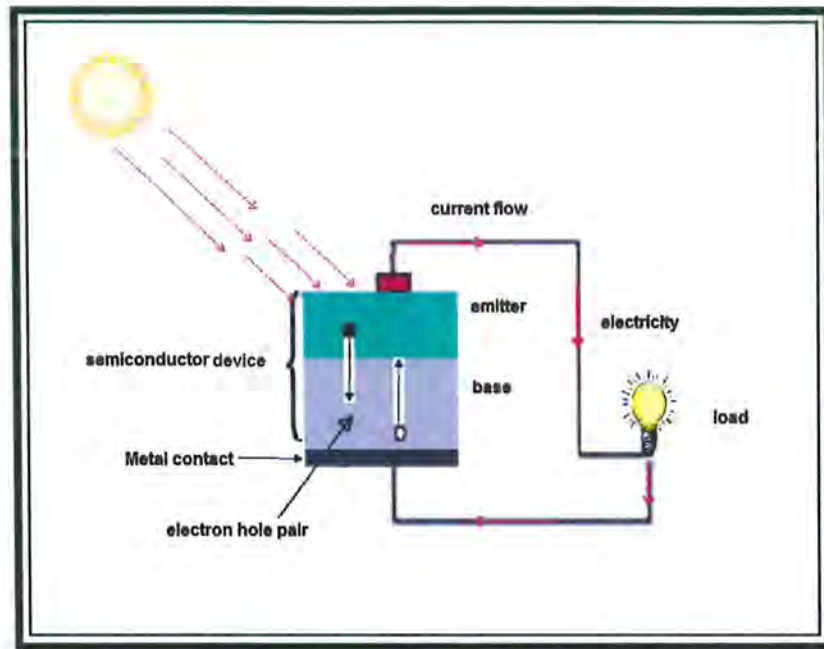
Figure 1.8. Solar cell cross section and working.

1.9. Different Generations of Solar Cells

According to the kind of material used in their construction, solar cells are often categorized into three generations. The silicon (crystalline in nature) based technology having its emphasis on wafers which can in turn either be in form of multi crystalline or single crystalline in structure, is used in the above mentioned first generation of solar cells. The technology of solar cells related to thin films does serve as the foundation for second-generation solar cells. The third and so far, last generation of solar cells uses innovations like concentrating and organic solar cells that are either currently being tested or are not yet commercially available[31]. The preliminary solar cells belonging to the first generation are the most common in the market and have the highest efficiency of all the generations, but they are quite expensive to produce. Second generation solar cells are also in commercial use and have low fabrication cost, but efficiency is still low. Third-generation solar cells are far more affordable and simpler to manufacture while still utilizing thin-film techniques and a variety of non-toxic materials. But have no commercial applications due to certain limitations[32].
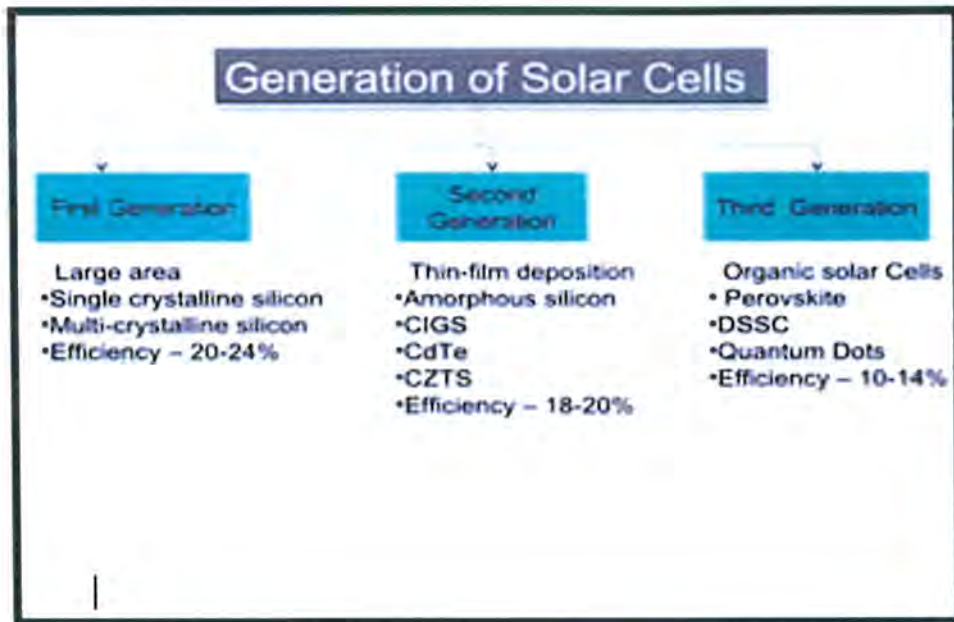
Figure 1.9. Generations of Photovoltaic cells.

1.9.1. First Generation Solar Cells

Solar cells based on silicon and belonging to the preliminary first generation are sometimes referred to as conventional, wafer-based, or classic solar cells. Two layers of various semiconductor materials that have been doped in various ways make up the structure of relevant solar devices. A diode having its basis on p-n junction is almost similar to a solar cell. To prevent direct solar irradiation from penetrating the electrode, silicon with embedded metal components is employed on the upper side of the electrode. Solar cells are made in a variety of sizes and forms to increase their useful surface area and minimize contact resistance-related losses. There are many kinds of solar cells, but around 90% of all solar cells are made from crystalline silicon wafers. However, a significant disadvantage of these cells is that they lose some of their effectiveness at high temperatures. This generation mainly includes the following type of solar cells[33].

- Emitter wrap-though cells (EWT)
- Monocrystalline silicon
- Gallium Arsenide (GaAs)
- Polycrystalline silicon

17

1.9.2. Second Generation Solar Cells

The technology corresponding to the second generation of solar cells, which used thin films instead of the crystalline silicon on which the first generation was based, proved to be far less expensive[32]. Despite taking into account the material of semiconductor, the more facile and effective thin films did provide opportunities for a significant decrease in the ongoing hype in prices of material by doing away with the wafer that did consist of far expensive silicon. Further benefits of such thin films do include the expansion of the production unit shift to a glass sheet (~ 1 m^2), from ordinary silicon wafer (~ 100 cm^2) which is roughly about one hundred times bigger[34]. The solar cell used in this technique is extremely thin, with a thickness ranging from 35-260 nm, because it uses less material. The following are the five types of cells having these new thin films that did prove out to be a commercial fruitful approach.

- Copper-Indium-gallium-Di selenide (CIGS) or Copper-Indium-selenide (CIS)
- Amorphous silicon type (a-Si)
- Cadmium sulfide (CdS) and cadmium telluride (CdTe)
- Tandem amorphous-Si as well as multi-crystalline-Silicon

1.9.3. Third Generation Solar Cells

To remove the restrictions on the greatest attainable extent of the previous two generations, the third and final generation was introduced at that time. For instance, the first generation requires high fabrication cost, and the second generation has limited material availability. The solar cell advancements that are in general associated with third generation still tend to be at the precommercial level and range in contrast to technologies that are demonstration such as concentrating solar cells having possession of multiple junctions and also unique perceptions and ideas that are so far in dire requirement of advanced as well as fundamental development & research to be carried out on them in future (e.g., solar cells possessing their quantum confinement in their respective structures). Several modern solar cell technologies are now being developed, and a major element of these technologies is the usage of quantum wells as well as dots, quantum mechanics-based wires or superlattices. The future use of such technologies in coming days seems to be most probable in assembly of solar cell technologies already based on concentration techniques,

where there is a chance of them that they might overcome the thermodynamic constraints of traditional (crystalline) cells and attain very high efficiencies[35]. They are not able to be operative on methods employed in junctions of p-n type which are overly simple. Several materials other than silicon have been used, including silicon wires, solar inks, and nanomaterials. To improve the light absorption in these devices, a great number of various elements have been tried to perform the function of sensitization. To cover a hell broad and great limit of solar spectra and to make in enhancement in spectral sensitivity, several stacking layers of materials with modified band gaps are utilized. As a result, the practical as well as desirable features of inorganic and organic solar cells were taken into consideration as a whole to create these hybrid solar cells. Low-cost manufacturing processes are used in the construction of these cells. The following are the certain categories of solar cells that are included in this so far ultimate generation[32].

- Solar cells have their origins in thin polymers.
- Dye-Sensitized solar cell (DSSC)
- Solar cells rely on the operation of sensitization of quantum dots.
- 'Smart' coatings
- Perovskites solar cells
- Solar cells are made of nano crystals.
- Polymer based solar cells.

Among all of them, the DSSCs are the primary focus of our attention.

1.10. Dye-Sensitized Solar Cells (DSSCs)

Dye-sensitized solar cells (DSSCs) in actual corresponding to the group of solar cells that have thin films within their systems are gaining attention due to certain desirable characteristics like ease in processing during production, simple yet facile preparation methodology, low cost, and low toxicity. Its fundamental principle has its basis lying on a certain photo as well as electrochemical system in which assembly of a semiconductor is resulted between a conventional electrolyte and an anode which is further sensitized by the virtue of light[36]. They are too termed to be as a class of the Gratzel cells, which were in turn originally assembled in the year of 1991 at UC Berkeley owing to the efforts made by corresponding first developer of this technology which are Michael Gratzel along with

Brian O'Regan. In case of an obsolete and old-fashioned solar cell, Si does provide us with a photoelectron's practical and nonstop source, and it does convey as basic mean for creation of a field which is naturally electric and in turn provides a basis for generation of effective amount of current which has resulted from separation of relative charges[37]. However, when we are taking into consideration DSSCs, the relevant semiconductor material that is present only performs the task of a charge transfer, and the photoelectrons are supplied by photosensitive dyes. The technically advanced new features that became associated with DSSC later did result when the nano sized grained coatings ,involving TiO₂ in structure, were made to subject to process taking into account photosensitization and that too combination of a visible dye that itself remains active in sense of optics for a longer amount of time, which in turn further makes conditions better by causing a rise in efficiency levels and taking them above 10%[38].
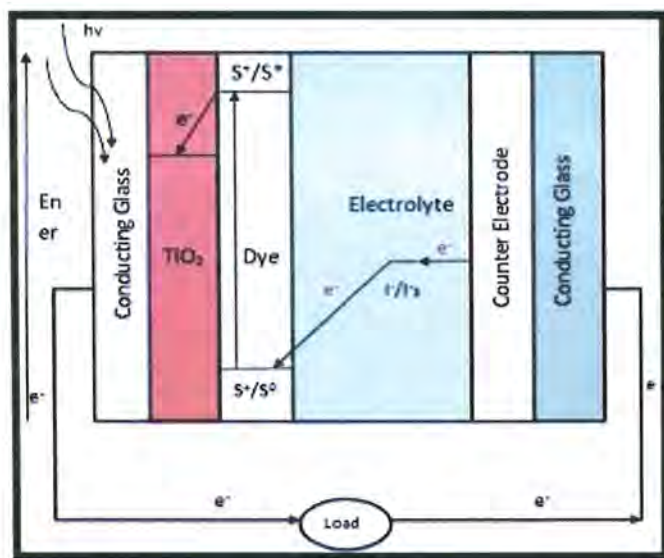
Figure 1.10. Principle and energy levels distribution for Nanocrystalline DSSC[39].

1.10.1. Photo electrochemical Solar Cells

Photo electrochemical types of cells use light to generate electricity. One or two semiconducting photoelectrodes, as well as auxiliary metal and reference electrodes submerged in an electrolyte, make up each cell. Semiconductors like ZnO, TiO₂, SnO₂, ZnS, etc are used as photoanode material[40]. The working principle of this type of DSSC

20

does take into consideration the following number of steps: current's collection, absorption of relevant light, charge separation and flow relevant to charges.

The below mentioned steps convert solar energy into voltage and current.

1) In the first step the dye molecules get excited when exposed to sunlight (s*). As a result, promotion of electrons does occur to states having relatively greater amount of energy from the previous default states of energy. The absorption of almost all dyes does take place at 700 nm of the wavelength, and which in turn almost equalizes the photonic energy levels at a value near about 1.72 eV[30].

$$S + photon (hv) \rightarrow S* \text{ (excitation)}................... (1.1)$$
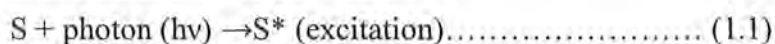
2) The basic contrast determines among various levels referring to LUMO and HOMO of the dye molecules determines how much photocurrent a DSSC can generate. Photoanode's conduction band, which is inherently active at certain levels which further do fall below the LUMO states adjacent to dye, is the place where electrons whose excitation has already been done are placed, and therefore, photosensitizer content's oxidation is carried out[30].

$$S* \rightarrow S^+ + e^- \text{ TiO2 (injection)}................... (1.2)$$
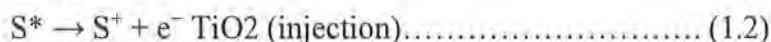
For kinetically favorable injection of electrons into LUMO of photoanode the LUMO of dye should have negative energy as compared to the LUMO of photoanode.

3) These injected electrons are then diffused through photoanode and move through external circuit and reaches towards counter electrode by dissipating their energy to load[30].

4) The consequent regeneration or reduction of the inherent default state belonging to a specific dye is carried out only when the electrolyte (I^-_3) does serve the function of collection of respective electrons and their original source if more specifically the electrode which does act as counter and finally, its reduction to (I^-) does take place. As a result of accepting an electron from the I^- ion redox mediator, the regeneration of dye takes place[30].

$$S^+ + e^- \rightarrow S \text{ (regeneration)}................... (1.3)$$

$$S^+ + 3I^- \rightarrow 2S + I^-_3 \text{ (regeneration)}................... (1.4)$$
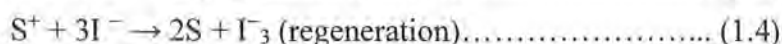
As a result, the ions of iodide (I⁻) which are already present within the medium regarding electrolyte therefore help in the regeneration of dye and also prevent the oxidized dye to recapture the electron of conduction band.

5) The oxidized mediator (I⁻₃) does make amendments for electrons that have already been lost from the electrodes acting as counter and it furthermore breaches the boundary adjacent to cathode, ultimately making the reduction of (I⁻₃) into much simpler (I⁻) plausible. The usual visible indicator for completion of a certain circuit is provided by subsequently when all of the (I⁻₃) have been completely reduced and as a result almost all of the (I⁻) are generally regenerated at the surface parallel to cathode[41].

$$I^-_3 + 2e^- \rightarrow 3I^- \text{ (reduction of electrolyte)} \dots\dots\dots\dots\dots (1.5)$$
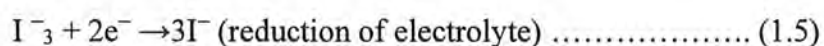
The use of liquid electrolytes as a charge carrier transporter offers maximum efficiency for DSSCs. But the use of liquid electrolytes offers certain limitations which includes solvent leakage, volatilization, photo-degradation, dye desorption, corrosion of counter electrode and ineffective sealing of cells. Due to these above drawbacks of using liquid electrolytes, these are replaced with stable solid or quasi-solid electrolytes leading to the formation of Solid State DSSCs.
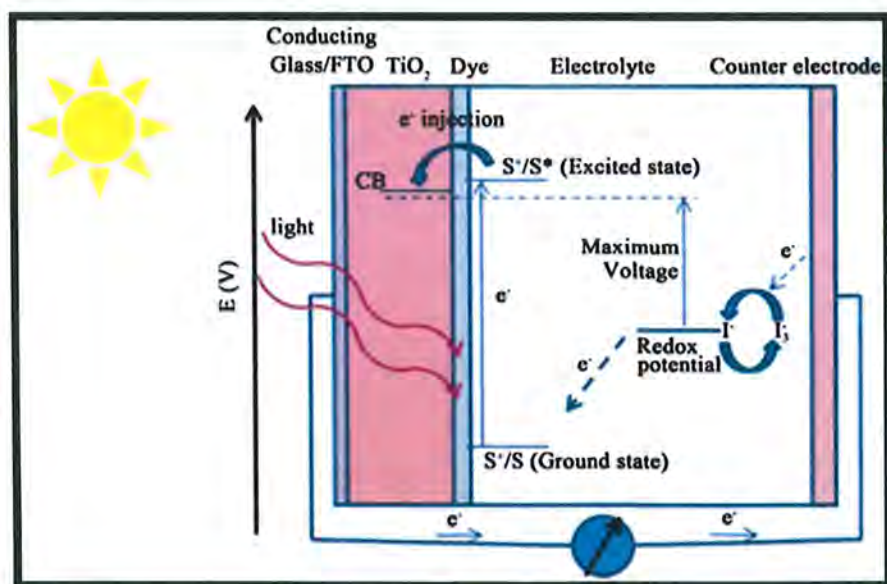
Figure 1.11. Working principle and energy levels distribution for Nanocrystalline DSSC[30].

1.10.2. Solid State Dye-Sensitized Solar Cells

In these cells, a material responsible for conduction of relevant holes, which is usually an organic conductive polymer, is used instead of the liquid electrolyte. The structural properties, working mechanism and charge transferring mechanism in these cells are like that of photo-electrochemical solar cells. But in contrast to other PEC cells, there is an absence of charged ions within the electrolyte, rather hole transfer takes place directly between the source responsible for providing holes and dye, meanwhile the necessary transportation of holes to a metallic counter electrode does take place sequential jumping among the available electronic states on the organic molecules[42].

1.10.2.1. Structure and operation principle

Whenever a hole conductor electrolyte that is solid state in nature and it is further present with a singular layer corresponding to a certain dye that is involved in the process of charge transfer and moreover, both of these are stuck to outer surface adjacent to film of TiO_2 which in turn is itself nanocrystalline in nature. Photoexcitation of given dye does provide a basis for the Insertion of an electron into the TiO_2's conduction band. Thus, restoration of the dye's original shape and state is achieved quite fruitfully, and this happens owing to hole conductors which do provide the task of donation of electrons. Further interception in the process by which a dye that is already oxidized and does perform the task of recapture of electrons belonging to conduction band does take place by virtue of hole conductor which favors the constant regeneration related to sensitizer substance. As a result, regeneration of conductor hole is carried out in turn at counter electrode and completion of circuit does occur with the aid of activity of migration of certain suitable electrons[39].

- In hole conducting polymer, the flow along with movement of respective holes tends to be very low as relative to the movement of ions in liquid electrolyte, which results in greater interfacial electron-hole recombination rates.
- Also, in comparison with liquid electrolyte, low interface interaction in hole conducting medium and larger distribution of trap sites inside the polymer.

Due to this overall conversion efficiency decreases. However simple and easy fabrication processes and low expenses encourage researchers to be active in this area.

1.10.3. Nanotechnology in DSSCs

In many respects, nanotechnology is essential in increasing cell's efficiency by providing,

➢ Higher surface area

➢ Tunability of band gap

1.10.3.1. Higher Surface Area

When our material size is significantly reduced to the nano scale, which is in turn 10^{-9} in meters from a prior level of bulk, a dramatic and rapid increase in surface area occurs with respect to the same as well as equal amount of the tested substance. As a result, the nanoparticles display intriguing physical and chemical characteristics that were previously unknown in bulk substances. The huge number of surface atoms for a nanostructure does make the chemical reactivity related to concerned nanomaterials stabilize and increase to a far greater extent[43]. There are more active sites for the adsorption of a substance on nanoparticles with greater surface area. Numerous applications, including storage devices related to energy, solar cells, catalysis that is chemical in nature, etc., take advantage of this resulted increased surface area referring to our most concerned nanostructures.

1.10.3.2. Band gap's tunability

The arrangement of single molecule generally does range in size from a value of 10 to 500 nm. Few atoms or molecules are assembled to form nanoparticles. Nanoparticles are really referred to as "artificial atoms/molecules". Quantum mechanics can be used to describe the features of our prepared nanostructures as well as nanoparticles that are linked to probabilities related to electricity along with levels of energy[43]. The lowest threshold energy that must be provided to an electron for excitation depends on the nanoparticle's subsequent size, which impacts the electron's confinement related to quantum mechanics. Thus, by varying the size of the nanoparticles, that particular light's wavelength whose absorption is taking place at the moment may be modified[43].

In many respects, nanotechnology is essential for increasing cell efficiency as discussed below.

1.10.3.3. Nanostructures as Semiconductive Metal Oxides

When used as semiconductor materials, nanostructures offer several benefits over bulk materials. The ability of the nanostructures to adsorb dye is substantially increased since they have a bigger surface area than bulk materials. The efficiency of solar cells increases due to greater dye adsorption's impact on higher light harvesting. One-dimensional (1-D) nanostructures and nanoparticles are the two basic categories for semiconductor materials utilized in DSSCs[43].

1. **Nanoparticles**

For the adsorption of dye, nanoparticles can provide a greater surface area which corresponds to better light harvesting. The use of semiconductor nanoparticle material rather than bulk material can significantly increase the efficiency of the cell. Therefore, the morphology and structure of the nanoporous layer will determine cell performance. However, because the nanoparticles have grain boundaries, the mesoporous semiconductor particles used in DSSCs experience "recombination of electrons that are already excited". Furthermore, the recombination of inherent charges does happen to the nearby electron acceptors and that too by the semiconductor's CB. In order to prevent the leakage as well spilling of electrons present in conduction band further to electrolyte, one method of decreasing charge recombination is to surround the nanoparticle with an exterior energy barrier[44].

2. **One Dimensional (1-D) Nanostructures**

Only because of the simultaneous occurrence of a recombination as well transport involving electron process, a DSSC's efficacy and accuracy calculating part tends be a more specifically suitable photoanode. Nanofibers, nanowires, and nanotubes are 1-dimensional (1-D) nanostructures that exhibit improved electrical conductivity. This is because electrons have a direct passage to the surface, resulting in a longer diffusion length than in nanoparticles. In a 1-D nanostructure, the grain boundary is minimized and can function as a single crystal[45]. It has been found that the rate of recombination in nanotubes is 10 times slower than that in nanoparticles. Due to their lesser surface area than nanoparticles, liquid electrolytes penetrate the 1-D lattice less readily.

1.10.4. Synthesis of Nanomaterials

The subsequent creation of materials in the nano size range relies on two distinct techniques, typically bottom-up and top-down, that have an impact on the synthesis process.[46]. The selection of method for obtaining nanoparticles depends upon the morphology and applications of the material to be manufactured. The incident spectrum that is made available to the solar cell must be changed for up or down-conversion[46].

1.10.4.1. Down-Conversion (Top-down method)

A single photon owning energy in the higher state will split and break part into photons which are two or more in quantitatively during down conversion, and the solar cell may then use these photons to hole electron pairs in certain numbers which will happen to be two or more[47].

1.10.4.2. UP-Conversion (Bottom-up method)

Up conversion is the process of combining two or more low energy photons into a single photon that the solar cell may use to create an electron hole pair[47].
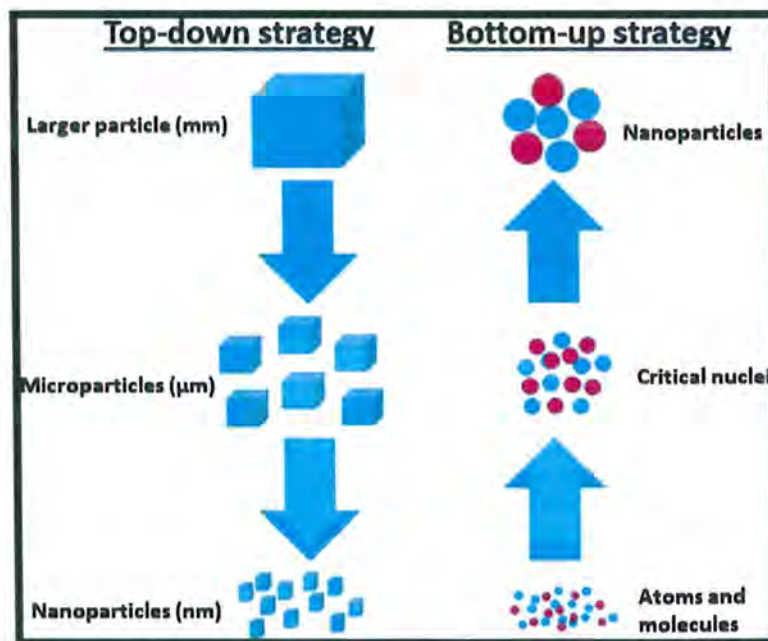
Figure 1.12. The schematic diagram for the representation of Top-down and Bottom-up conversions for the fabrication of nanomaterials[48].

1.11. Introduction of Components of DSSC

Some of the crucial components that we utilized while assembling a desired dye sensitized solar cells are given as follows.

1. Semiconducting nanoparticles (NiO) as photoanode
2. Dyes (Carminic Acid, Coomassie Violet R200, Arsenazo III)
3. Electrolytes (Poly-3-hexylethiophene P3HT, PEDOT: PSS)

1.11.1. Semiconducting Photoanode Material

The DSSCs' structural core is made up of metal oxides. They serve two crucial functions as dual function materials: (i) they do serve the purpose of being certain centers that tend to be naturally photoactive centers, and which can further be modified by the virtue of dye, while (ii) They operate as a pathway for electrons from dye molecules that are still photoexcited to transfer to contact at the back as well. Therefore, a greater available extent of porosity as well as surface area that are required for efficient, accurate and facile loading of desired dye, excellent and far more reaching features related to the scattering of light and an effective as well as influential level of crystallinity for a facile transport of already present electrons make up key variables useful for determination of efficiency linked to activity of photovoltaic of our DSSCs. An essential need for the electron injection is the proper alignment of the conduction band (CB) edge that belongs to the semiconductor material with respect to the dye's LUMO. Effective electron injection becomes impossible in certain cases like whenever LUMO of the dye is equal or lower than the CB of semiconductor's material[45].

1.11.1.1. NiO Nanoparticles

Nickel oxide NiO is a cubic lattice structure transition metal oxide. Due to its potential for usage in several applications, including electrochromic films, catalysis, gas sensors, magnetic materials, and cathodes of battery, it further has gained growing interest. Additionally, it is widely considered for its utilization in photocathodes that are still dye-sensitized in nature. It does display a range of production options, electrochromism linked to subsequent anode, a greater value of optical density related to spin and outstanding stability as well as endurance related to a particular electrochemical system. NiO

semiconductors tends to rise as a domain of substantial scientific interest in the new areas of particular study due to their low material cost as a material who can efficiently as well accurately utilized for serving the purpose of storage material[49]. Nickel oxide that is nanocrystalline in size is anticipated to possess much superior qualities to nickel oxide nanoparticles that have their sizes in the range of micrometer and this does happen due to the macroscopic quantum tunnel effect, the effect created as a result of size in quantum, effect arising because of volume and the effect produced due to surface[50].
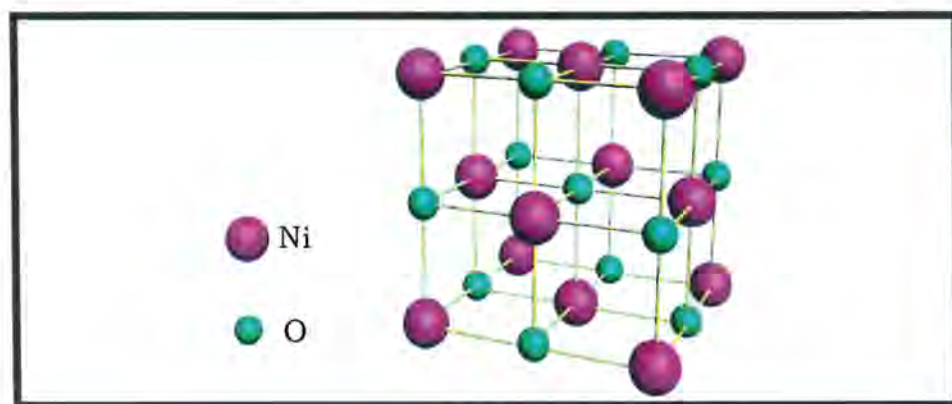
Figure 1.13. Structure of NiO[51].

1.11.2. Dyes as a Photosensitizer

The dye is crucial in making the semiconductor sensitive to absorption in particular infrared as well as visible ranges of certain spectrum related to solar power. For this reason, a few requirements; including the already present chemical potential linked originally to redox system of corresponding electrolyte, a broad spectrum related to absorption, non-toxicity, a plausible matching of edges related to VB and CB od in-use semiconductor respectively to the LUMO and HOMO levels adjacent our employed dye and substantial stability, must be satisfied at the same time. The almost full amount of the light that is at lower level corresponding to a level lower than the minimum required wavelength must be absorbed by the ideal sensitizer. Additionally, it must behave as a possessor of have an influential orbital bonding as well as interactions with the nanoparticles of nickel oxide. In this work, some of the dyes such as Carminic acid, Coomassie Violet R200, and Arsenazo III, were used to increase the optical property of pure and doped NiO nanoparticles. These

dyes adsorbed on the surface of nanoparticles and act as photosensitizer to enhance their corresponding optical properties.

1.11.2.1. Carminic Acid Dye

An organic dye with a blood-red color. Its molecular formula is $C_{22}H_{20}O_{13}$ with a core consisting of anthraquinone bonded to a glucose sugar. Carboxyl, hydroxyl, and phenolate groups make up the structure of carminic acid. Due to its strong anchoring groups and high oxidation states in excited condition, carminic acid is considered as an efficient sensitizer for DSSCs. Phenolate group is an electron source in carminic acid while the hydroxyl and carboxyl anchor to the semiconducting photoanode material[52]. It is present in a number of species of scale insects called cochineals, such as Dactylopius coccus. It has vast applications in cosmetics, drinks, food, and pharmaceutical products.
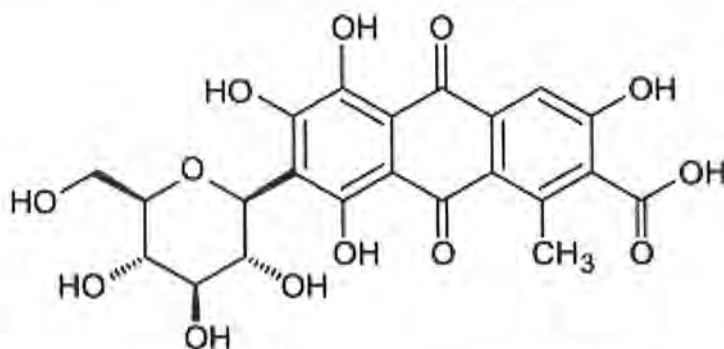
Figure 1.14. Structure of Carminic Acid dye[53].

Table 1.1. General properties of Carminic Acid dye.

Molecular formula	$C_{22}H_{20}O_{13}$
Molar mass	492.39 g/mol
Appearance	The particular dye of carminic acid tends to seem like dark red, bright red or a mass of dark purplish brown in color, powder. The color associated with it tends to generally darken at a temperature of 248 °F. It does own a violet to yellow like type

	of color when submersed in aqueous solutions having a pH in range of acid, while in water, it does exhibit a deep red type of color.
Melting temperature	136 ° C
Extent of Solubility while employing water as solvent	1.3g/ L

1.11.2.2. Coomassie Violet R200 Dye

It is an anionic organic dye and it has various applications in leather, textile, rubber, cosmetic, printing, paper and plastic industries to color the products[54]. In the structure of comassie violet R200 sulphonic acid group (-SO₃H) is acting as an anchoring group.
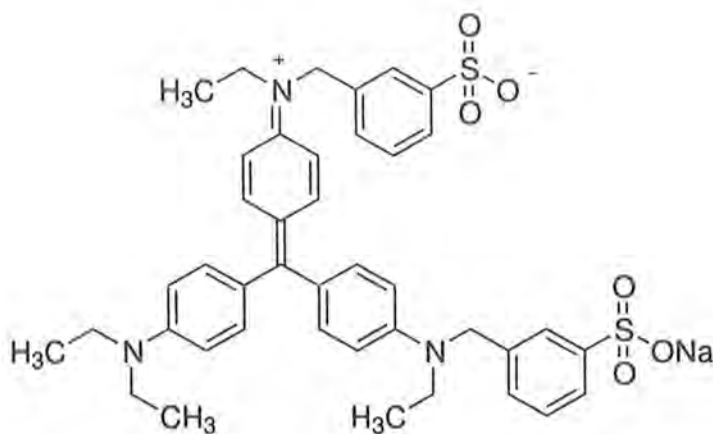
Figure 1.15. Structure of Coomassie Violet R200 dye[54].

Table 1.2. General properties of Coomassie Violet R200 dye.

Molecular formula	$C_{41}H_{44}N_3NaO_6S_2$
Molecular weight	761.93
Molecular structure	triarylmethane class
Appearance	Bright blue purple or deep navy powder, easily soluble in water and ethanol. Purple in water and violet blue in ethanol.

1.11.2.3. Arsenazo III Dye

Arsenazo III, a chelating indicator dye[55]. This dye has already been investigated for the purpose of detection related to calcium that is naturally present in tissues and cells along with its presence in solution[56]. It is safe to be said as a selective as well as efficient, sensitive and facile chemical for its subsequent purpose related to calcium[57]. The sulphonate group ($-SO_3H$) in its structure acts as an anchoring group.
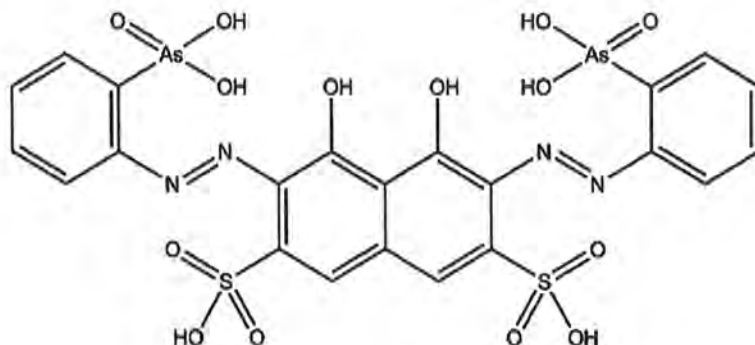
Figure 1.16. Structure of Arsenazo III dye[56].

Table 1.3. General properties of Arsenazo III dye.

Molecular Formula	$C_{22}H_{18}As_2N_4O_{14}S_2$
Molecular Weight	776.37
Solubility in solvents	Soluble in alcohol as well as water
Melting temperature	>320 °C

The advantages attained by making use of organic dyes are:

1. They do possess a greater value of coefficient linked to absorption where moreover plenty of transitions of the type $\pi \rightarrow \pi^*$ do take place within our in-use dye's molecules.

2. Designing and modifying dyes with the help of continually changing structures and modifying the associated range and limit of the relevant wavelength linked to the phenomena of absorption.

3. Does not use metal and has no resource restrictions.

4. Enables synthesis and is less expensive than organic metal dyes.

1.11.3. Electrolytes

Electrolytes are a crucial component of the DSSC because they regenerate the oxidized sensitizers and, as a result, make possible the flow which is smooth as well as continuous of electrons between electrode linked to photoanode and the electrode acting as a counter, completing given electric circuit. Certain familiar electrolytes which can be used for practical purposes in DSSC are able to be categorized into classes of quasi-solid, liquid, or solid states and these in turn have further their origins based on the viscosity along with composition of already present components. Since the electrolyte related to redox couple which further consists of iodide/triiodide (I^-/I_3^-) owns a distinctively slow recombination rate, it is extensively investigated[41]. Leakage is the main problem of using liquid electrolytes. That is why, DSSC in the available nature of solid state which are further denoted by (s-DSSC), in which the tasks related to electrolyte are substantially carried out with the virtue of material that is organic in nature and is employed for hole-transport, has been developed to address this drawback.

1.11.3.1. Poly-3-hexylthiophene (P3HT)

P3HT is an organic semiconducting polymer and belongs to the polythiophenes (having polymerized thiophene monomer) family. In solid-state DSSCs P3HT acts as a redox electrolyte because of its hole conducting properties. Charged units which act as hole carriers are produced, when P3HT is doped with p-type dopants like organic acids and halogens.
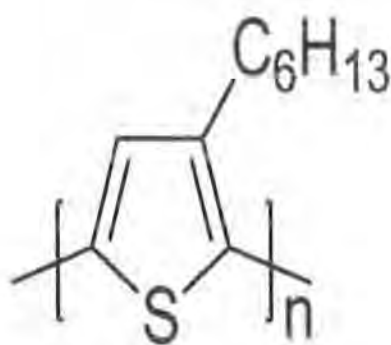
Figure 1.17. Structure of P3HT[58].

In organic solvents, P3HT shows a broad absorption maximum at about 550nm. The absorption spectra of P3HT shows hypochromic and bathochromic shift as it depends upon the length of conjugated system[59]. The corresponding band gap does tend to make a rise and that in turn is associated with a certain improvement in the length of conjugated system, hence the absorption peak shifts towards the longer wavelength end. In the same way, our in-use band gap tends to fall in value and following is regarded with a drop in the length of conjugated system and as a result the absorption peak shifts towards lower wavelength end. There are various factors that may affect the length of conjugated system such as temperature, solvent etc. P3HT does have efficiency to play almost equal part in solid-state DSSCs, as compared to electrolyte consisting of liquid tends to carry out in liquid state DSSCs. If the respective level of LUMO of hole conducting polymer is more in extent as compared to the LUMO level of the dye, it can perform its function effectively.

P3HT plays two important functions in DSSCs.

1) By accepting holes from dye, it carries them towards counter electrode.

2) It also contributes to the generation of photocurrent.

1.11.3.2. PEDOT: PSS

Poly (3,4-ethylenedioxythiophene) polystyrene sulphonate consists of two ionomers; one of the ionomers is negatively charged sulphonated polystyrene as the sulphonate group loses a proton, and the other ionomer is PEDOT [poly(3,4-ethylenedioxythiophene)] which carries a positive charge. This polymer is transparent and

conductive. A macromolecular structure is formed by the combination of these two oppositely charged components[60] as shown below.
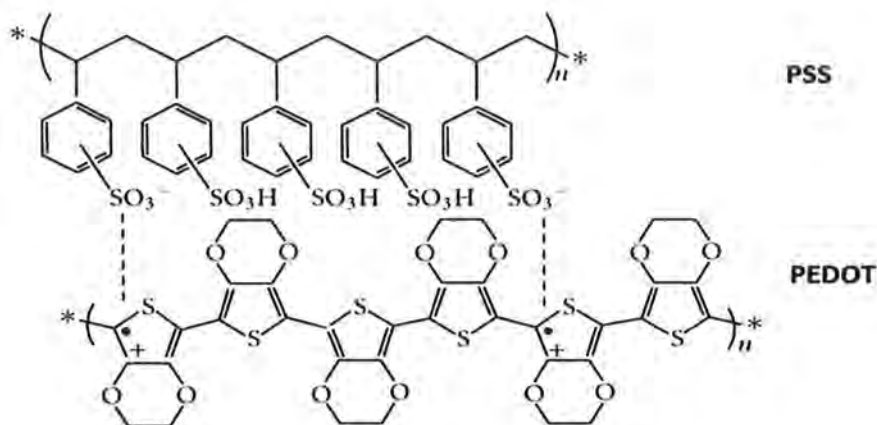
Figure 1.18. Structure of PEDOT: PSS[61].

The conductivity of PEDOT: PSS is about 1000 S/cm which can be further increased by its treatment with various compounds such as geminal diols, ethylene glycol, acids, and phenol etc. This polymer offers several applications such as used as an antistatic agent in photography and used as a conductive polymer. The stability of device is improved by thin film coating of PEDOT: PSS on the surface of conducting substrate (ITO) that does fulfil the purpose of hindrance to certain extent of diffusion regarding oxygen and indium, that too is in practical condition only because of anode. It also has the potential to smoothen the surface of the conducting substrate[61].

1.12. Characterization of Solar Cell by Current-Voltage Measurements

The power conversion's efficiency, stability, and cost serve as the indicators of DSSC's performance. The characterization of solar cell does involve the study of, theoretical power that is PT, open circuit voltage which is V_{oc}, energy conversion efficiency expressed by η, maximum power point that is shown by M_{pp}, current at maximum power (I_{MPP} or Imax), voltage at certain point referring to maximum power as is expressed by V_{MPP} or Vmax, current density due to short circuit represented by J_{sc} and fill factor denoted by FF, and to

34

assess the efficiency of fabricated cells. Some standard conditions have been assigned to investigate the performance of the fabricated device which include spectrum, intensity of light, and temperature[41].

- Fill Factor (FF)
- Short Circuit Current Density (J_{sc})
- Maximum Power Point (M_{pp})
- Open Circuit Voltage (V_{oc})

1.12.1. Short Circuit Current Density (J_{sc})

The short-circuit current (I_{sc}) is the current flowing through the solar cell when there is no voltage across it (i.e., given cell tends to be in environment of short circuit) is termed as short circuit current density (J_{sc}). It is abbreviated as I_{sc} or J_{sc}, which does further serve the function of expression of current that is generally available per unit area with having units of mA/cm^2. Various parameters such as the volume of incident photons, the solar spectrum, optical qualities like reflection and absorption, and the surface area including that of our solar cells as well can also be utilized for providing a control for current density arising due to short circuit and explain the properties like carrier separation and transport efficiency. The J_{sc} is affected by the relationship between the absorption coefficient belonging to dye sensitizer, dye sensitizer itself and photoanode overall. Hence, the following characteristics decide the high J_{sc} values:

- The strong dye adsorption that extends over a long distance as well as limits of available amount of sunlight.
- A greater insertion of available number of electrons into CB that is further relevant to our prepared photoanode, by photoexcited dyes.
- The successful regeneration of the dye that has already been oxidized and that too by the aid of I^-[41].
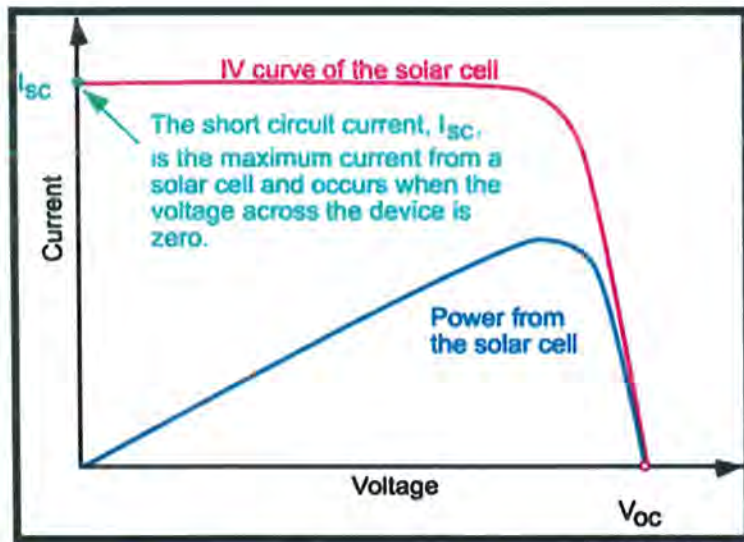
Figure 1.19. Graphical representation of J_{sc}[62].

1.12.2. Open Circuit Voltage (V_{oc})

The maximum available amount of voltage that can be garnered from a certain solar device is called V_{oc} and is defined as the maximum value of the potential difference between two electrodes when resulting circuit is not closed (J=0) and is ultimately facing the consequences of illumination. V_{oc} is due to the difference in the two electrode's work function. The difference in amount of all available energy between the respective photoanode's fermi level and that of available material making electrolyte defines the V_{oc}. If under illumination, unfortunately the circuit is generally an open one (J=0) current is no longer able to flow and under these circumstances, the voltage tends to be at the maximum plausible value and is subsequently referred to as the voltage present due to an open circuit (V_{oc}). Generally, the photogenerated current is produced when the circuit is reverse biased. Mainly because of a sharp but regular rise in corresponding values of voltage that is generally forward biased, travelling of current that is photogenerated tends to fall and a certain time reaches where current flow becomes zero and at this stage the voltage is called open-circuit voltage.
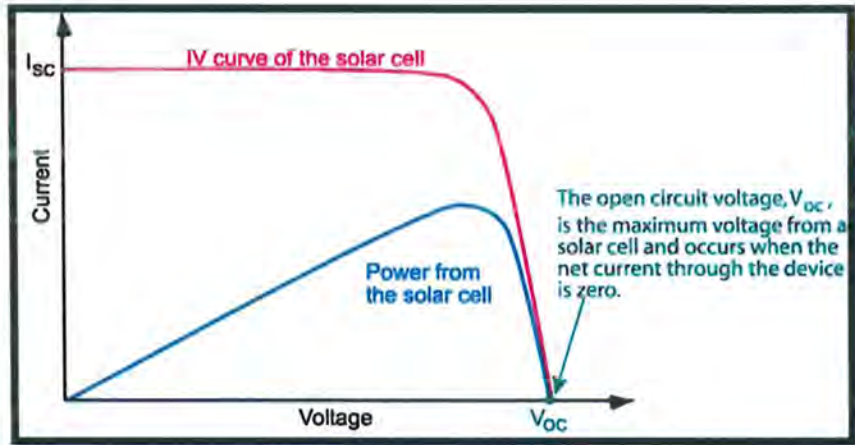
Figure 1.20. Graphical representation of V_{oc}[62].

1.12.3. Maximum Power Point (Mpp)

It is the respective point that corresponds to the maximum plausible value related to multiplication product of current and voltage at our given curve regarding I-V. So corresponding maximum power point (M_{pp}) increases and reaches its maximum value with an increase in voltage. It has nil value at the respective point of open circuit ($V=V_{oc}$) as the current density also tends to become zero and also void at the point of short circuit ($I=I_{sc}$) since the voltage becomes nothing at this point. The maximum power that a solar cell is capable of producing is represented by the equations V=Vmax and I=Imax. The point related to maximum power (Pmax), or the point of generation of maximum value of power in electrical form, corresponds to the point because of inflection of a conventional curve of I-V.

$$M_{PP} = V_{max} \times J_{max} \dots\dots\dots\dots\dots\dots\dots\dots\dots\dots (1.6)$$
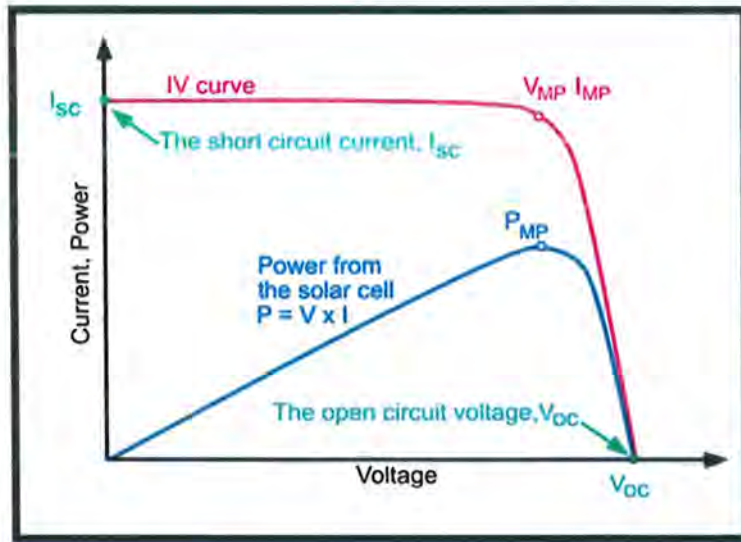
Figure 1.21. I-V curves showing maximum power point[62].

1.12.4. Fill Factor (FF)

The term fill factor (FF) tends to be identified as the ratio between power referring to maximum point and product of the voltage due to open circuit (Voc) and the current because of short circuit (Isc). It is abbreviated as FF and gives information about the overall output activity of the photovoltaic cell. The solar cell's quality is measured by the fill factor (FF). It is difficult to calculate maximum power from cell because both J_{sc} and V_{oc} never gives maximum value at same time as both the parameters are interdependent and the maximum value of one makes the other zero. So, another parameter fill factor is introduced to overcome this difficulty of measuring the maximum power of the cell. Its value ranges from 0 to 1.

$$FF = \frac{V_{MPP} \cdot I_{MPP}}{V_{OC} \cdot I_{SC}}$$ .... (1.7)

1.12.5. Efficiency related to Solar Cell (η)

The most important characterization parameter in relation to a solar cell is its efficiency (η) and it can broadly be defined as the ratio between the maximum power that has already been produced (P_{max}) and the power (P_{in}) that is incident or the power of incident photon. More precisely, it is gotten by division of output energy obtained from

38

corresponding solar cell in our use with energy in form of input that is ultimately coming from the sun[30].

Efficiency of a certain solar cell (η) = Output Power (P_{max})/Power of incident photon (P_{in})

$$\eta = \frac{FF \times V_{OC} \times J_{SC}}{P_{in}} \times 100\% \quad \dots\dots\dots\dots\dots\dots\dots\dots\dots\dots (1.8)$$

The efficiency of solar cells is directly related to I_{sc}, V_{oc}, and FF which indicates that an increase in these parameters will surely cause a betterment in the ability of considered solar cells and vice versa. The measurements regarding the efficacy of a particular solar cell are performed under the incident power of 100 mW/cm² which almost equals irradiance value in relation with spectrum linked with AM 1.5. The efficiency of solar cell (η) gives information about the light conversion into electricity, photovoltaic parameters, and the generated power of DSSC.

1.12.6. Air Mass

The efficiency measurements of almost all solar cells are carried out under conditions of AM 1.5. These AM 1.5 conditions correspond to the incident radiation of 100 mW/cm²· and this irradiance of solar spectrum exists on a clear shiny and sunny day. AM 1 is the shortest distance that sunlight can cover through the atmosphere, and it happens when the sun is exactly above the head during midday. AM 1.5 condition means the sunlight can cover the distance through the atmosphere which is 1.5 times larger than that of AM 1 condition.

The air mass can be calculated using the formula below.

$$AM = \frac{1}{Cos\theta} \quad \dots\dots\dots\dots\dots\dots\dots\dots\dots\dots\dots (1.9)$$

Here θ is termed as angle of zenith and it has value of 48.2° for AM 1.5 and 0° for AM 1 conditions.
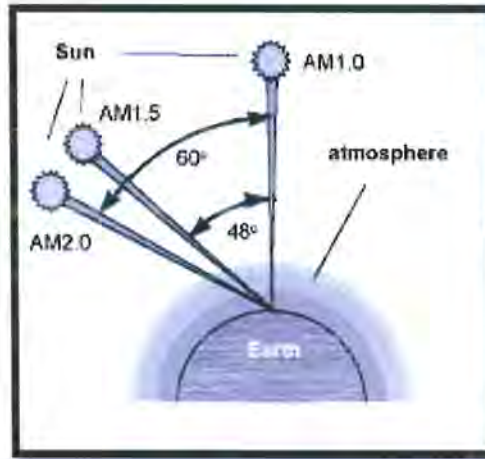
Figure 1.22. Air Mass.

1.12.7. Ohmic Resistances in Solar Cells

Ohmic resistances are of two types, one is series resistance and the other is shunt resistance. These resistances affect solar cell efficiency.

1.12.7.1. Series Resistance (Rs)

It is the resistance experienced by the electrons when they come across each other while passing through different component layers of the cell such as counter electrode, electrolyte etc. Or the resistance which is experienced because of interactions of electrons present at the interface of semiconductor material[63]. The voltage is decreased at much greater values which are in turn corresponding to resistance of series (R_s) and hence it does result in the fall of value related to the fill factor (FF).

1.12.7.2. Shunt Resistance (Rsh)

It is the resistance that appears at the donor-acceptor interface. The shunt resistance (R_{sh}) arises due to the current leakage because of recombination process at a certain junction of the cell which is p-n. The decrease in shunt resistance (R_{sh}) does cause a drop in FF as it does account for subsequent losses in our corresponding cells by making arrangement of an alternate route for required generation current.
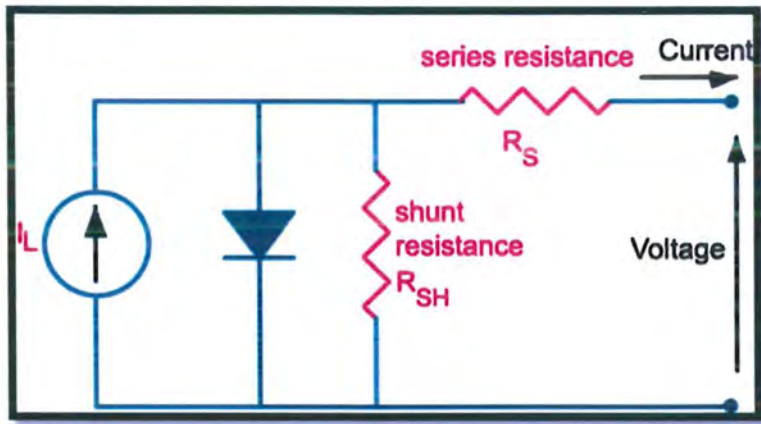
Figure 1.23. Impact of Series and Shunt resistance[64].

1.13. Literature Review

DSSCs prove to be an effective technology for future energy supplies. In contrast to the customary solar cells of silicon, DSSCs are generally customized at a much lower cost and provide substantial power conversion efficiency (PCE)[65]. Semiconducting metal oxide nanoparticles are well known to be used in catalysis, photodetectors, light emitting diodes, optoelectronics, and solar cells. Several wide band gap semiconductors are used in DSSCs[66]. The material performing the function of photoanode does play a significant part in deciding given efficiency of DSSCs as it becomes responsible for emission of electrons. As a result, significant effort has been put into developing innovative materials that have greater light absorption, high electron mobility, and a wide surface area for dye absorption. NiO is a large band gap p-type semiconductor material (E_g=3.17eV) due to which NiO turns out to be acceptable host material. NiO is a crucial cubic lattice structure transition metal oxide[67]. Due to its potential for usage in several applications, including magnetic materials, battery cathodes, electrochromic films, catalysis and gas sensors[68]. So far, it already has gained growing interest as reported by Khodair, ZT. et al[69]. Nanocrystalline NiO is anticipated to have much more superior qualities than the nickel oxide nanoparticles having size in range of micrometer and this becomes plausible owing to the macroscopic quantum tunnel effect, volume effect, the surface effect and the quantum size effect as studied by El-Kemary, M. et al[50].

The effective doping of transition metals such as Ag^{+2} and Zn^{+2} into NiO to change its electronic structure has been reported. By doping, the light harvesting efficiency of the devices have improved because it extends the absorption spectra into the visible region[70]. The material doped with metallic ions offers less electron-hole recombination as compared to the undoped NiO[71]. For performing the quick as well as efficient separation operation between holes and electrons, doping ions provide the sink. The band gap of NiO is either reduced or increased by the metal concentration. Through the use of diverse NiO-based materials and a variety of dyes, the total sunlight harvesting efficacy regarding our desired dye-sensitized solar cells has increased over time[72].

Farooq, M. et al. did report in their original work, the experimental preparation of NiO NPs by application of sol-gel technique and that too by making use of nickel nitrate hexahydrate as precursor salt[73]. NiO nanoparticles are thought to be simple to make by

substituting positive transition metals, such as Ag and Zn, to bring the absorption at longer wavelength region[74]. Al Boukhari, J. *et al.* did intentionally report fruitful preparation of NiO NPs whose doping has further been performed with the aid of metal ions specifically nickel oxide NPs being doped with zinc and further synthesized by a method taking into account co-precipitation at calcination temperature 550 °C[75].

Ghazal, S. *et al.* reported the effective formation of nickel oxide NPs further doped with silver through sol–gel preparation method and she did make use of $AgNO_3$ and Ni $(NO_3)_2 \cdot 6H_2O$ as a valuable origin for silver along with nickel. The materials that were prepared while considering above mentioned steps were further used as photoanode in DSSCs. The maximum efficiency of 1.50% was attained by photoanodes with an ideal metal content[76].

Using different dopants has increased current density, as reported by most studies, although a significant rise in the value regarding voltage (open circuit) has received less attention so far. The resulting difference that does arise in the values regarding the redox potential corresponding to electrolyte's materials and subsequent quasi fermi level referring to oxide of metal when exposed to light determines the open circuit potential[77]. So, in order to change the electrical structure of NiO. V_{oc} might be increased by elemental doping[78].

It is well-known that dye adsorbs on semiconductor's surface generates electrons, which are then transferred to photoanodes by semiconductor material. Therefore, attempts have been undertaken to increase the photo-conversion efficiency through improving light absorption, increasing electron-hole production, or expanding optical absorption into the visible spectrum[37].

The optical absorption is increased when Ru-based dyes are used as sensitizers, but their cost is very high[79]. To address the economic difficulties, research has been done on natural dyes, metal-free organic dyes, and metal complexes.

In recent years, cost-effectiveness has been increased by using various metal-based complexes and organic dyes. Kamil, A.F. *et al.* did report the inherent preparation of nanoparticles belonging to NiO with the aid of photo irradiation (photolysis)[80], the standard p-type semiconductor used as photoanode in p-DSSC. Cibacron brilliant red B is a synthetic dye that belongs to the azo dye family, was reported which was used as a photosensitizer for making an improvement in the efficiency of corresponding DSSCs[81].

Ansir, R. *et al.* reported utilization of an organic dye *i-e*; carminic acid as an effective sensitizer in dye-sensitized solar cells. Due to its strong anchoring groups and exceptional oxidation potential in the excited state, computational studies have demonstrated the effectiveness of carminic acid for performing the task of sensitizer in a recently developed dye-sensitized solar cells[82].

The DSSC manufacturing structure also plays a beneficial part in limiting the commercialization of these devices, furthermore, even after excepting the photoanode materials and sensitizers. Due to its instability and toxicity, liquid electrolyte I^-/I^-_3 usage results in a reduction in overall efficiency. The dye sensitized solar cells in solid state form , which does utilize polymers suitable for conduction of holes like P3HT and PEDOT: PSS as an electrolyte, are the solution to this issue[37].

The solid-state DSSCs have higher portability and durability than liquid state DSSCs, but they have much lower efficiency. The introduction of novel photoactive materials and specific dyes is a successful strategy for making a substantial rise in the activity of a given solid state DSSCs. The durability referring to solar cells has also been made sufficiently well by making the use of a certain solid-state electrolyte or a general quasi-solid electrolyte. To develop potential electrolytes for photochemical cells, Polymer blending is the best route.

The use of polymer gel electrolyte for DSSC was reported by Aram, E. *et al.* which contains PEO/PMMA. Using DSC, the temperature effect on ionic conductivity was studied. A significant increase in the stability of devices was observed[83].

To replace liquid electrolyte, the blended heterojunction of P3HT was used reported by Yue, Gentian. *et al.* It was shown that this blend not only increases stability but also increases solar spectrum absorption into the visible range. Using this electrolyte, a photo-conversion efficiency of 1.43% was obtained[84].

In DSSCs, for Titania films, the role of P3HT as an electrolyte was investigated by Lin, song. *et al.* The enhanced stability of devices was observed in the presence of P3HT electrolyte[85].

1.14. Aims and Objectives

The potential aims and objectives of following research work are to synthesize cost effective and highly efficient NiO based photoactive materials and then further utilization of these photoactive materials in heterojunction dye sensitized solar cell devices.

1.15. Work Plan

To achieve these aims the following work plan is adopted.

- To synthesize and characterize small band gap nanostructured photoactive material.
- To investigate the efficient functionalization of nanostructures with various organic dyes and the impact of various parameters on the photoconversion efficiency of DSSCs.
- To study the photovoltaic performance of photoactive materials by using solid state electrolyte.

Chapter 2: Experimental

2.1. Experimental

The following chapter contains information regarding utilized chemicals, followed experimental procedures, and characterization methods used to synthesize nanostructured materials. The optical, morphological, and structural properties of the as-synthesized materials were taken into consideration. Such properties are further discussed in the section that follows.

2.1.1. List of chemicals

The table lists the chemicals utilized in the synthesis.

Table 2.1. List of chemicals utilized for material synthesis.

Sr No.	Compound name	Chemical Formula	Molar mass (g/mol)	Percentage Purity	Supplier
1	Nickel Chloride Hexahydrate	$NiCl_2.6H_2O$	237.69	99.9%	Sigma Aldrich
2	Sodium Hydroxide	NaOH	39.99	>98.0%	Fish CHEM
3	Silver Nitrate	$AgNO_3$	169.87	97.8%	AnalaR
4	Zinc Nitrate	$Zn(NO_3)_2$		>97.0%	Sigma Aldrich
5	Carminic Acid	$C_{22}H_{20}O_{13}$	492.39	99.0%	Sigma Aldrich
6	Coomassie Violet R200	$C_{41}H_{44}N_3NaO_6S_2$	761.92	98.9%	Sigma Aldrich
7	Arsenazo III	$C_{22}H_{18}As_2N_4O_{14}S_2$	776.36	99.2%	Sigma Aldrich

2.2. Synthesis of Materials

The synthesis of NiO based nanoparticles has been done by adopting the Co-precipitation method.

2.2.1. Synthesis of pure NiO nanoparticles

The synthesis of pure and transition metals (Ag & Zn) doped nickel oxide NPs was done by using co-precipitation technique. Following pathway is adopted. 3.2g of nickel chloride hexahydrate was dissolved in 30ml of deionized water in a two neck round bottom flask. Magnetic stirrer was used for stirring the mixture for about 15 minutes for the complete dissociation of salt in the solvent. A green color solution was formed. Take 1g of sodium hydroxide in 25ml of deionized water and then dropwise transfer of this solution into the reaction mixture with the help of dropper along with constant magnetic stirring, precipitates begin to form. The stirring of the above reaction mixture is carried out for about 2 hours and kept for 24 hours. Green color precipitates of nickel oxide nanoparticles were settled at the bottom of flask. The obtained green color precipitates were then washed for a lot of times utilizing deionized water and ultimately dried by an oven at a temperature of 80°C overnight. The dried green color precipitates of nickel oxide nanoparticles were grinded into fine powder with the help of mortar and pestle and then calcined in furnace at 500°C for 3hours. The resultant black powder of nickel oxide nanoparticles was obtained[73].
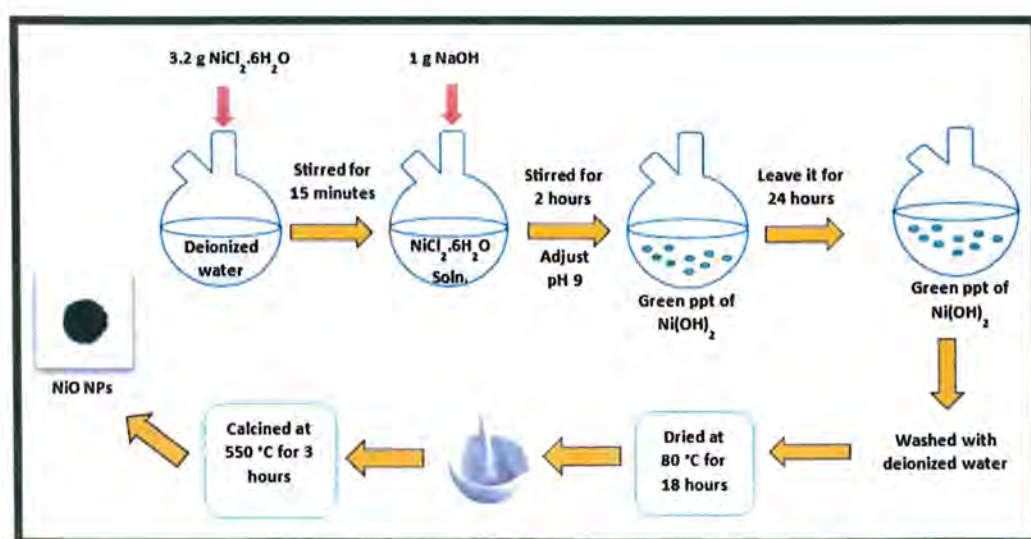
Figure 2.1. Schematic representation of NiO NPs synthesis.

2.2.2. Synthesis of transition metals (Ag & Zn) doped NiO NPs

- For Ag doped nickel oxide nanoparticles, weighted (1-6) percentages of silver nitrate in deionized water were added and stirring of resulting mixture was done well to get an almost homogenous kind of solution, transparent color of final solution was obtained. And for Zn doped nickel oxide nanoparticles, weighted (1-6) percentages of zinc nitrate in deionized water were added and again stirring was done to a good extent for attainment of a homogenous type of solution, again transparent color solution obtained.

- Then 3.2g of nickel chloride hexahydrate was added into the above-mentioned solution and stirring was continued for a time frame of about 20 minutes and subsequently repeat the above followed procedure. The resultant (1-6) % composition of both silver and zinc doped nickel oxide nanoparticles was formed.
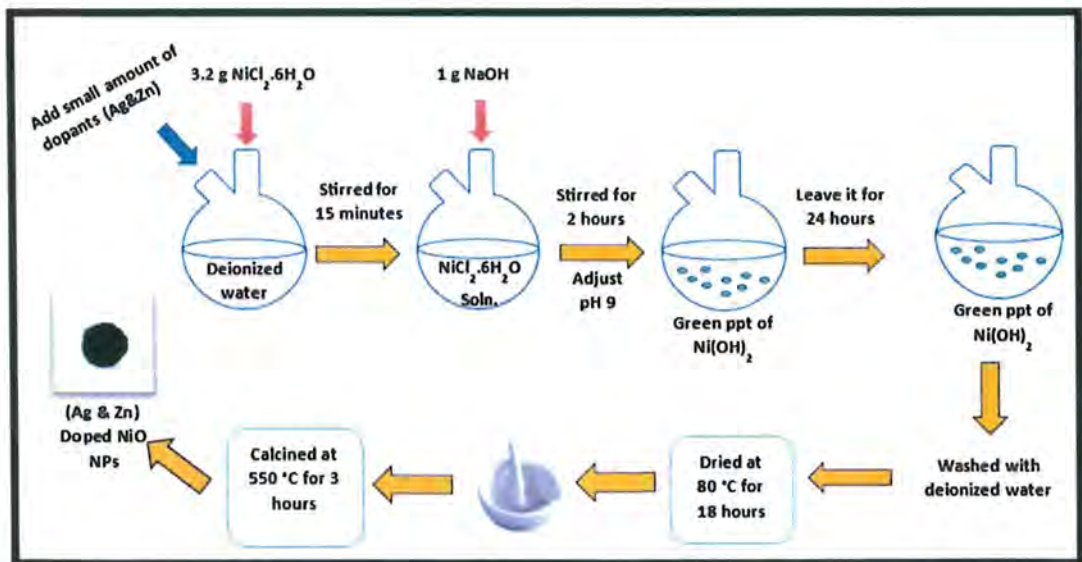
Figure 2.2. Schematic representation of transition metals (Ag &Zn) doped NiO NPs.

2.3. Functionalization (grafting) of dyes on pure and doped NiO NPs

2.3.1. Solution preparation for dyes (Carminic acid, Coomassie Violet R200, Arsenazo III)

To check the solubility, different solvents were used to prepare dye solutions. All the dyes stated above were completely soluble in deionized water. The preparation of various concentrations of Carminic acid, Coomassie Violet R200 and Aesenazo III ranging 5 μM to 70 μM was done, and the results were examined using UV-Visible spectroscopy.

2.3.2. Chemisorption of Carminic Acid, Coomassie Violet R200 and Arsenazo III on pure & doped NiO NPs

For the chemisorption of above-mentioned dyes on the surface of nanoparticles, following steps were followed:

In deionized water, 4 ml of 1 mg/ml solution of NiO NPs was prepared in glass vial. In the 2 ml of above NiO NPs solution, 4 ml of dye's solutions were added. For all the optimized concentrations *i-e*; 70 μM of Carminic acid, 30 μM of Coomassie violet R200 and 50 μM of Arsenazo III, the same composition was prepared as for above solution in separate glass vials. The solutions were stirred on a hot plate, the colors of the dyes altered, indicating chemisorption of the dyes onto the surface of the nanoparticles.

For Ag and Zn doped NiO NPs, the previously indicated procedure was repeated.
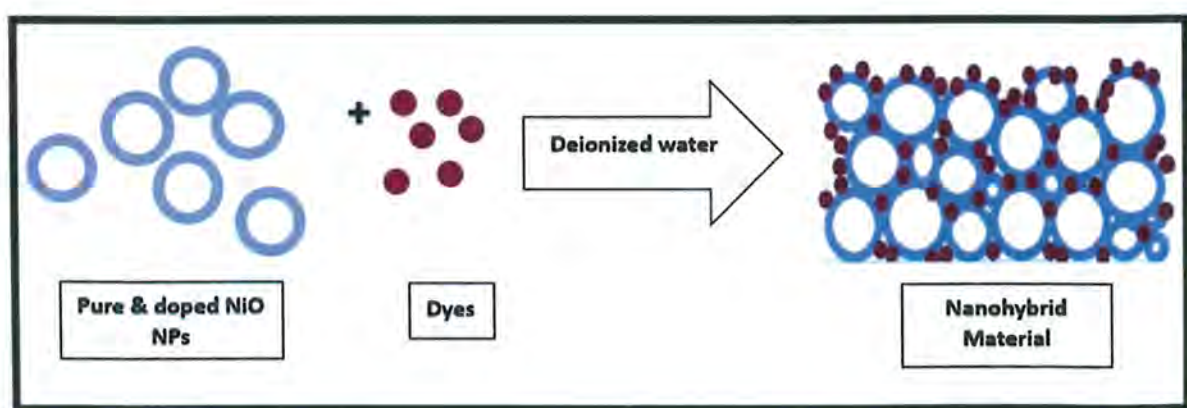
Figure 2.3. Photosensitization of pure and doped NiO NPs.

2.4. Fabrication of Solid-State Dye-Sensitized Solar Cell

The manufacturing of DSSCs involves the steps below.

2.4.1. Preparation of Active Layer of NiO and P3HT Solution

Step-by-step procedure was followed to serve the purpose of preparation of the solution.

For the formation of P3HT solution, 4 ml of chloroform was used to dissolve 80 mg of P3HT polymer. Then, in an atmosphere of argon, heat the above polymer solution at 60 °C for approximately 15 minutes. Consequently, a P3HT solution with a 20 mg/ml concentration was prepared. The active layer of grafted NiO NPs was created by mixing the polymer solution with the grafted NiO NPs solution in an equal volume. The doped NiO NPs' active layer was made using a similar procedure.

2.4.2. Substrate Treatment

As a substrate, sheets made of glass having dimensions nearly about 3 by 2 cm^2 while their thickness was kept around 80 nm. Indium tin oxide was then used to coat these sheets. The small piece of ITO was de-coated for an hour using HCL, but the leftover was covered with scotch tape. After removing the acid, it was dried overnight in an oven. After one day passed, the protective Scotch tapes were taken off, and the substrate was cleaned with the aid of acetone that took in environment of an ultrasonic bath[86]. It was then prepared for PEDOT: PSS spin coating.

2.4.3. PEDOT: PSS Spin Coating

A thin film consisting of polymer that is further of p-type. PEDOT: PSS deposited at the surface of ITO to smooth the substrate's surface and facilitates hole conduction towards the ITO. The deposition of polymer on substrate's surface was done by spin coating of thin layer of conducting polymer for 50 seconds at 5000 rpm speed at an acceleration of 7000 rpm/min after a little drop of the polymer was placed in the middle of the glass sheet[87]. Then, a small portion of PEDOT: PSS was de-coated by repeatedly washing with water. By spreading the polymer across a glass sheet owing to centripetal acceleration, uniform distribution of the polymer on the substrate's respective surface was made possible. The

ultimate substrate was subsequently annealed in an oven at 140 °C. Rotational speed, exhaust fumes, centripetal acceleration, etc. all affect the characteristics of a polymer film[88].

2.4.4. Active Layer Deposition

A hole conducting polymer P3HT and dyes (Carminic acid, Coomassie Violet R200 and Arsenazo III) sensitized pure/doped NiO nanoparticles blend with a ratio of 3:7 respectively was used as active material[89]. On a PEDOT: PSS-coated glass substrate, a thin film of this active substance was spin coated while spinning was done at two distinct speeds. At first, the spin coater's speed was maintained at 1500 rpm for 20 minutes, then it was lowered around 500 rpm. Repetitive spinning at 500 rpm was done to remove any leftover solvent to prevent the miscibility of the donor and accepter, which significantly decreased the efficiency of solar cells[88].

2.4.5. Cathode Deposition

Due to high conductivity of Pt and Al metals, Pt or Al coated ITO were used as a counter electrode[90]. Pt was deposited using a thermal metal evaporator under a highly vacuumed environment. Metal evaporator and cathodic contacts with a thickness of 80 nm were utilized for effective extraction of electrons from the external circuit[91]. After completing all processes of manufacture, the annealing of the respective device was carried out for a time frame of 15 minutes and that too at a temperature of 90 °C and this was allowed to take place in presence of regular flow of argon gas which in turn does account for a uniform as well continuous distribution of respective blend (active) which is in turn related to morphology of itself. Soon after getting done with annealing the corresponding cells were chilled under the regular flow of argon that too at the starting pint of the sintered tube made of glass for 15 minutes[88]. Thus, the dye sensitized bulk hetero-junction device was prepared for characterization.
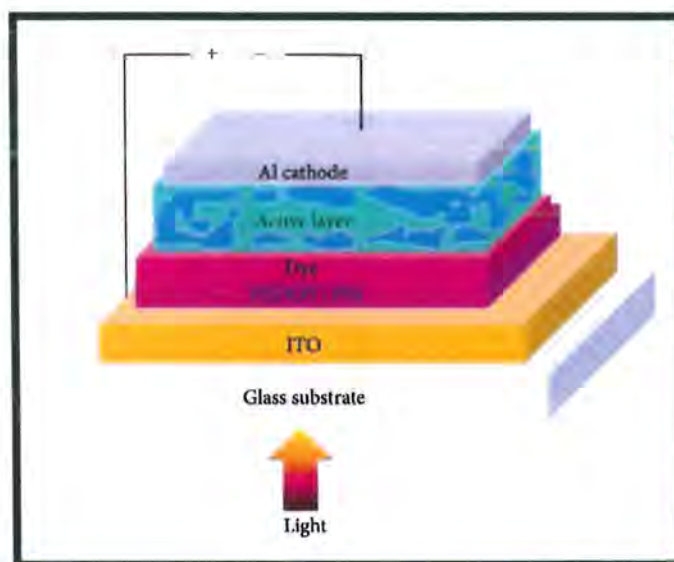
Figure 2.4. Construction of ssDSSC[88].

2.5. Characterization Techniques

The morphological, optical, and structural analysis of as-synthesized nanoparticles was done to check their potential for application in photovoltaic devices.

2.5.1. Structural Characterization

The structural analysis of synthesized material was done by using the following of all the available techniques related to characterization.

➢ X-ray Diffraction analysis (XRD)

➢ Fourier-transform infrared spectroscopy (FTIR)

2.5.1.1. X-ray Diffraction (XRD)

XRD in maximum cases is employed for the fruitful analysis of thin films as well as materials. The crystalline structure and purity of material was analyzed by using XRD. It is a highly sensitive analytical technique, and its efficiency depends upon the crystallinity of material. It is used for determining atomic arrangements in crystal and solid crystalline material structure. It may be utilized to give information about crystal defects, crystallinity, phases, and grain size. Information about morphology and optical properties of materials

may also be obtained[92]. The atoms of the crystalline substance which are under consideration diffract the incident x-rays into many directions. Size distribution function is used to characterize completely the particles having nonuniform sizes. However, in majority of methods, the average particle size is investigated[93].

0.2 mg of sample was used to assess pure and doped NiO NPs samples. PANalytical X-ray diffractometer model 3040/60 X'Pert PRO at an accelerating voltage and current was used. The samples were tested throughout a 2θ range from 20° to 80°. Debye Scherer's equation was used for the determination of crystallite size of pure and doped nickel oxide NPs.
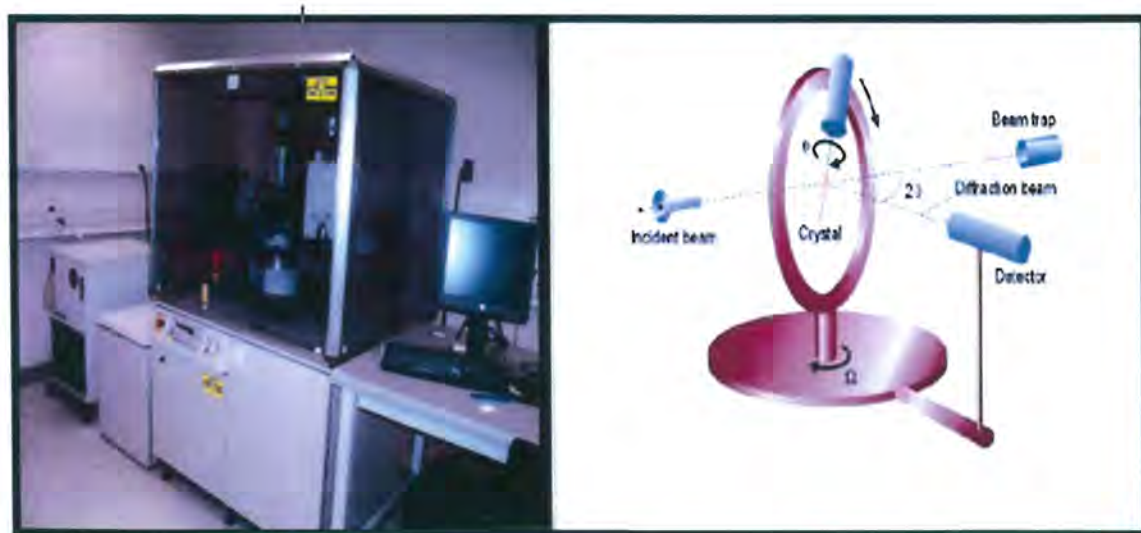
Figure 2.5. X-ray diffraction beam and schematic diagram of x-ray Diffraction Analysis[93].

2.5.1.2. Fourier Transform Infrared (FTIR) Spectroscopy

A corresponding spectrum of infrared radiations belonging to either emission or absorption of a gas, liquid, or solid can be obtained using the above mentioned method of spectroscopy (FTIR)[94]. A wide range of high-resolution spectral data is simultaneously collected by an FTIR spectrometer. In FTIR a beam of light with multiple frequencies shines at the sample at once, and its absorption is measured. To obtain FTIR spectrum IR radiations are passed through the sample.

The various kinds of compounds in the prepared samples, either organic or inorganic, are identified by FTIR analysis. The basic compositional structural information of the synthesized nanomaterials due to functional group specificity is obtained by FTIR spectra. Information about different vibrational bands of elements in the sample was also obtained. This technique also gives information about the purity of samples. This technique is used for quantitative analysis, and it is non-destructive.

The different kinds of peaks which represent different vibrational bands within the sample appeared in spectrum. The information about the nature of sample was given by peak's intensity[95].
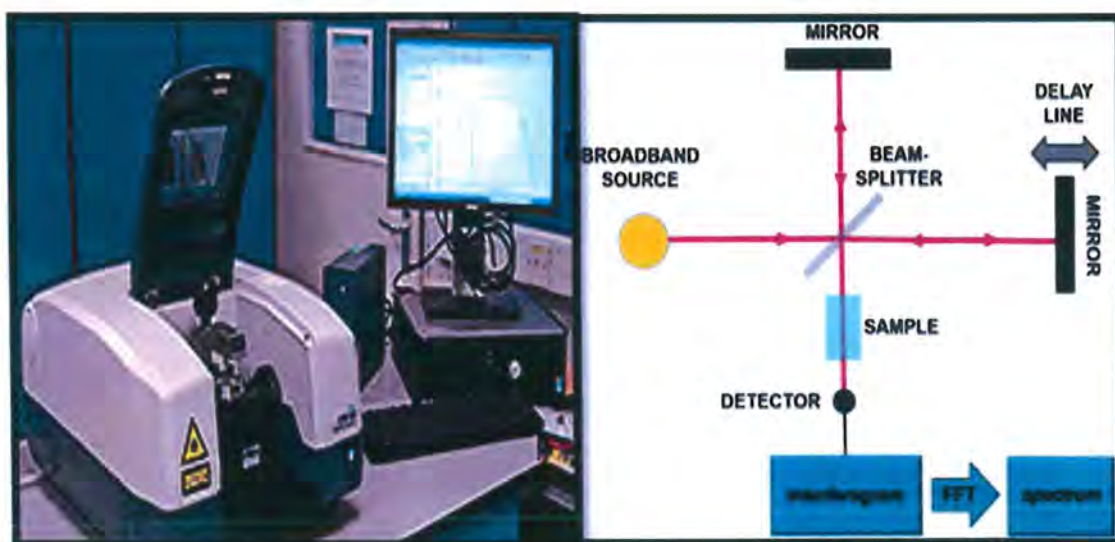
Figure 2.6. (a) FTIR machine (b) Schematic representation of FTIR[96].

2.5.2. Optical Analysis by UV-Visible Absorption Spectroscopy

There are various factors that do play their part in influencing the optical properties related with certain nanoparticles such as solvent polarity, surface charges, surface defects, surface ligands and imperfection of lattice.

UV-Visible is a fast and effective technique which can frequently by employed for studying the properties related to absorption of our concerned materials, where assessment of absorbance of the material does take place while only serving as wavelength's function. The general spectrometer has the ability of measurement of the concerned spectrum which

is solar between 200 to 800 nm where 200 to 400 nm corresponds to the UV region and 400 to 800 nm does refer to region of the spectrum(solar) that falls in visible region.

The transitions related to electrons to excited state (conduction band) taking place from ground state (valence band) can only be measured with the assistance of UV-Visible spectroscopy. Absorption taking place at a certain wavelength as well as the intensity of that absorption at each and every wavelength can be accurately and efficiently recorded by assistance of a UV-Visible spectrophotometer[97]. UV-Visible spectroscopy helps to determine nanoparticle geometry, nanoparticle aggregation state, and nanoparticle surface composition. Electronic spectroscopy or absorption spectroscopy are other names of ultraviolet-visible spectroscopy. The resultant spectra are termed absorption spectra.

The relationship between absorption spectra and bandgap energy is reported by Tauc's expression which is reported as:

$$\alpha h\nu = A(h\nu - E_g)^n \dots\dots\dots\dots\dots\dots\dots\dots\dots\dots\dots (2.1)$$

Where "h" does denote plank's constant, while "v" is a representation of the frequency of the concerned photon, α does express absorbance, "A" represents a specific constant, and "E_g" is energy of the band gap.
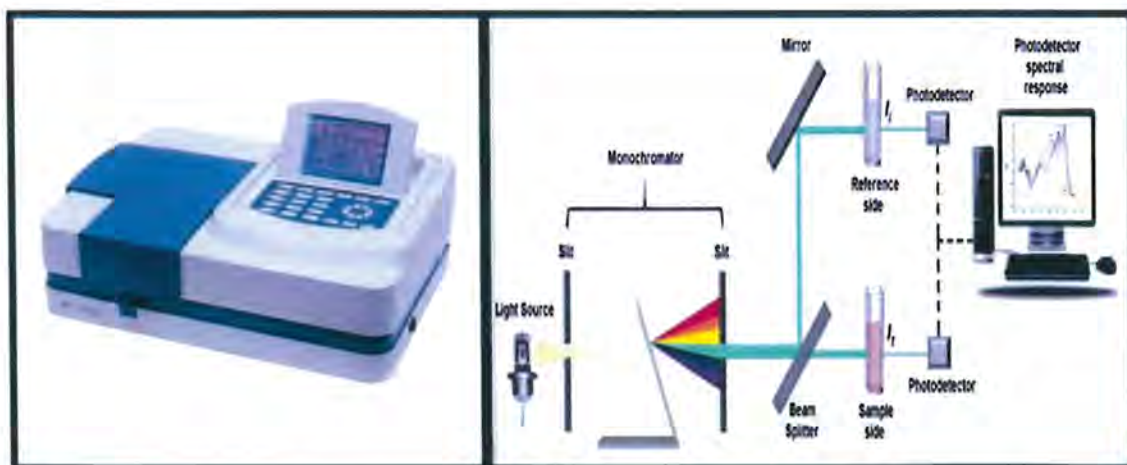
Figure 2.7. (a) UV-Vis double beam spectrophotometer (b) Working principle of UV-Vis spectrophotometer[98].

2.5.3. Morphological and Elemental Characterization

These characterization techniques are:

> Scanning electron microscopy (SEM)
> Energy dispersive X-rays spectroscopy (EDX)

2.5.3.1. Scanning Electron Microscopy (SEM)

A continuous beam of electrons having a large amount of energy, which is generally generated by a desirable source which normally tends to be an emission gun (field), or filament made of tungsten, does provide the basis for a certain scanning electron microscope which tends to be most effective tool for maximization or magnification. The SEM does make use of electrons instead of light for the purpose of generation of a three-dimensional image that too resolved to a greater extent of a given specimen that is usually in form of solid.

By considering the above-mentioned method, detailed set of information based on phase distribution, external morphology also known as topography, composition, and crystalline structure, that too are dependent on extensive magnification area, can be easily obtained. Information about porosity, particle size and homogeneity of sample can also be assessed by this technique.

The production of an electronic beam takes place whenever a filament made of metal is subjected to strong heat. The travel path of electronic beam is usually a vertical one and it finally permits the beam to go through the column of respective microscope. The corresponding beam then goes by the lenses (electromagnetic) whose function is to provide the focus to beam and eventually, pointing it downward towards the sample. After its collision with the sample, both backscattered as well as secondary electrons' emission from respective sample does occur. In the creation of material's SEM image, photons or distinctive x-rays are also collected. The specified region at which the electron beams collide with the sample is known as the "interaction volume" region, which generates a variety of signals. Since the creation of x-rays by electron contact does not result in volume damage, it is a non-destructive technique. The signals are collected by a cathode ray detector tube. Strong signal-producing regions of the sample appear to be brighter.
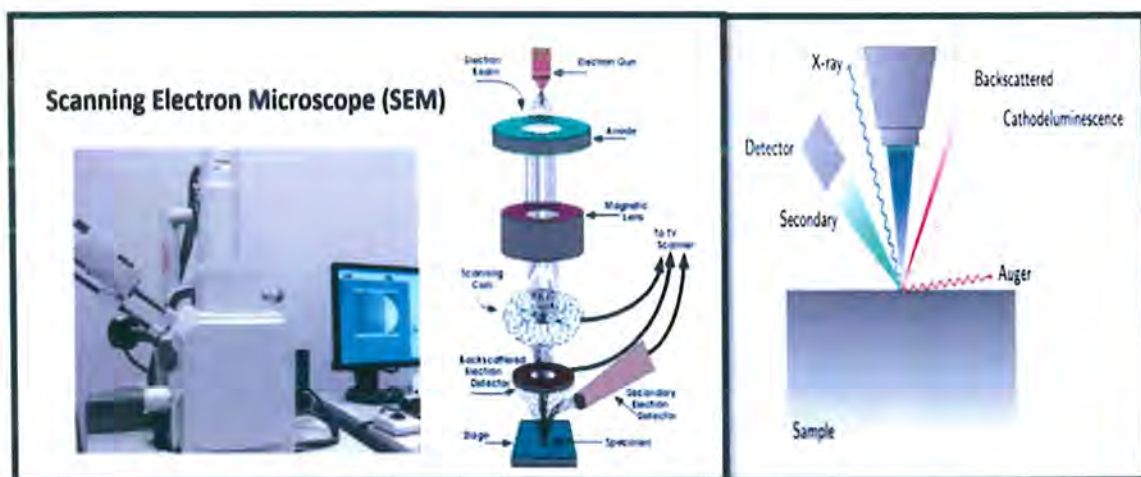
Figure 2.8. (a) SEM machine and its (b)working principle[99].

2.5.3.2. Energy Dispersive X-ray (EDX) Spectroscopy

EDX is one other fundamental technique utilized for analysis, which is pretty much useful in determination of the chemical as well as elemental composition of the material with X-rays. This is based on the interaction of the material with X-rays. One important aspect of EDX characterization capabilities is the foremost idea that each element does own a unique structure of its atoms that allows for only a singular peaks' set on the emission spectrum related to X-ray of itself. A specific stream of protons, x-rays, or electrons withholding a high intensity is forced to target the adjacent sample regarding production of X-rays of the given specimen having certain extraordinary features. A hole is left behind when the electron from an inner shell is knocked out by the specified beam, and an electron from the adjacent highly energetic shell jumps into it to fill the gap. X-rays are produced because of the difference in the energies of shell. With the aid of spectrometer working on the principle of energy dispersion, the quantity along with energy of these X-rays, whose emission is taking place, is estimated. The chemical composition and the presence of the desired components are both confirmed by EDX.
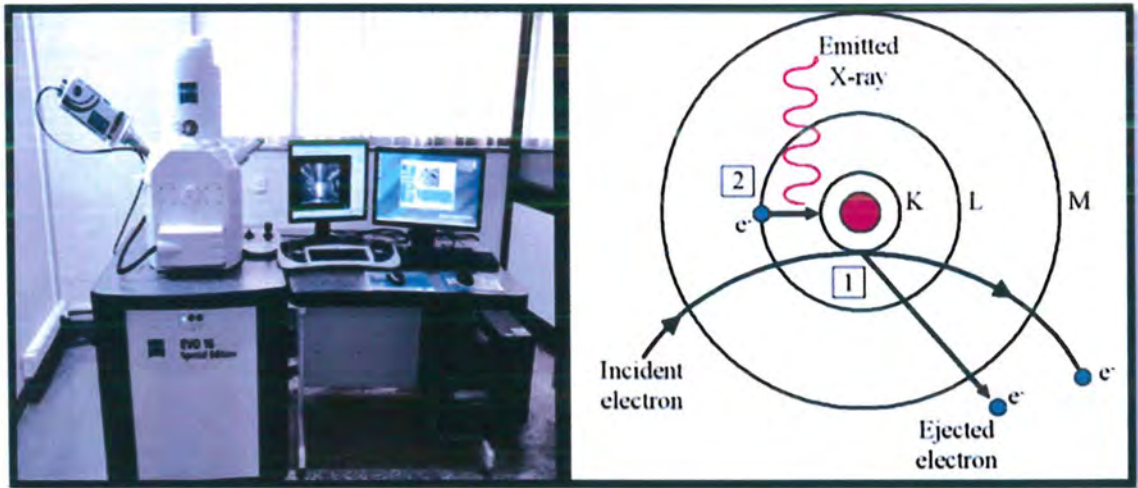
Figure 2.9. (a) EDX machine (b) working principle of EDX[100].

Chapter 3: Results and Discussion

Undoped Nickel oxide nanoparticles along with the ones which did use Ag and Zn as dopant were more specifically prepared by employment of technique of co-precipitation. There are various characterization techniques that were applied to these nanoparticles to check their purity, morphology, crystallinity, and optical behavior. The dye which does act as sensitizer was adsorbed on the surface of nanoparticles because of which the optical properties of these materials were increased, and they were successfully used as photoanode in the fabrication of desired solar cells.

3.1. Morphological and Optical Properties belonging to Pure NiO and (Ag & Zn) Doped NiO NPs

The following approaches were used to investigate the structural, morphological, and optical characteristics of pure and doped NiO nanoparticles.

- ➤ UV-Visible Spectroscopy (UV-Vis)
- ➤ X-ray Diffraction (XRD)
- ➤ Scanning Electron Microscopy (SEM)
- ➤ Energy Dispersive X-rays (EDX)
- ➤ Fourier Transforms Infrared Spectroscopy (FTIR)

3.2. Optical Studies

3.2.1. UV-Visible Spectrum of Pure NiO NPs

The absorption spectrum resulting from interaction of pure NiO NPs with light is shown in figure (3.1). NiO absorbs light in UV regions of the solar spectrum. The as-synthesized NiO nanoparticles possess a strong maximum absorption peak at 317nm.
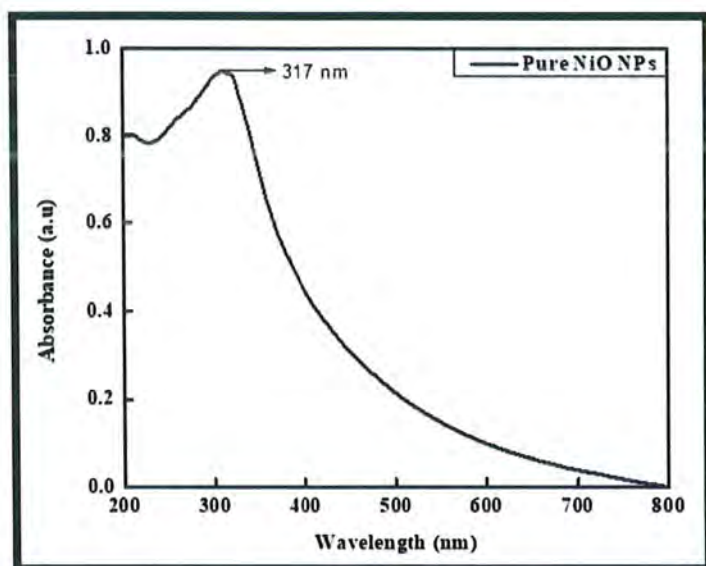
Figure 3.1. UV-Visible absorption spectrum of pure NiO NPs.

3.2.1.1. Band Gap of Pure NiO NPs

Figure (3.2) shows the relevant band gap of pure NiO, obtained from UV-Visible spectroscopy by using tauc plot. Tauc plot is obtained from equation $(\alpha h\nu)^2 = A(h\nu - E_g)^n$. The E_g value was obtained by drawing tangent on graph. The obtained E_g value of NiO is 3.17 eV.
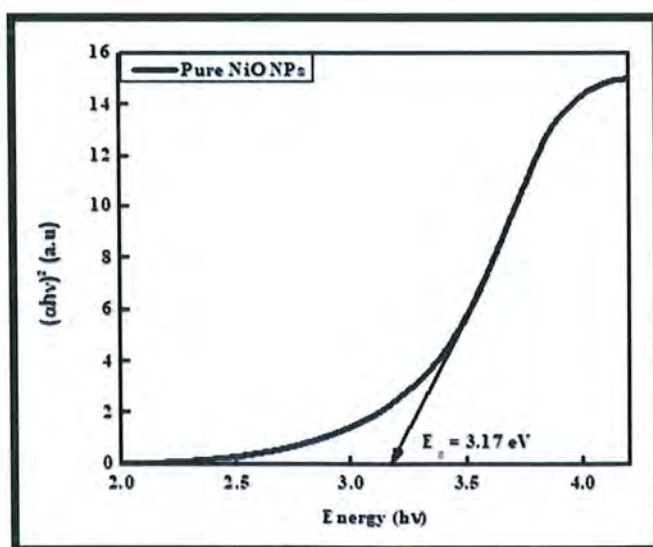
Figure 3.2. Tauc plot of Pure NiO NPs.

3.2.2. UV-Visible Spectrum of Ag doped NiO NPs

The absorption spectrum of Ag doped NiO nanoparticles is shown in figure (3.3). It shows that by the addition of weight percentages (1 to 6%) of Ag dopant in NiO nanoparticles, the absorption peak was further shifted to higher wavelength region from 317 nm to 348 nm (Red shift), which shows that the crystallite size of nanoparticles has been increased[101].

The Ag doped NiO nanoparticles could absorb light in higher wavelength regions, because by adding the Ag transition metal as an impurity the band gap of doped nanoparticles reduced according to this relation.

$$E = \frac{hc}{\lambda} \quad .... \quad (3.1)$$

Figure 3.3. UV-Visible absorption spectra of Ag doped NiO NPs.

3.2.2.1. Band Gap of Ag doped NiO NPs

Figure (3.4) shows the relevant band gaps of Ag doped NiO obtained from UV-Visible spectroscopy by using Tauc's plots. The E_g value of pure NiO is 3.17 eV which tends to decrease regularly by increasing the concentration of Ag dopant. For Ag-NiO NPs, Tauc's plots show tuning in band gap from 3.17-2.10 eV.

Figure 3.4. Tauc's plots of **(a)** 1% Ag-NiO **(b)** 3% Ag-NiO **(c)** 5% Ag-NiO.

Table 3.1. Band gaps of prepared Ag-NiO samples.

Sr No.	Nanoparticles	Band gap (eV)
1	Pure NiO	3.17
2	1% Ag-NiO	2.55
3	3%Ag-NiO	2.33
4	5%Ag-NiO	2.10

Table (3.1) shows tuned band gaps for all Ag doped NiO NPs. The bandgap of NiO NPs is reduced by incorporating Ag dopant having narrow bandgap due to which it

62

generates impurity energy levels above the valence band edge. Consequently, less energy is needed to excite charge carriers, lowering the optical bandgap. Also the existence of a direct optical transition, an increase in grain size, and the presence of single phase may be responsible for the increase in absorbance with an increase in the Ag concentration[102].

3.2.3. UV-Visible Spectrum of Zn doped NiO Nps

The absorption spectrum of Zn doped NiO nanoparticles is shown in figure (3.5). It shows that by the addition of weight percentages (1 to 6%) of Zn dopant in NiO nanoparticles, the absorption peak was further shifted to higher wavelength region from 317 nm to 341 nm (Red shift), which shows that the crystallite size of nanoparticles has been increased[103].

The Zn doped NiO nanoparticles could absorb light in higher wavelength regions, because by adding the Zn transition metal as an impurity the band gap of doped nanoparticles reduced according to this relation.

$$E = \frac{hc}{\lambda}$$ .... (3.1)
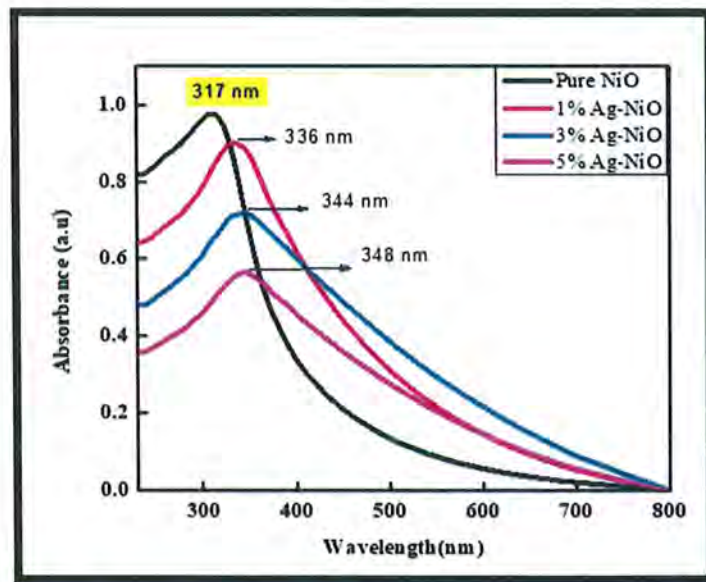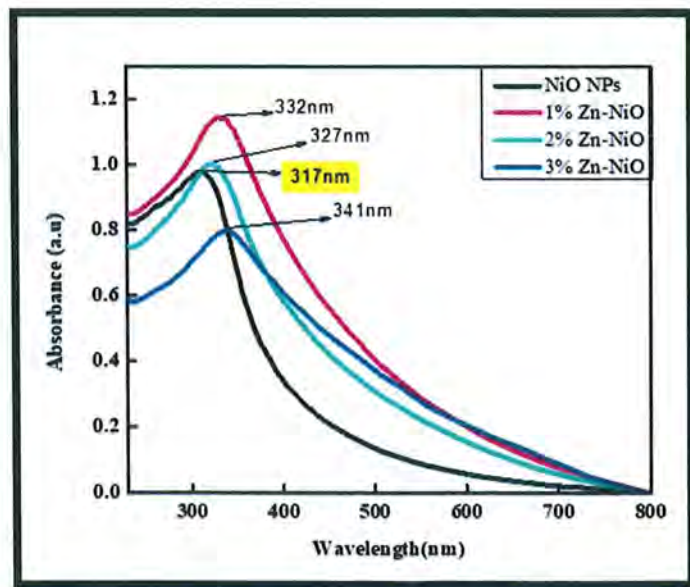

Figure 3.5. UV-Visible absorption spectra of Zn doped NiO NPs.

3.2.3.1. Band Gap of Zn doped NiO NPs

Figure (3.6) shows the relevant band gaps of Zn doped NiO obtained from UV-Visible spectroscopy by using Tauc's plots. The E_g value of pure NiO is 3.17 eV which tends to decrease regularly by increasing the concentration of Zn dopant. For Zn-NiO NPs, Tauc's plots show tuning in band gap from 3.17-2.00 eV.
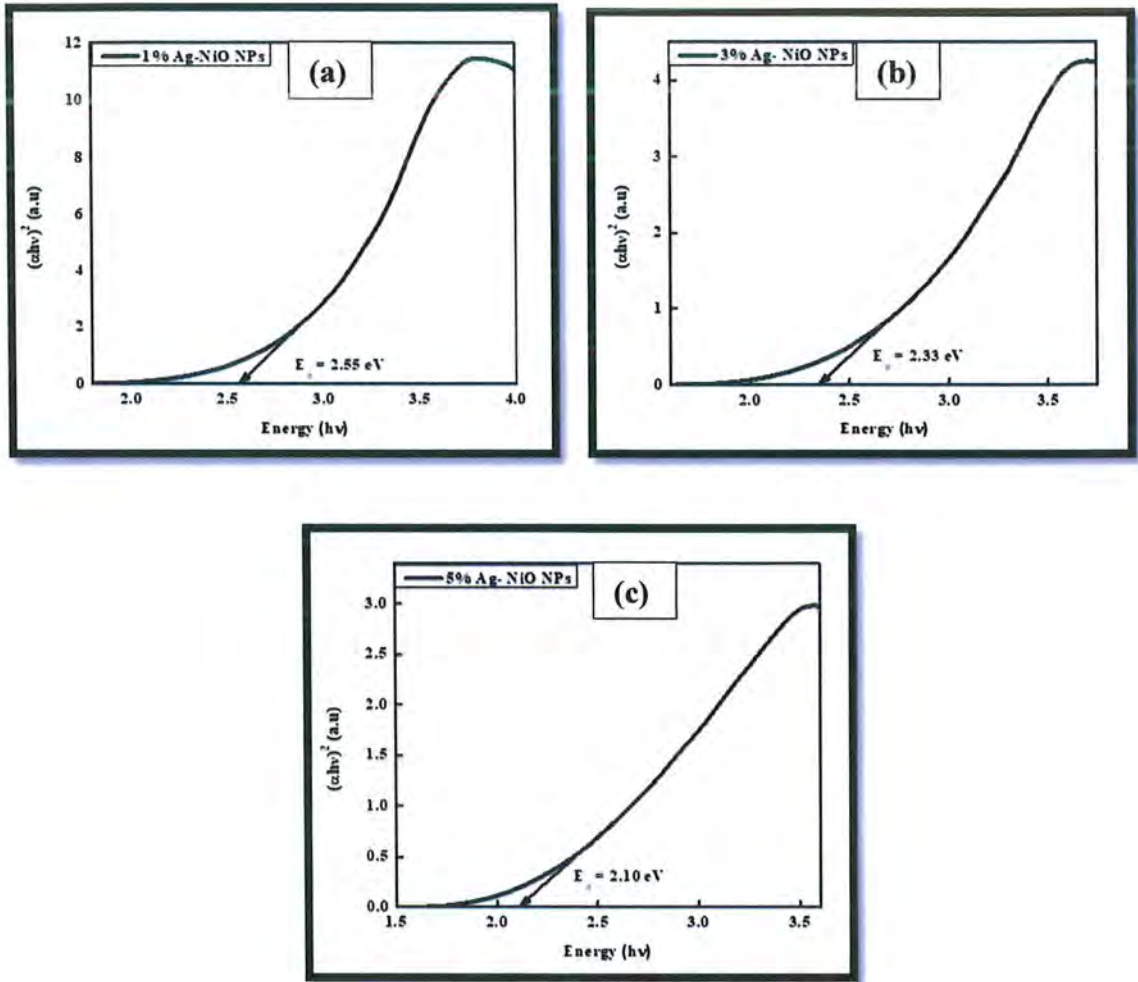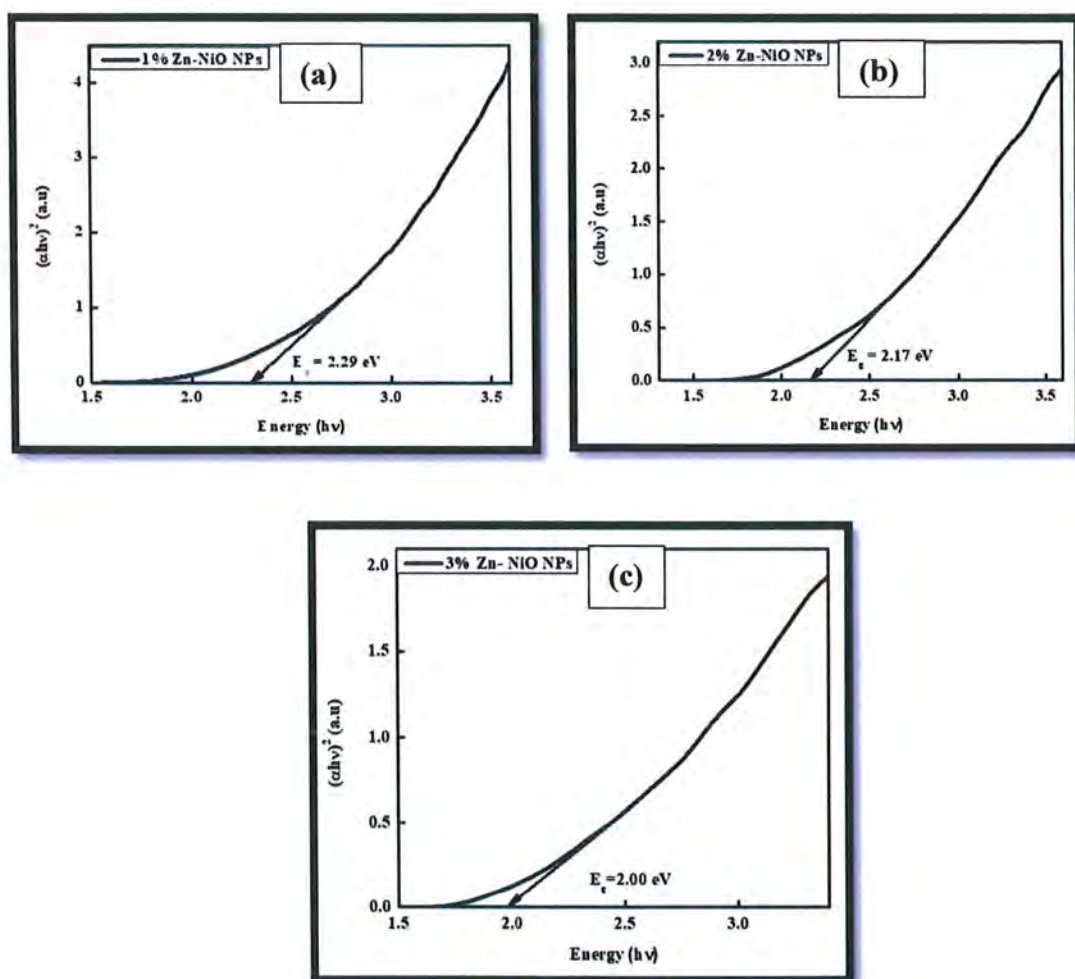

Figure 3.6. Tauc's plots of **(a)** 1% Zn-NiO **(b)** 2% Zn-NiO **(c)** 3% Zn-NiO.

Table 3.2. Band gaps of prepared Zn-NiO samples.

Sr No.	Nanoparticles	Band gap (eV)
1	Pure NiO	3.17
2	1% Zn-NiO	2.29
3	2% Zn-NiO	2.17
4	3% Zn-NiO	2.00

Table (3.2) shows tuned band gaps for all Zn doped NiO NPs. The bandgap of NiO NPs is reduced by incorporating Zn dopant[104]. In a NiO semiconductor material, the concentration of free carriers is raised because of Zn doping due to which the separation distance of an electron-hole pair will become smaller as a result band gap decreases[105]. Consequently, less energy is needed to excite charge carriers, lowering the optical bandgap.

3.3. XRD Studies

3.3.1. XRD Pattern of Pure NiO NPs

To observe the subsequent structure, size, and crystallinity of NiO Nanoparticles, these were subjected to X-ray diffraction (powdered technique). The resulting XRD pattern of pure NiO nanoparticles in the following figure (3.6) shows (111), (200), (220), (311), crystallographic planes respectively which corresponds to the detected diffraction peaks at 2θ values of 37°, 43°, 63°, 75°[106]. The XRD pattern confirms the high crystallinity and face centered cubic structure (fcc) of NiO NPs as reported in standard reference card (JCPDS Card No. 073-1523). The average crystallite size of NiO NPs calculated by using Debye Scherrer's equation ($D = K\lambda/\beta cos\theta$) is 28.73 nm.
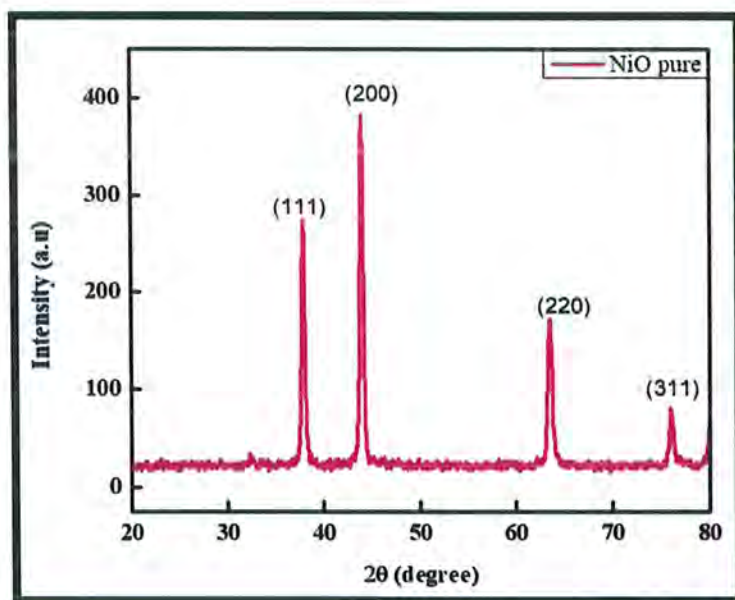
Figure 3.7. XRD pattern of pure NiO NPs.

3.3.2. XRD Pattern of Ag doped NiO NPs

Figure (3.8) shows the resulting pattern of XRD of Ag doped NiO NPs, which clearly shows that upon doping there were no additional peaks found representing the purity of nanoparticles, it means that Ag^{+2} and Ni^{+2} ions are uniformly homogenized and Ag ion successfully replaced Ni ion without distorting its face centered cubic crystal structure and the sample remains in single phase. Also, there was a slight broadening of peaks observed at higher concentrations along with shifting towards lower 2θ upon doping with Ag. This may be due to unequal ionic radii of both ions Ni^{+2} (0.69Å) and Ag^{+1} (1.15Å) due to which lattice dislocations occur and micro strain produced, and peaks shifts towards lower 2θ[102]. The information about the crystallinity of sample was also obtained that gradually decreases with the increase in dopant concentration.
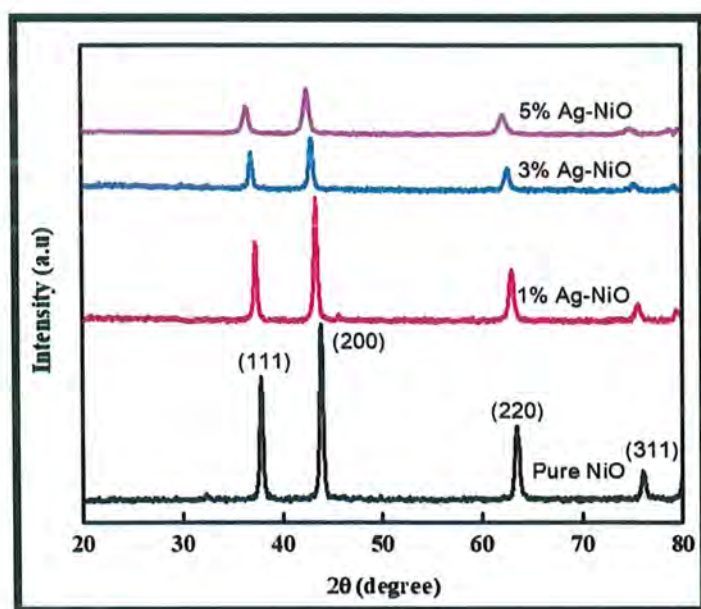
Figure 3.8. XRD pattern of pure NiO and (1,3,5%) Ag doped NiO NPs.

3.3.2.1. Average Crystallite Size of Ag doped NiO NPs

Using Debye Scherrer's formula, the average crystallite sizes of Ag doped NiO NPs can be calculated.

$$D = K\lambda/\beta cos\theta \quad\text{................................} (3.2)$$

Here,

"**D**" is defined as average crystallite, while "**λ**" does imply the X-ray's wavelength which is (1.54 Å), "**β**" does stand for full-widths-at-half-maximum (FWHM) and is taken in units of radian, and "**θ**" does denote the Bragg's angle taken in degree and "**K**" does represent a specific dimensionless shape factor and its value equals 0.9.

Table 3.3. Crystallite size of pure and Ag-NiO NPs.

Sr No.	Materials	Crystallite size (nm)
1	Pure NiO	28.73
2	1% Ag-NiO	28.90
3	3% Ag-NiO	30.65
4	5% Ag-NiO	31.40

Table (3.3) shows that with the increase in dopant's concentration, the crystallite size of NiO lattice also tends to increase which may be due to increased lattice parameters of NiO crystal upon doping with Ag.

3.3.3. XRD Pattern of Zn doped NiO NPs

Figure (3.9) shows that upon doping of Zn in NiO, no impurity peaks were found also it shows a single crystalline phase, confirming that Zn and Ni ions are equally dispersed and successful replacement of Ni ions by Zn ions without violating its face centered cubic crystal structure. The stable crystal structure on Zn doping shows that the Zn ion was incorporated as a substitution ion. Also, a slight shift in peaks towards lower 2θ was observed which may be due to unequal ionic radii of both ions due to which lattice dislocations occur and micro strain produced[107]. The ionic radii of Zn^{+2} is (0.74Å) which is slightly large as compared to ionic radii of Ni^{+2} (0.69Å). The regular increase in the intensity of peaks was observed that gives information about crystallinity of sample.
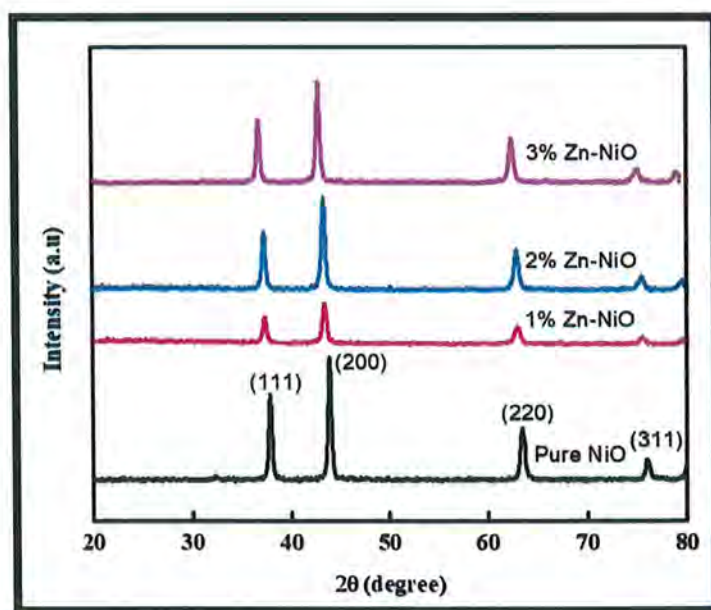
Figure 3.9. XRD pattern of pure NiO and (1,2,3%) Zn doped NiO NPs.

3.3.3.1. Average Crystallite Size of Zn doped NiO NPs

The average crystallite sizes of Zn doped NiO NPs can be calculated by using Debye Scherrer's formula.

$$D = K\lambda/\beta cos\theta \dots\dots\dots\dots\dots (3.2)$$

Here,

"D" is defined as average crystallite, while "λ" does imply the X-ray's wavelength which is (1.54 Å), "β" does stand for full-widths-at-half-maximum (FWHM) and is taken in units of radian, and "θ" does denote the Bragg's angle taken in degree and "K" does represent a specific dimensionless shape factor and its value equals 0.9.

Table 3.4. Crystallite size of pure and Zn-NiO NPs

Sr No.	Materials	Crystallite size (nm)
1	Pure NiO	28.73
2	1% Zn-NiO	28.89
3	2% Zn-NiO	29.01
4	3% Zn-NiO	29.54

Table (3.4) shows that with the increase in dopant's concentration, the crystallite size of NiO lattice also tends to increase which may be due to increased lattice parameters of NiO crystal upon doping with Zn.

3.4. FTIR Analysis

3.4.1. FTIR Spectrum of Pure NiO NPs

To investigate various functional groups and the purity of samples FTIR analysis was done. The FTIR spectra was investigated in area of wavenumber ranging from 500 to 4000 cm⁻¹. In the FTIR spectra of pure NiO as shown in figure (3.10), a broad peak located in the region of 3690-3100 cm⁻¹ is specifically allocated to stretching vibrations of O-H of water molecule as little it remained adsorbed at the surface of nanoparticles during washing of product. An additional peak appears in graph at 2359 cm⁻¹ which shows stretching

vibrations due to CO_2 which may be incorporated from air[108]. Below 1000 cm^{-1} at the certain area of graph at 668 cm^{-1}, a peak associated with the stretching vibration of Ni-O bond also exists[108].
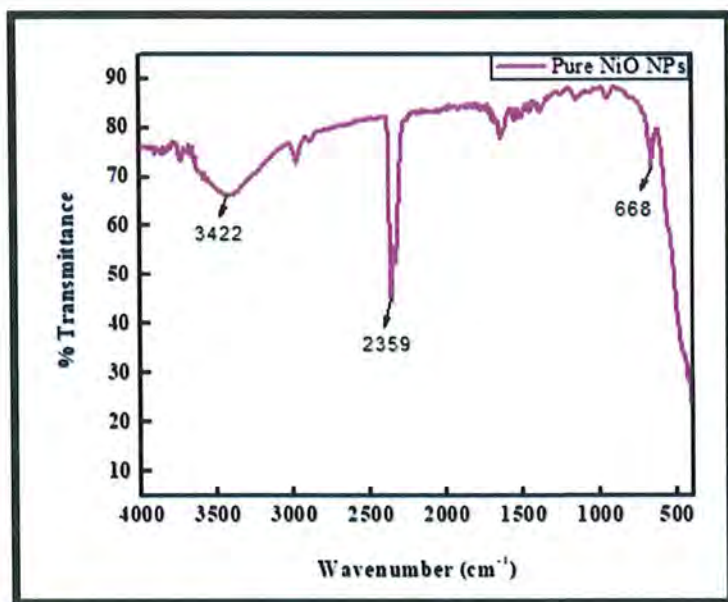
Figure 3.10. FTIR spectra of Pure NiO NPs.

Table 3.5. FTIR peaks of pure NiO NPs and their corresponding functional groups.

Sr No.	Wavenumber (cm^{-1})	Functional Group
1	3690-3100	O-H stretching of water
2	2359	CO_2 stretching
4	668	Ni-O stretching

3.4.2. FTIR Spectrum of Ag doped NiO NPs

Figure (3.11) shows the FTIR spectra of Ag doped NiO NPs. FTIR spectrum shows that for all Ag doped samples all the vibrations are similar to pure NiO except a new peak appears at 1126 cm^{-1} due to doping which was attributed to C-N symmetrical stretching[109].
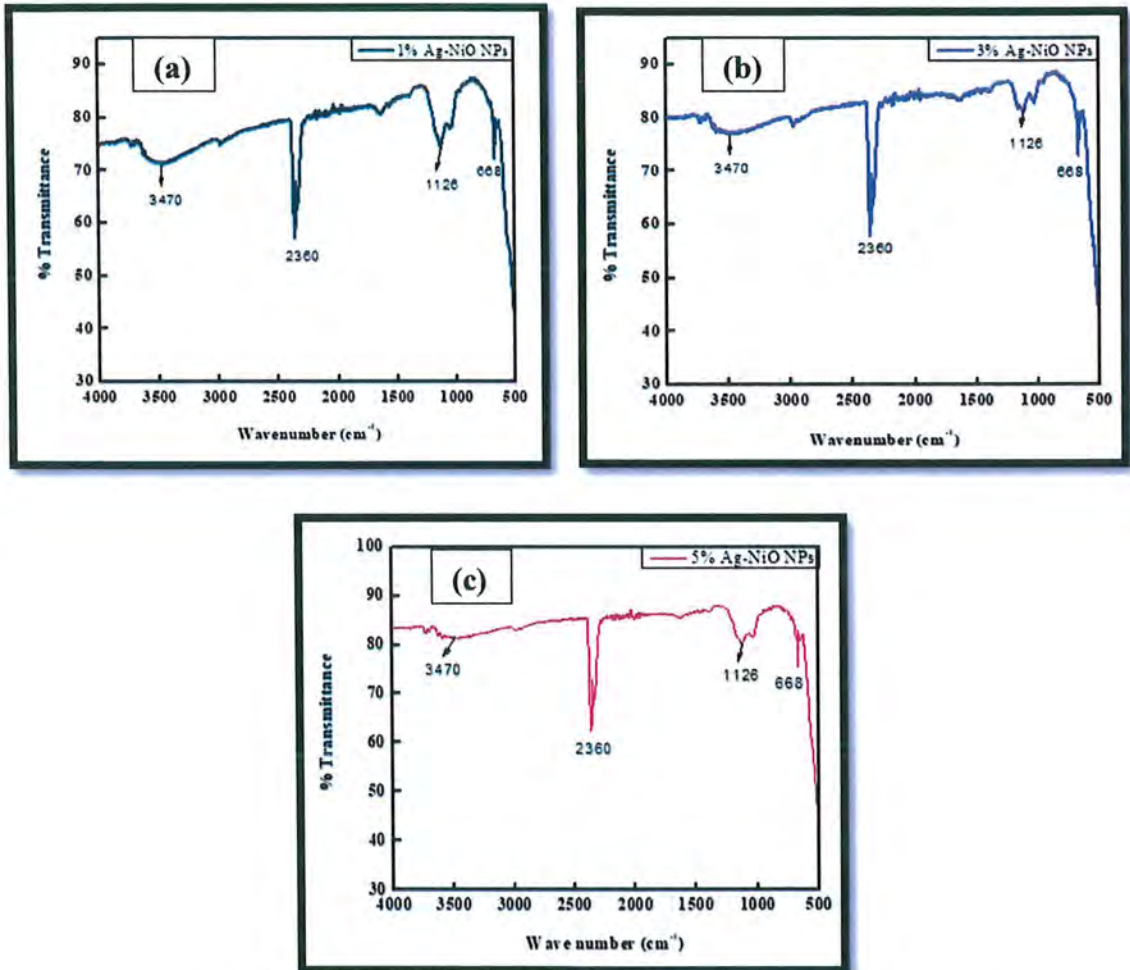
Figure 3.11. FTIR spectra of **(a)** 1% Ag-NiO **(b)** 3% Ag-NiO **(c)** 5% Ag-NiO.

3.4.3. FTIR Spectrum of Zn doped NiO NPs

Figure (3.12) shows the FTIR spectrum of Zn doped NiO NPs. FTIR spectrum reveals that for all Zn doped samples all the vibrations are similar to pure NiO except two close peaks appear in the range of 1300-1000 cm^{-1} due to doping which may be attributed to C-O stretching vibrations[75].
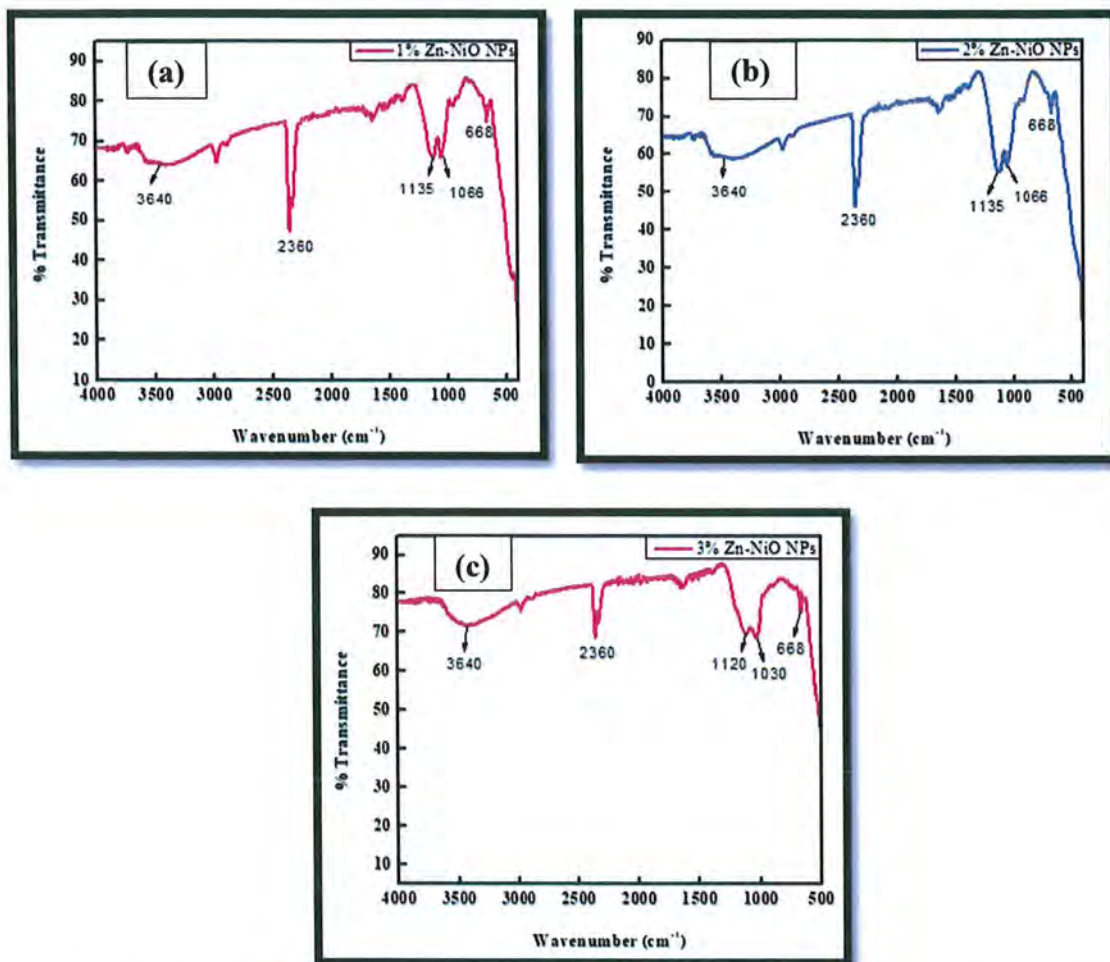
Figure 3.12. FTIR spectra of **(a)** 1% Zn-NiO **(b)** 2% Zn-NiO **(c)** 3% Zn-NiO.

3.5. SEM Analysis

3.5.1. SEM Images of Pure and Doped (Ag & Zn) NiO NPs

SEM (Scanning Electron Microscopy) was used to study the morphological changes that occurred in nanoparticles. This technique is basically used for surface studies

of material. Surface morphology revealed that due to the surface-active nature of nanoparticles, both pure and doped (Ag & Zn) NiO nanoparticles existed in agglomerated form. Figure (3.13), (3.14), and (3.15) shows spherical morphologies of both pure and doped (Ag & Zn) nanoparticles, this is because both pure and doped NPs were calcined under same temperature condition (550 °C). SEM scans reveals that the material was made up of agglomerated, non-uniform, irregular structures[110].
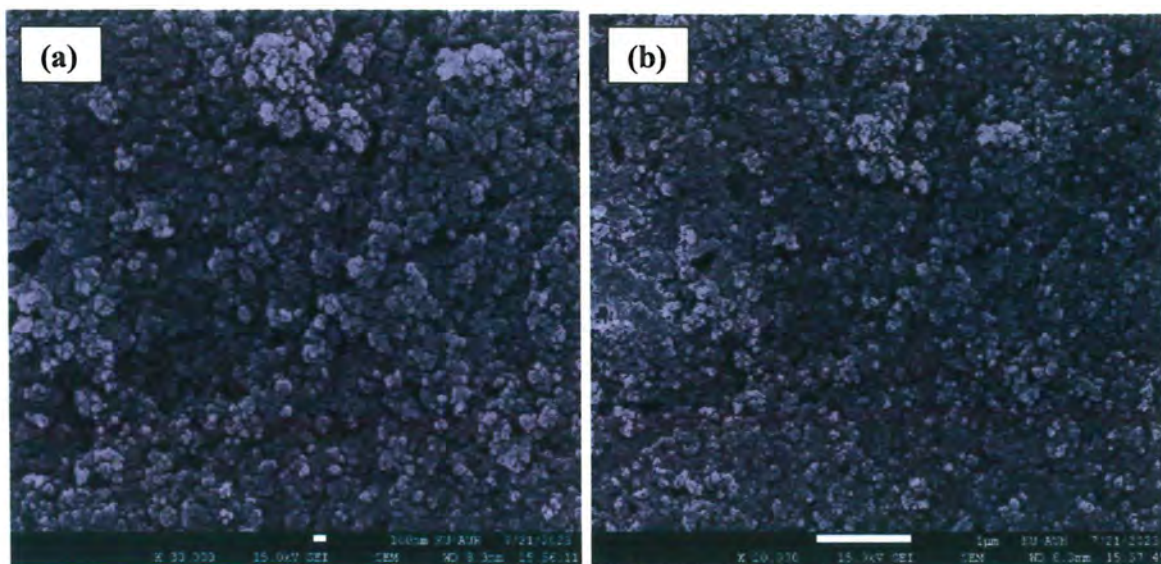
Figure 3.13. (a),(b) SEM images of Pure NiO NPs.
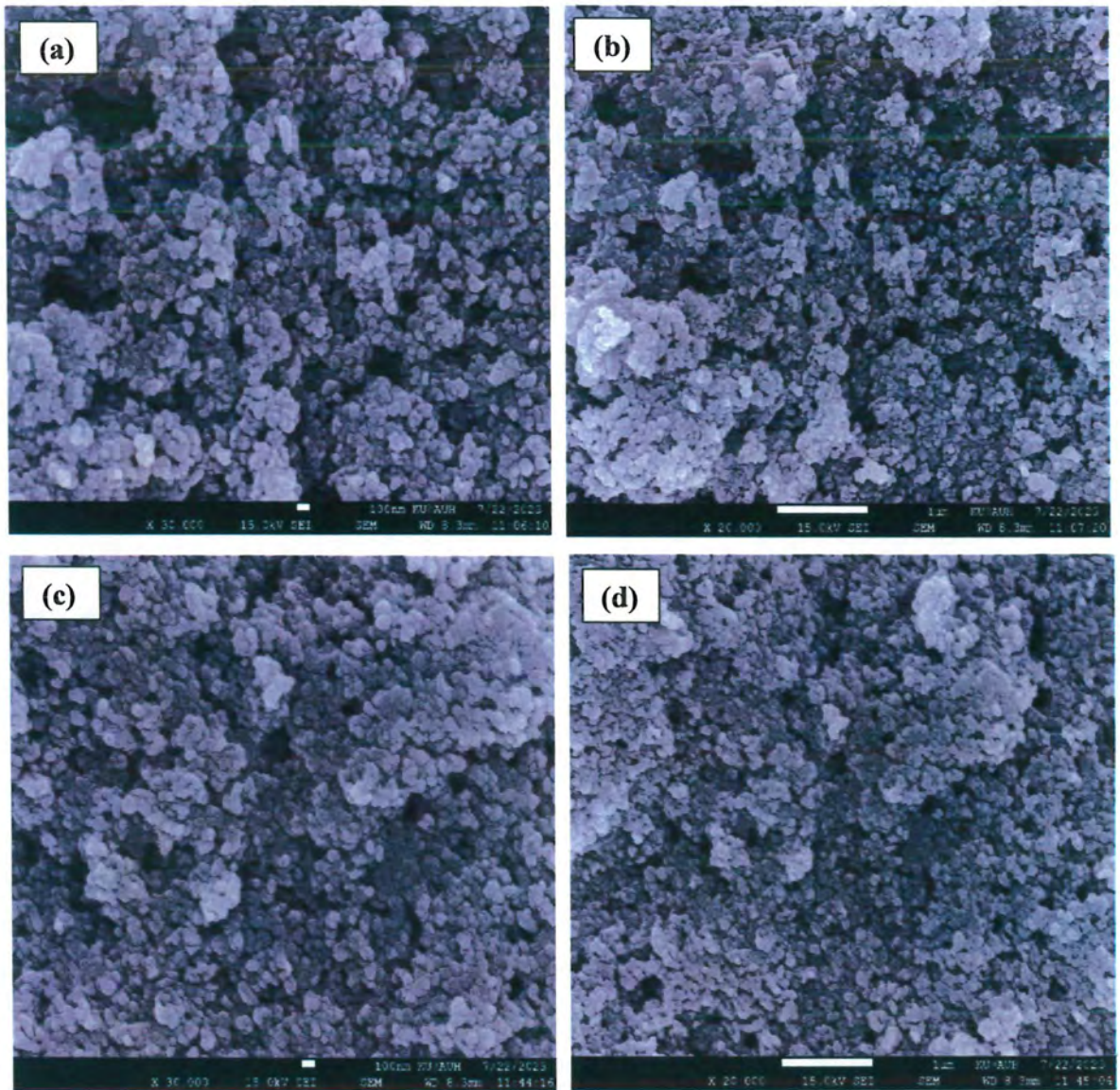
Figure 3.14. SEM images **(a)**,**(b)** 3% Ag-NiO NPs & **(c)**,**(d)** 5% Ag-NiO NPs.
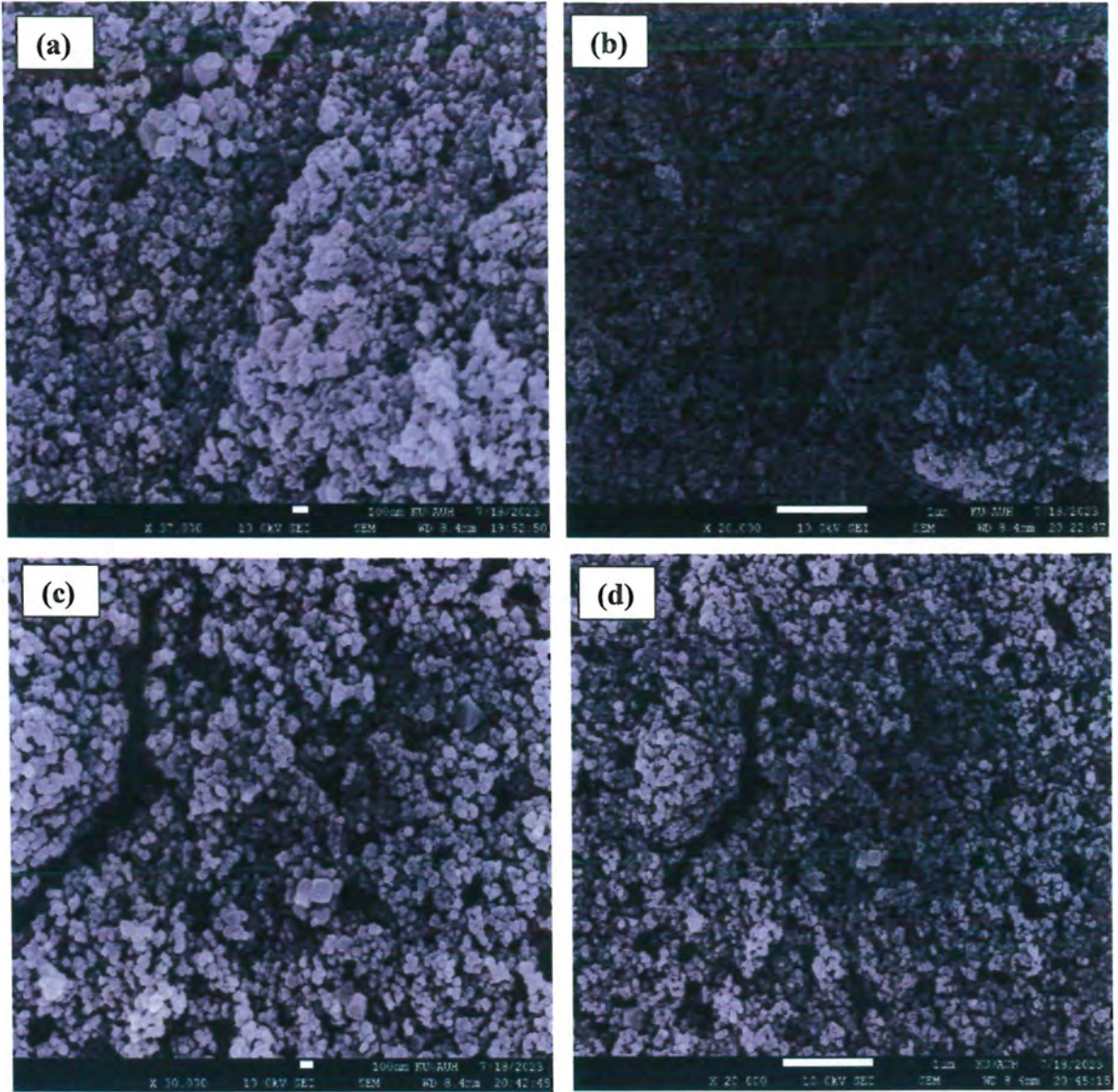
Figure 3.15. SEM images **(a),(b)** 2% Zn-NiO NPs & **(c),(d)** 3% Zn-NiO NPs.

3.6. EDX Studies

3.6.1. EDX Spectra of Pure and Doped (Ag & Zn) NiO NPs

EDX (Energy Dispersive X-ray) is an elemental analysis technique, used to study the composition of the elements in sample. Figure (3.16) verify the weight percentages of nickel, oxygen, silver, and zinc to be in close proximity with the as-synthesized material. However, certain impurity peaks of carbon, sulfur and chlorine elements were also observed which may be added during sample preparation procedure before analysis. Because EDX is a surface approach and cannot identify the whole amount of the sample, the obtained ratio of the elements deviated somewhat from the nominal content.
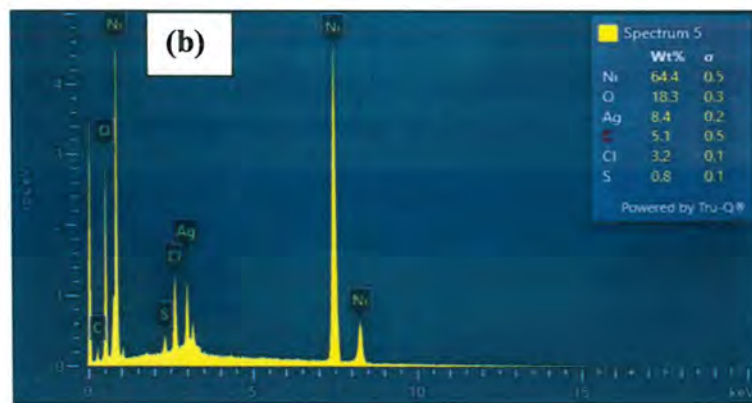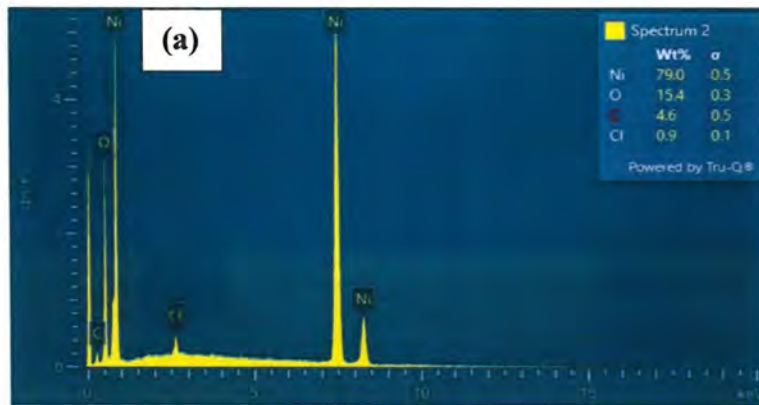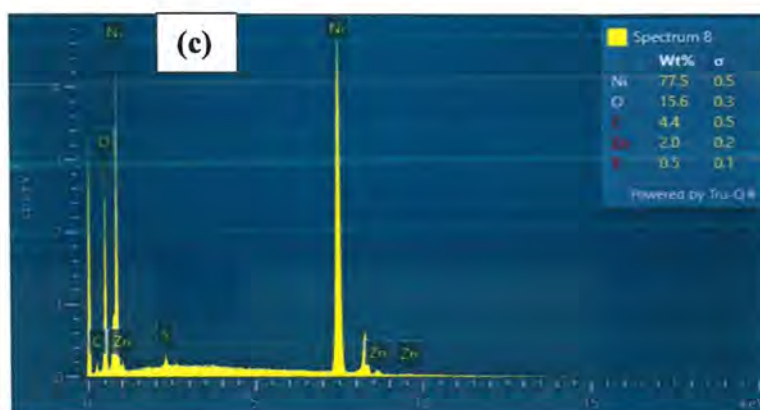
Figure 3.16. EDX spectra of **(a)** Pure NiO NPs **(b)** Ag-NiO **(c)** Zn-NiO NPs.

3.7. Optical Study of Dyes and Nanohybrid materials

3.7.1. UV-Visible Spectroscopy of Dyes

Carminic acid, Coomassie Violet R200, and Arsenazo III dyes were used in DSSC. The optical properties of dyes were checked by preparing 1mM parent solution of each dye. The mother solution (1 mM) was further diluted to 5 µM, 10 µM, 20 µM, 30 µM, 40 µM... and so on respectively by using dilution formula.

3.7.1.1. UV-Visible Spectroscopy of Carminic Acid Dye

Figure (3.17) represents the UV-Vis spectra of pure Carminic acid dye. Sharp peak of Carminic acid at 280 nm which lies in the UV region of solar spectrum and broad band appeared in the region 400-600 nm which represents the visible region of solar spectrum. The sharp peak of dye is due to $\pi \rightarrow \pi^*$ transitions and broad peak is due to $n \rightarrow \pi^*$ transitions.
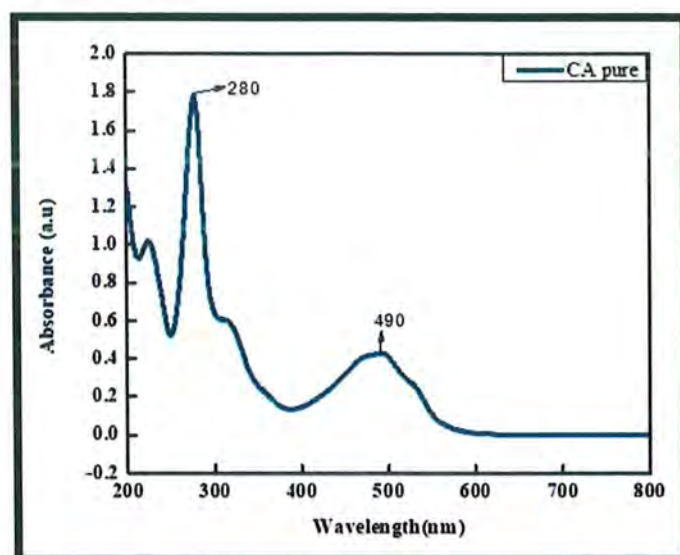
Figure 3.17. UV-Vis spectrum of pure Carminic acid dye.

3.7.1.2. UV-Visible Spectroscopy of Coomassie Violet R200 Dye

Figure (3.18) represents the UV-Vis spectra of Coomassie Violet R200 dye. Sharp peak of Coomassie violet R200 is at 551 nm which is in the visible region and two small peaks also noticed in the range of 200-320 nm which lies in the UV region of solar spectrum. The sharp peak of dye is due to $\pi \rightarrow \pi^*$ transitions and broad peak is due to $n \rightarrow \pi^*$ transitions.
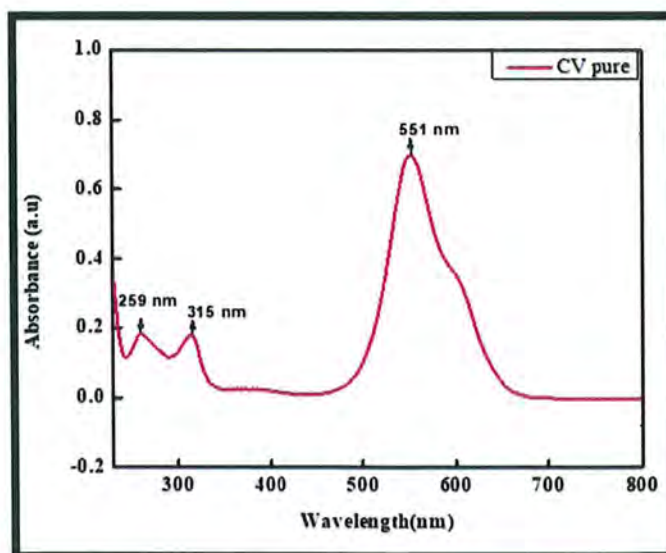
Figure 3.18. UV-Vis spectrum of pure Coomassie Violet R200 dye.

3.7.1.3. UV-Visible Spectroscopy of Arsenazo III Dye

Figure (3.19) represents the UV-Vis spectra of Arsenazo III dye. Arsenazo III showed a sharp peak at 535 nm which lies in visible region and broad peak at 310 nm which represents the UV region of solar spectrum. The sharp and broad peak of dye is due to $\pi \rightarrow \pi^*$ and $n \rightarrow \pi^*$ transitions.
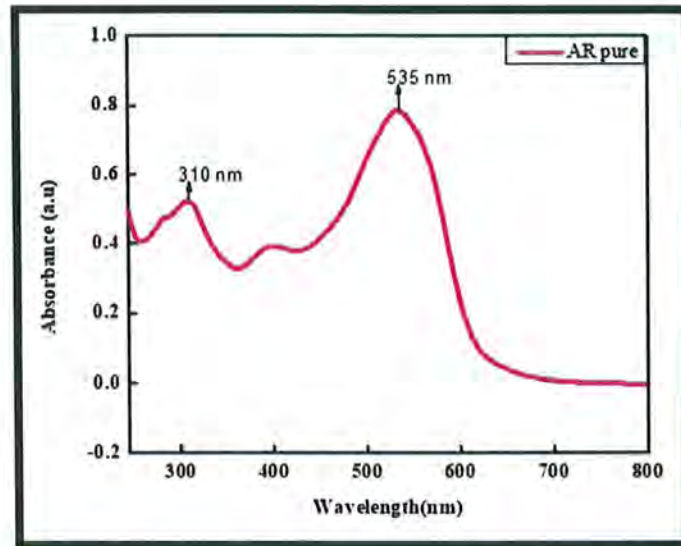
Figure 3.19. UV-Vis spectrum of pure Arsenazo III dye.

3.7.2. UV-Visible Spectroscopy of Nanohybrid Materials

3.7.2.1. UV-Visible Spectroscopy of Carminic acid Sensitized Nanohybrid Materials

Figure (3.20) represents the absorption spectra of Carminic acid sensitized nanohybrid assembly. Optimized concentration of dye like 70 μM for Carminic acid was utilized for grafting. As the chemisorption of dye (Carminic acid) does take place on the surface of nanoparticles, already present sharp peak corresponding to dye is getting disappear and an additional peak of nanoparticles was appeared along with the shifting of absorption spectra or broad peak of dye towards longer wavelength (red shift) as shown in figure (3.20). The significant drop in the intensity of relative sharp peak as well as red shift

79

in the absorption spectra of Carminic acid dye, when grafted with both pure and Zn doped NiO nanoparticles confirms the dye's chemisorption (grafting) on the surface of NPs.
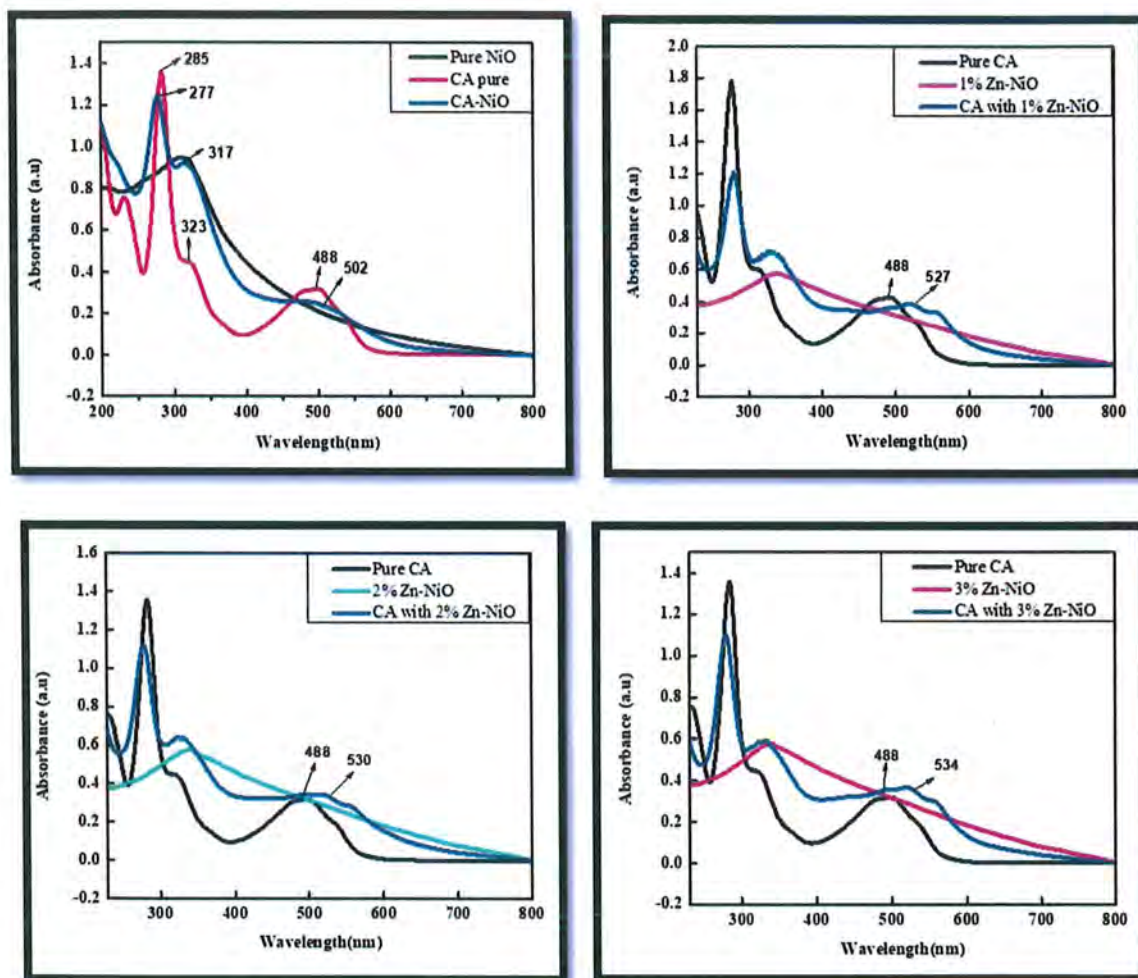
Figure 3.20. Absorption spectra of Carminic acid sensitized NiO and (1,2,3%) Zn-NiO nanomaterials.

3.7.2.2. UV-Visible Spectroscopy of Coomassie Violet R200 Sensitized Nanohybrid Materials

Figure (3.21) represents the absorption spectra Coomassie Violet R200 sensitized nanohybrid assembly. Optimized concentration of dye like 30 μM for Coomassie violet was utilized for grafting. As the chemisorption of dye (Coomassie Violet R200) does take place on the surface of nanoparticles, a clear blue shift was observed as shown in figure (3.21). The decrease in the intensity of sharp peak and blue shift in absorption spectra of

dye on grafting with pure and Ag doped NiO nanoparticles confirm the chemisorption of dye on the surface of nanoparticles as shown below.
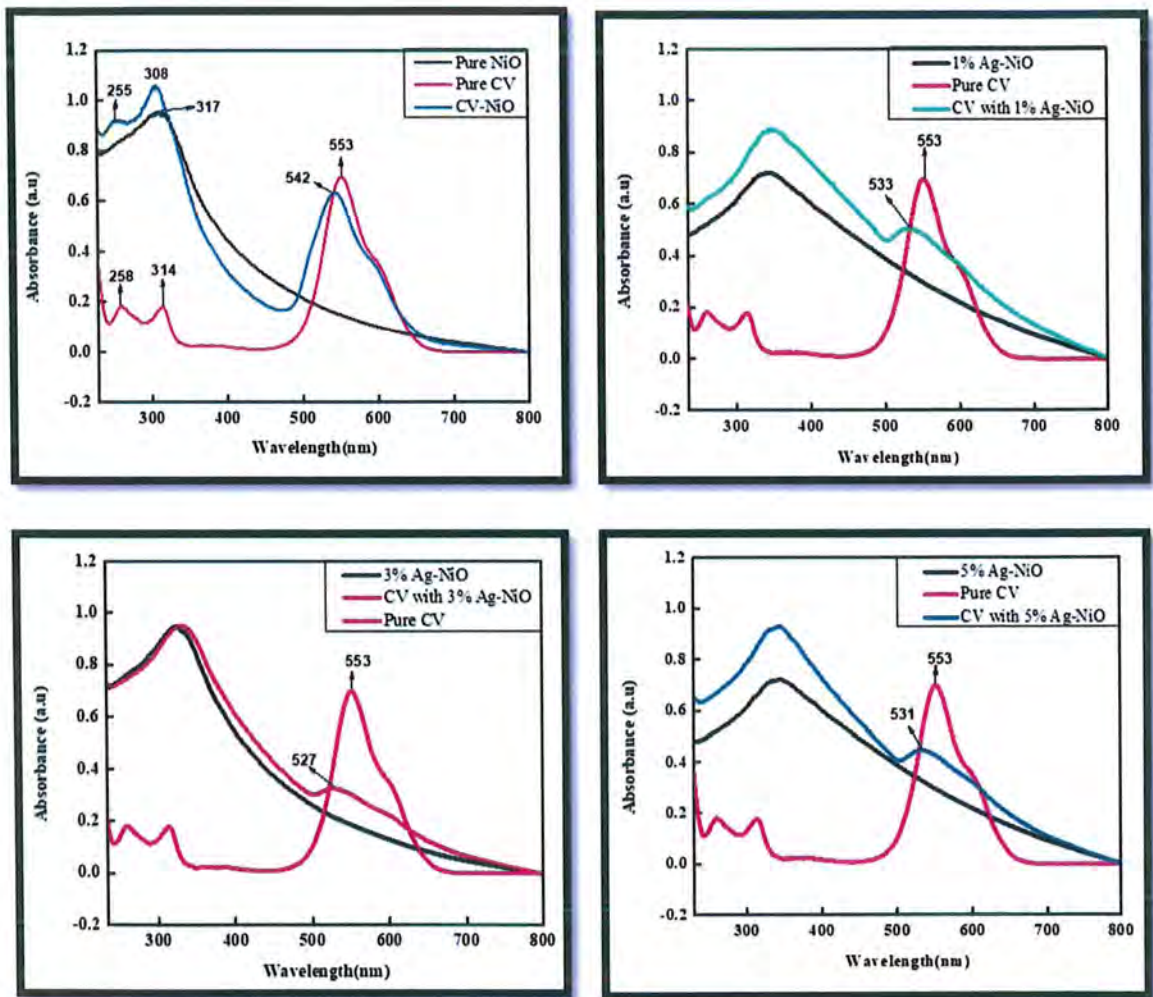
Figure 3.21. Absorption spectra of Coomassie Violet R200 sensitized NiO and (1,3,5%) Ag-NiO nanomaterials.

3.7.2.3. UV-Visible Spectroscopy of Arsenazo III Sensitized Nanohybrid Materials

Figure (3.22) and (3.23) represent the absorption spectra of Arsenazo III sensitized nanohybrid assembly. Optimized concentrations of dye like 50 μM for Arsenazo III was utilized for grafting. As the chemisorption of Arsenazo III dye does take place on the surface of nanoparticles, already present sharp peak corresponding to dye is getting disappear and an additional peak of nanoparticles was appeared along with the shifting of

absorption spectra or broad peak of dye towards longer wavelength (red shift) as shown in figure (3.22) and (3.23). The significant drop in the intensity of relative sharp peak as well as red shift in the absorption spectra of Arsenazo III dye, when grafted with both pure and doped (Ag & Zn) nanoparticles confirm the chemisorption (grafting) of dye on the surface of NPs.
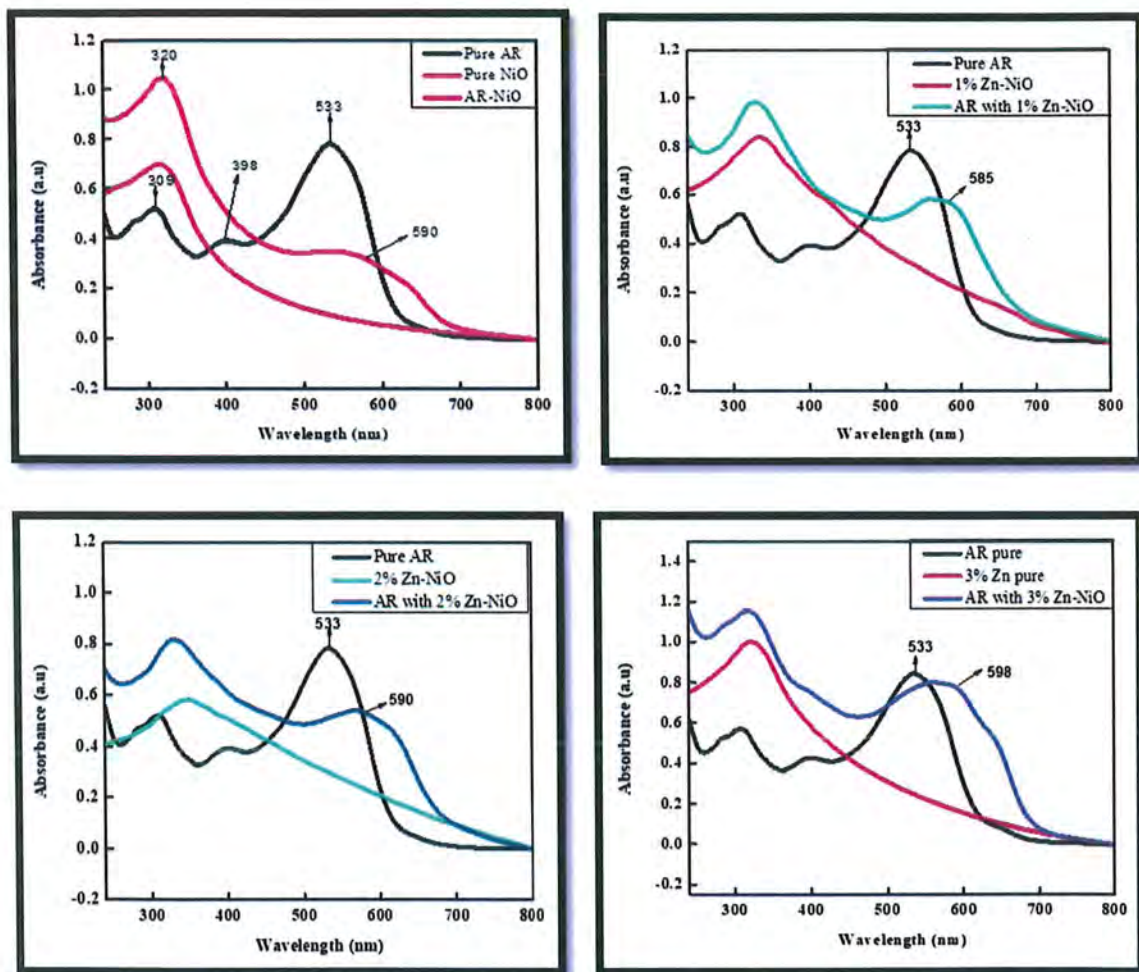
Figure 3.22. Absorption spectra of Arsenazo III sensitized NiO and (1,2,3%) Zn-NiO nanomaterials.
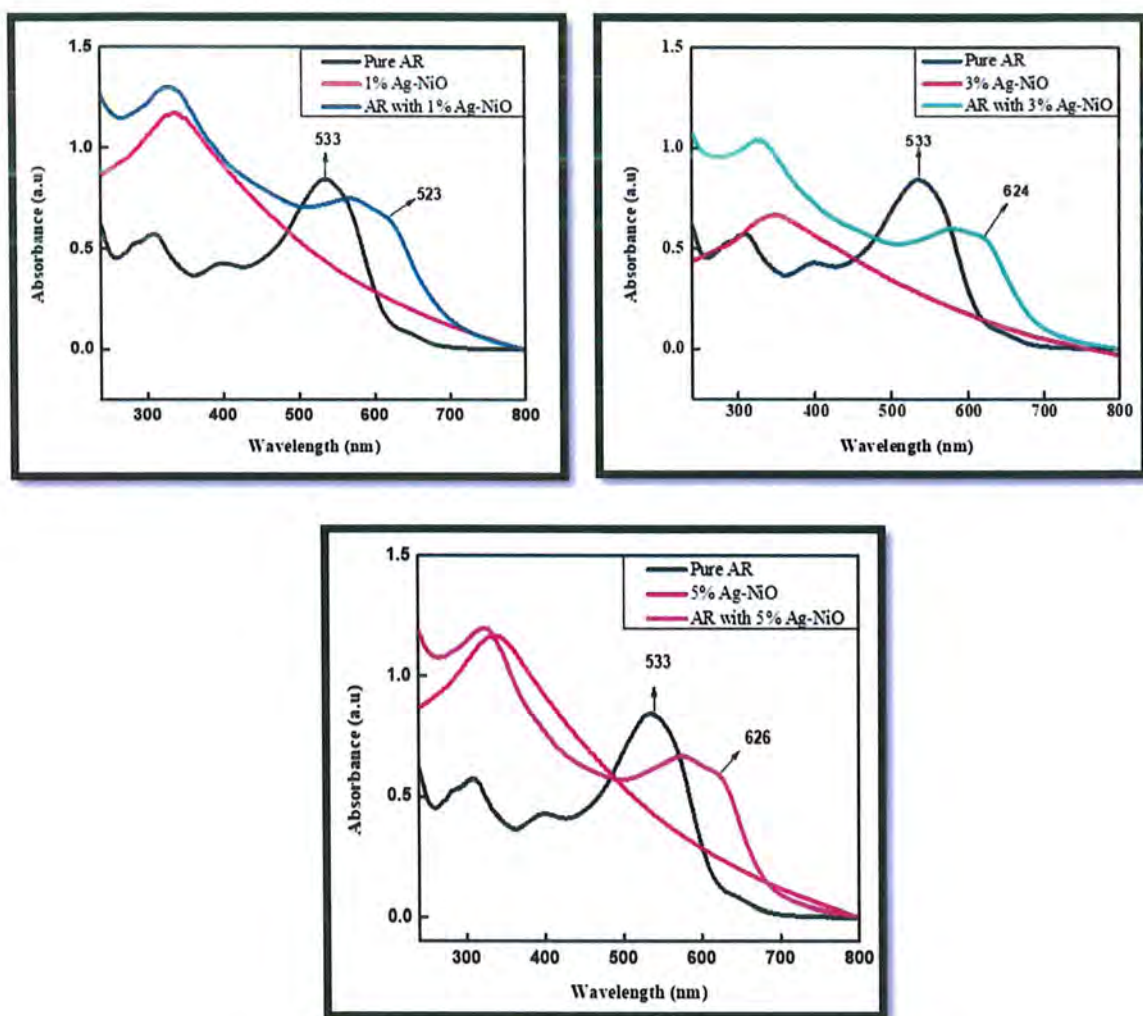
Figure 3.23. Absorption spectra of Arsenazo III sensitized (1,3,5%) Ag-NiO nanomaterials.

3.8. FTIR Study of Nanohybrid Materials

3.8.1. Carminic acid Sensitized Nanohybrid Assembly

Figure (3.24) and (3.25) shows FTIR spectra of pure Carminic Acid dye and Carminic acid grafted NiO and Zn-NiO NPs. In the FTIR spectra of pure Carminic acid dye, appearance of a broad peak at 3239 cm^{-1} indicated the occurrence of O-H stretching vibrations. While a noticeable peak at 1735 cm^{-1} shows the stretching vibrations due to the

carbonyl functional group corresponding to C=O which is used as an anchoring group. The peaks corresponding to region 1000 to 1500 cm^{-1} are attributed to C-C of the ring, C-H out of the plane and C-OH scissoring vibrations. The FTIR spectra of grafted Carminic acid dye shows the disappearance of peak at 1735 cm^{-1} which confirms the chemisorption of dye on nanoparticle's surface. The FTIR spectra of grafted Carminic acid dye shows a little peak at 1735 cm^{-1} which confirmed that some of the material remains un-grafted.
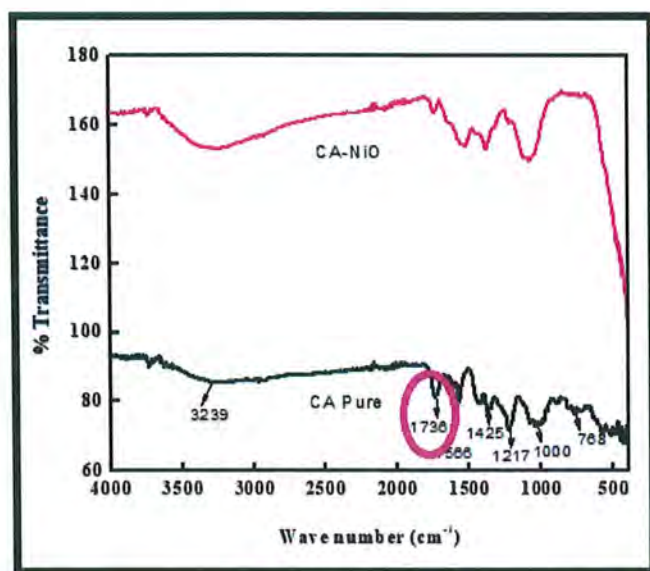
Figure 3.24. FTIR spectra of pure Carminic acid and Carminic acid grafted NiO NPs.
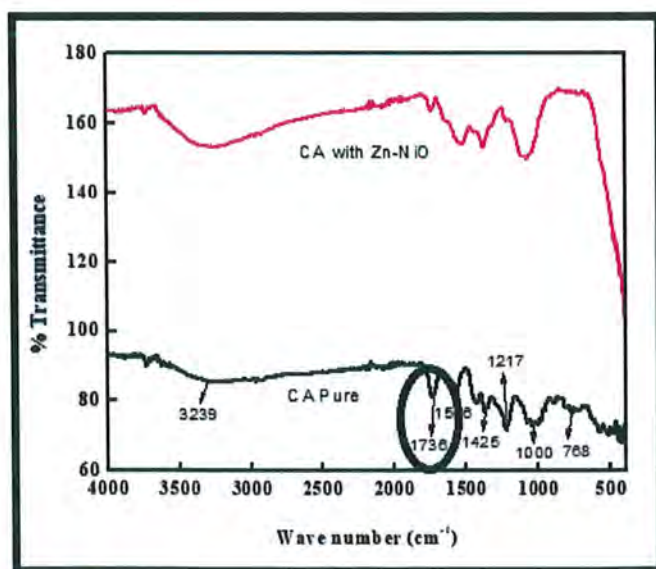
Figure 3.25. FTIR spectra of pure Carminic acid and Carminic acid grafted Zn-NiO NPs.

3.8.2. Coomassie Violet R200 Sensitized Nanohybrid Assembly

Figure (3.26) and (3.27) represent the FTIR spectra of pure Coomassie Violet R200 dye and Coomassie Violet R200 grafted NiO and Ag-NiO NPs. FTIR spectra of pure Commassie violet R200 shows a peak at 3403 cm^{-1} which is attributed to O-H stretching, and a peak observed at 1573 cm^{-1} which may be due to S=O vibrations of -SO$_3$H group which is acting as an anchoring group. Another small peak was noticed at 613 cm^{-1} which shows M-O stretching vibrations. The successful chemisorption of dye on the surface of nanoparticles was assessed due to complete disappearance of peak at 1573 cm^{-1} in the grafted spectra of Coomassie violet R200.
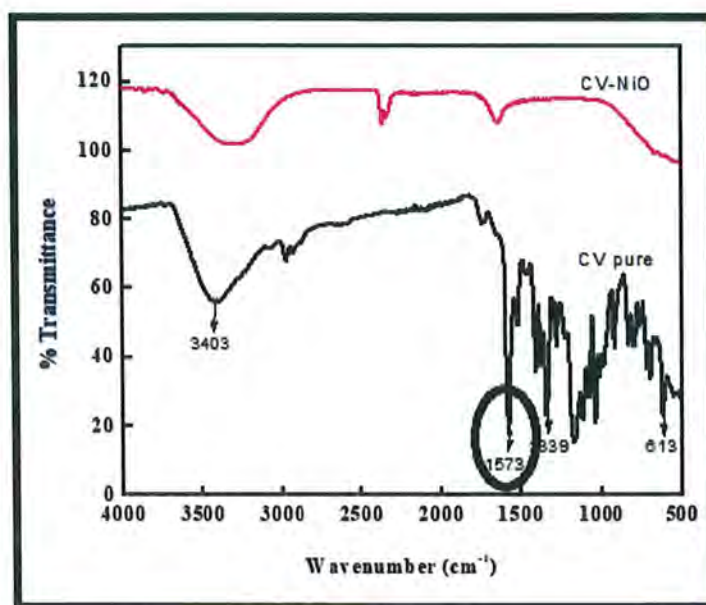
Figure 3.26. FTIR spectra of pure Coomassie Violet R200 and Coomassie Violet R200 grafted NiO NPs.
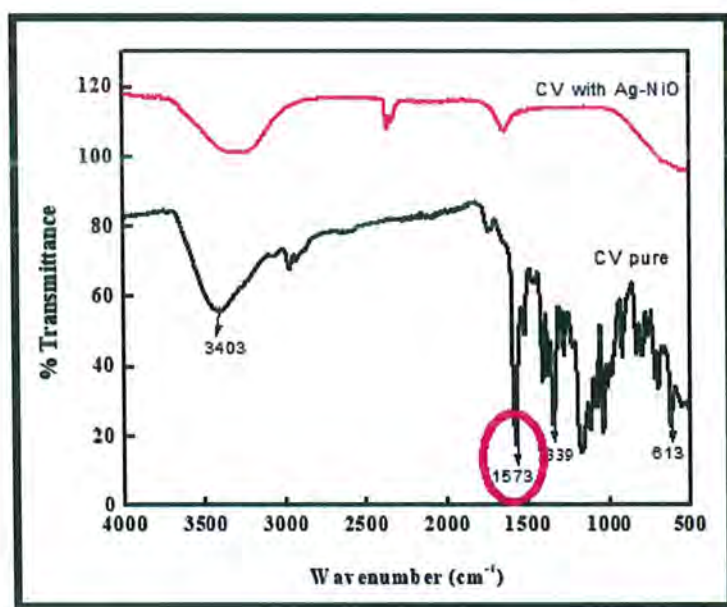
Figure 3.27. FTIR spectra of pure Coomassie Violet R200 and Coomassie Violet R200 grafted Ag-NiO NPs.

3.8.3. Arsenazo III Sensitized Nanohybrid Assembly

Figure (3.28), (3.29) and (3.30) represent the FTIR spectra of pure Arsenazo III dye and Arsenazo III grafted NiO, Zn-NiO and Ag-NiO NPs. FTIR spectra of pure Arsenazo III shows a peak at 2828 cm^{-1} which may be due to O-H stretching, and a peak observed at 2359 cm^{-1} which may be attributed to C-H vibrations, also a peak noticed at 1576 cm^{-1} which is due to S=O vibrations of -SO$_3$H group which is acting as an anchoring group. Another peak was noticed at 1472 cm^{-1} which shows N=N stretching vibrations. The complete disappearance of peak at 1576 cm^{-1} in the grafted spectra of Arsenazo III confirms the successful chemisorption of dye on the surface of nanoparticles.
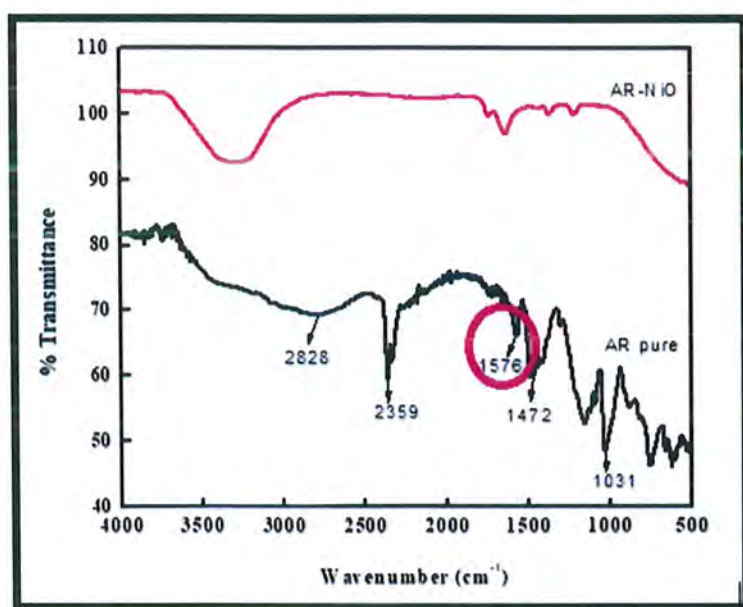
Figure 3.28. FTIR spectra of pure Arsenazo III and Arsenazo III grafted NiO NPs.
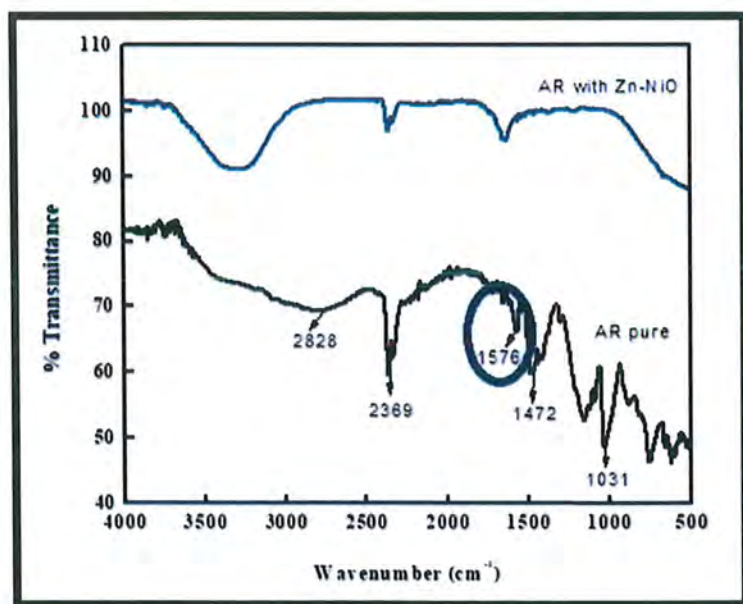
Figure 3.29. FTIR spectra of pure Arsenazo III and Arsenazo III grafted Zn-NiO NPs.
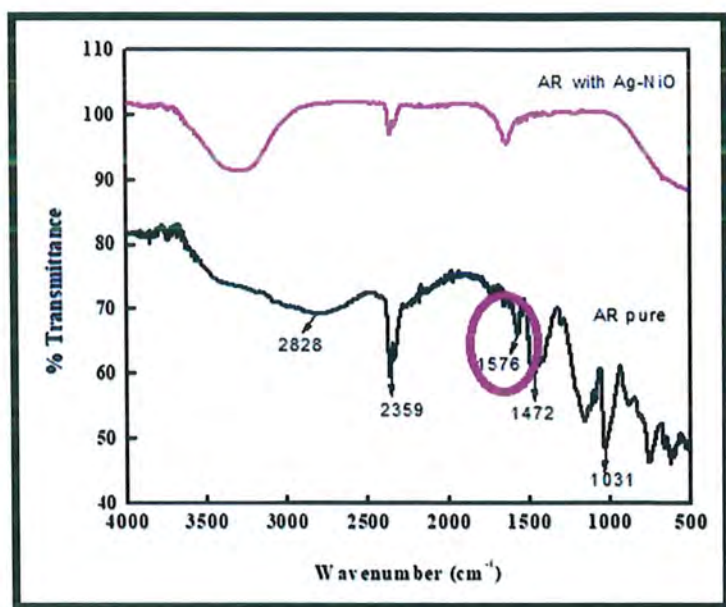
Figure 3.30. FTIR spectra of pure Arsenazo III and Arsenazo III grafted Ag-NiO NPs.

3.9. I-V Characterization of the Fabricated DSSCs

In addition to Ag-NiO that had been successfully tested in DSSCs and loaded with Carminic acid and Arsenazo III, this work investigated the usage of P3HT as a hole conducting material. In figure (3.37), I-V plots represent the photovoltaic study of the devices fabricated by using Ag-NiO as photoanode material. Table summarizes all the parameters of the devices. In this work, we fabricated ungrafted and grafted solar cell devices. The device which consists of NiO as photoanode when placed in dark it gives no current and is represented by black line in the graph. But when this device is exposed to light, current begins to flow, and it gives an efficiency of 0.07% with J_{sc} of 0.54 mA/cm^2 and V_{oc} of 0.31 V and it is taken as reference cell to compare the efficiency of other fabricated solar cell devices. The open-circuit potential (V_{oc}) of NiO (0.31 V) is lower than Ag-NiO (0.43 V). The V_{oc} was enhanced from 0.31 to 0.43 V due to Ag doping in NiO nanoparticles, which serves as an energy barrier to lessen electron-hole recombination and responsible for the rise in V_{oc} of nanostructured Ag-NiO. Similarly, compared to individual material, current density (J_{sc}) was also increased in case of Ag-NiO. The increased absorption of light and the production of free charge carriers lead to an increase in current density. When the Ag-NiO nanomaterial was sensitized using dyes, further rises in J_{sc} values were noticed. It is clear from the table that the DSSC made of Ag-NiO and sensitized with Carminic acid (CA) dye showed an efficiency of 0.40 % with J_{sc} value of 3.10 mA/cm^2. It is also evident from the table that the maximum efficiency was obtained for DSSC based on Arsenazo III sensitized Ag-NiO nanomaterial which is 1.03% with J_{sc} value of 7.90 mA/cm^2 and V_{oc} of 0.31 V, as compared to the reference cell of 0.07%.
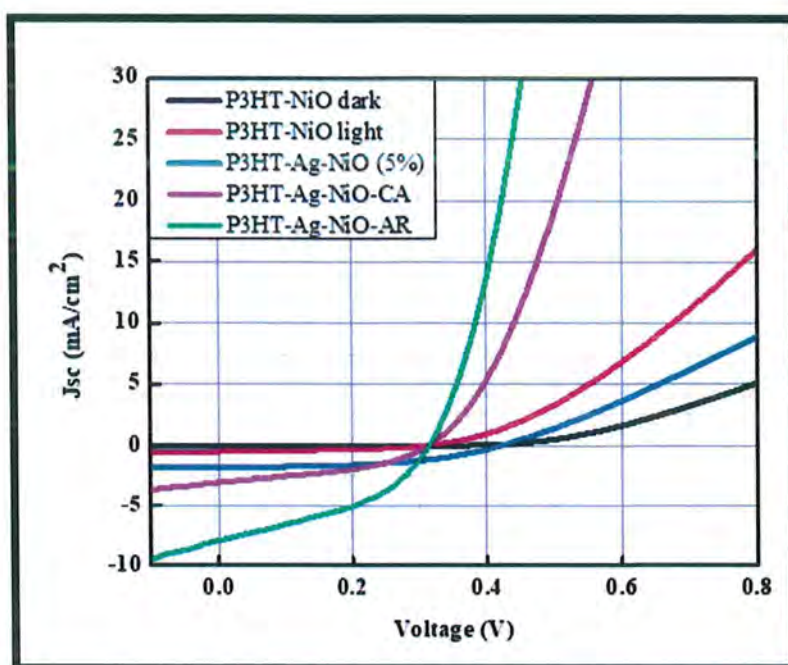
Figure 3.31. Current-voltage(I-V) plots of P3HT-NiO Dark **(black solid line)**, P3HT-NiO light **(red line)**, P3HT-Ag-NiO 5% **(blue line)**, P3HT-Ag-NiO-CA dye **(pink line)** and P3HT-Ag-NiO-AR dye **(green line)**.

Table 3.6. Calculated parameters of the I-V measurement curves.

Cell Composition	J_{sc} (mA/cm^2)	V_{oc} (V)	M_{pp} (mW/cm^2)	FF	(η%)
P3HT-NiO Light	0.54	0.31	0.07	0.42	0.07
P3HT-Ag-NiO 5%	1.82	0.43	0.39	0.50	0.40
P3HT-Ag-NiO-CA	3.10	0.31	0.40	0.42	0.40
P3HT-Ag-NiO-AR	7.90	0.31	1.01	0.42	1.03

Conclusions

Co-precipitation approach was effectively used to synthesize pure NiO and 1 to 6% transition metals (Ag & Zn) doped NiO NPs. XRD, FTIR, UV-visible spectroscopy, SEM, and EDX were successfully used to characterize the as-synthesized nanoparticles. NiO has an absorption peak with λ_{max} = 317 nm, according to an optical analysis carried out using UV-visible spectroscopy. By effectively doping Ag and Zn into NiO, the maximum absorption was shifted towards longer wavelengths (Red shift), and the λ_{max} was increased from 317–348 nm, respectively. Tauc's plots showed tuning in band gap of NiO from 3.17-2.10 eV in case of Ag-NiO and 3.17-2.00 eV in case of Zn-NiO respectively. XRD studies showed that the average crystallite size of pure and doped (Ag & Zn) NiO nanoparticles lies in the range of 28.73 to 31.40 nm. The elemental composition of nanostructured material was examined by EDX. And the surface morphology was examined by the aid of SEM analysis which showed spherical morphologies with little bit agglomeration of nanoparticles. FTIR analysis demonstrates the vibration bands of required materials and reveals the absence of any impurity. When compared to the pure dye spectrum, the FTIR peak for the -COOH group in the case of Carminic acid and the -SO$_3$H group in the case of Coomassie Violet R200 and Aesenazo III gets disappeared in the nanohybrid spectrum, demonstrating efficient functionalization (grafting) of the nanoparticles with the corresponding dyes. The absorption into the visible range was noticeably expanded by the functionalization of the pure as well as doped NiO nanoparticles with Carminic acid and Arsenazo III dyes. The fabricated (grafted and ungrafted) solar cell devices were characterized by I-V measurement curves. For DSSC based on Carminic acid dye sensitized Ag-NiO, the efficiency was observed to be 0.40% with J_{sc} of 3.10 mA/cm^2 and V_{oc} of 0.31 V. The maximum efficiency was obtained for DSSC based on Arsenazo III dye sensitized Ag-NiO, which is 1.03% with J_{sc} of 7.90 mA/cm^2 and V_{oc} of 0.31 V, as compared to the reference cell (0.07 %).

References

1. Umbach, F., Global energy security and the implications for the EU. *Energy Pol.* **2010,** *38* (3), 1229-1240.

2. Jayaraman, T.; Murthy, A. P.; Elakkiya, V.; Chandrasekaran, S.; Nithyadharseni, P.; Khan, Z.; Senthil, R. A.; Shanker, R.; Raghavender, M.; Kuppusami, P., Recent development on carbon based heterostructures for their applications in energy and environment: a review. *J. Ind. Eng. Chem.* **2018,** *64,* 16-59.

3. Jacoby, M., Tapping the sun. *Chem. Eng. News* **2007,** *85* (35), 16-49.

4. Güney, T., Renewable energy, non-renewable energy and sustainable development. *Int J. Sustain. Dev. World Ecol.* **2019,** *26* (5), 389-397.

5. Øvergaard, S., Issue paper: Definition of primary and secondary energy. *Stat. Norway, Osl.* **2008.**

6. Kannan, N.; Vakeesan, D., Solar energy for future world:-A review. *Renew. Sust. Energ. Rev.* **2016,** *62,* 1092-1105.

7. Mishra, A.; Powar, S.; Dhar, A., Solar Thermal powered bakery oven. *Adv. Sol. Energy Res.* **2019,** 577-592.

8. Banos, R.; Manzano-Agugliaro, F.; Montoya, F.; Gil, C.; Alcayde, A.; Gómez, J., Optimization methods applied to renewable and sustainable energy: A review. *Renew. Sust. Energ. Rev.* **2011,** *15* (4), 1753-1766.

9. Devabhaktuni, V.; Alam, M.; Depuru, S. S. S. R.; Green II, R. C.; Nims, D.; Near, C., Solar energy: Trends and enabling technologies. *Renew. Sust. Energ. Rev.* **2013,** *19,* 555-564.

10. Ahmed, A.; Ge, T.; Peng, J.; Yan, W.-C.; Tee, B. T.; You, S., Assessment of the renewable energy generation towards net-zero energy buildings: A review. *Energy Build.* **2022,** *256,* 111755.

11. Zain-Ahmed, A.; Sopian, K.; Othman, M.; Sayigh, A.; Surendran, P., Daylighting as a passive solar design strategy in tropical buildings: a case study of Malaysia. *Energy Convers. Manag.* **2002,** *43* (13), 1725-1736.

12. Rabah, K., Development of energy-efficient passive solar building design in Nicosia Cyprus. *Renew. energy* **2005,** *30* (6), 937-956.

13.   Goetzberger, A.; Greube, W., Solar energy conversion with fluorescent collectors. *App. phy.* **1977**, *14*, 123-139.

14.   Hoppmann, J.; Huenteler, J.; Girod, B., Compulsive policy-making—The evolution of the German feed-in tariff system for solar photovoltaic power. *Res. pol.* **2014**, *43* (8), 1422-1441.

15.   Eker, B., Solar powered water pumping systems. *Trakia J. Sci.* **2005**, *3* (7), 7-11.

16.   Loferski, J. J., Recent research on photovoltaic solar energy converters. *Proc. IEEE* **1963**, *51* (5), 667-674.

17.   Adejumobi, I.; Oyagbinrin, S.; Akinboro, F.; Olajide, M., Hybrid solar and wind power: an essential for information communication technology infrastructure and people in rural communities. *IJRRAS* **2011**, *9* (1), 130-138.

18.   Raghavendra, K. V. G.; Zeb, K.; Muthusamy, A.; Krishna, T.; Kumar, S. V. P.; Kim, D.-H.; Kim, M.-S.; Cho, H.-G.; Kim, H.-J., A comprehensive review of DC–DC converter topologies and modulation strategies with recent advances in solar photovoltaic systems. *Electronics* **2019**, *9* (1), 31.

19.   Sekar, N.; Ramasamy, R. P., Recent advances in photosynthetic energy conversion. *J. Photochem. Photobiol., C* **2015**, *22*, 19-33.

20.   Chang, C.; Wang, Z.; Fu, B.; Ji, Y., High-efficiency solar thermoelectric conversion enabled by movable charging of molten salts. *Sci. Rep.* **2020**, *10* (1), 20500.

21.   Mahmud, M. P.; Huda, N.; Farjana, S. H.; Lang, C., Environmental impacts of solar-photovoltaic and solar-thermal systems with life-cycle assessment. *Energies* **2018**, *11* (9), 2346.

22.   Mehrdel, B.; Nikbakht, A.; Aziz, A. A.; Jameel, M. S.; Dheyab, M. A.; Khaniabadi, P. M., Upconversion lanthanide nanomaterials: basics introduction, synthesis approaches, mechanism and application in photodetector and photovoltaic devices. *Nanotechnology* **2021**, *33* (8), 082001.

23.   Benda, V., Development of a course on photovoltaic systems. *Solid State Phenom.* **2004**, *97*, 133-138.

24.   Hall, R., Recombination processes in semiconductors. *Proc. Inst. Electr. Commuc. Eng.* **1959**, *106* (17S), 923-931.

25.   Mahdouani, M.; Bourguiga, R.; Jaziri, S.; Gardelis, S.; Nassiopoulou, A., Investigation of Auger recombination in Ge and Si nanocrystals embedded in SiO2 matrix. *Physica E Low Dimens. Syst. Nanostruct.* **2009,** *42* (1), 57-62.

26.   Cheng, H.; Feng, Y.; Fu, Y.; Zheng, Y.; Shao, Y.; Bai, Y., Understanding and minimizing non-radiative recombination losses in perovskite light emitting diodes. *J. Mater. Chem. C* **2022.**

27.   Bang, J.; Sun, Y.; Song, J.-H.; Zhang, S., Carrier-induced transient defect mechanism for non-radiative recombination in InGaN light-emitting devices. *Sci. Rep.* **2016,** *6* (1), 24404.

28.   Crabtree, G. W.; Lewis, N. S., Solar energy conversion. *Phys. Today* **2007,** *60* (3), 37-42.

29.   Kuno, H., Analysis and characterization of PN junction diode switching. *IEEE T ELECTRON DEV.* **1964,** *11* (1), 8-14.

30.   Sharma, K.; Sharma, V.; Sharma, S., Dye-sensitized solar cells: fundamentals and current status. *Nanoscale Res. Lett.* **2018,** *13,* 1-46.

31.   Bagher, A. M.; Vahid, M. M. A.; Mohsen, M., Types of solar cells and application. *Am J Opt Photonics.* **2015,** *3* (5), 94-113.

32.   Sharma, S.; Jain, K. K.; Sharma, A., Solar cells: in research and applications—a review. *Mater. sci. appl.* **2015,** *6* (12), 1145.

33.   Khatibi, A.; Razi Astaraei, F.; Ahmadi, M. H., Generation and combination of the solar cells: A current model review. *Energy Sci. Eng.* **2019,** *7* (2), 305-322.

34.   Green, M. A., Third generation photovoltaics: solar cells for 2020 and beyond. *Physica E Low Dimens. Syst. Nanostruct.* **2002,** *14* (1-2), 65-70.

35.   Abdin, Z.; Alim, M. A.; Saidur, R.; Islam, M. R.; Rashmi, W.; Mekhilef, S.; Wadi, A., Solar energy harvesting with the application of nanotechnology. *Renew. Sust. Energ. Rev.* **2013,** *26,* 837-852.

36.   Hagfeldt, A.; Boschloo, G.; Sun, L.; Kloo, L.; Pettersson, H., Dye-sensitized solar cells. *Chem. Rev.* **2010,** *110* (11), 6595-6663.

37.   Nazeeruddin, M. K.; Baranoff, E.; Grätzel, M., Dye-sensitized solar cells: A brief overview. *Sol. energy* **2011,** *85* (6), 1172-1178.

38.   Raut, K. H.; Chopde, H. N.; Deshmukh, D. W., A review on comparative studies of diverse generation in solar cell. *Int. J. Electr. Eng. Ethics* **2018,** *1*, 1-9.

39.   Ghernaout, D.; Boudjemline, A.; Elboughdiri, N., Electrochemical engineering in the core of the dye-sensitized solar cells (DSSCs). *oalib.* **2020,** *7* (3), 1-12.

40.   Pandey, R.; Babu, K. C.; Srivastava, O., High conversion efficiency photoelectrochemical solar cells. *Prog. Surf. Sci.* **1996,** *52* (3), 125-192.

41.   Yahya, M.; Bouziani, A.; Ocak, C.; Seferoğlu, Z.; Sillanpää, M., Organic/metal-organic photosensitizers for dye-sensitized solar cells (DSSC): Recent developments, new trends, and future perceptions. *Dyes Pigm.* **2021,** *192*, 109227.

42.   Iftikhar, H.; Sonai, G. G.; Hashmi, S. G.; Nogueira, A. F.; Lund, P. D., Progress on electrolytes development in dye-sensitized solar cells. *Materials* **2019,** *12* (12), 1998.

43.   Reddy, K. G.; Deepak, T.; Anjusree, G.; Thomas, S.; Vadukumpully, S.; Subramanian, K.; Nair, S. V.; Nair, A. S., On global energy scenario, dye-sensitized solar cells and the promise of nanotechnology. *Phys. Chem. Chem. Phys.* **2014,** *16* (15), 6838-6858.

44.   Mourdikoudis, S.; Pallares, R. M.; Thanh, N. T., Characterization techniques for nanoparticles: comparison and complementarity upon studying nanoparticle properties. *Nanoscale* **2018,** *10* (27), 12871-12934.

45.   Janani, M.; Nair, S. V.; Nair, A. S., Photovoltaics: Role of Nanotechnology in Dye-Sensitized Solar Cells. *Nanotechnol. Energy Sus.* **2017,** 101-132.

46.   Arole, V.; Munde, S., Fabrication of nanomaterials by top-down and bottom-up approaches-an overview. *J. Mater. Sci* **2014,** *1*, 89-93.

47.   Abid, N.; Khan, A. M.; Shujait, S.; Chaudhary, K.; Ikram, M.; Imran, M.; Haider, J.; Khan, M.; Khan, Q.; Maqbool, M., Synthesis of nanomaterials using various top-down and bottom-up approaches, influencing factors, advantages, and disadvantages: A review. *Adv. Colloid Interface Sci.* **2022,** *300*, 102597.

48.   Shyam, A.; Chandran S, S.; George, B.; E, S., Plant mediated synthesis of AgNPs and its applications: an overview. *Inorg. Nano-Metal Chem.* **2021,** *51* (12), 1646-1662.

49.   Nwanya, A. C.; Ndipingwi, M. M.; Ikpo, C. O.; Obodo, R.; Nwanya, S. C.; Botha, S.; Ezema, F. I.; Iwuoha, E. I.; Maaza, M., Zea mays lea silk extract mediated synthesis of

nickel oxide nanoparticles as positive electrode material for asymmetric supercabattery. *J. Alloys Compd.* **2020**, *822*, 153581.

50.   El-Kemary, M.; Nagy, N.; El-Mehasseb, I., Nickel oxide nanoparticles: Synthesis and spectral studies of interactions with glucose. *Mater. Sci. Semicond.* **2013**, *16* (6), 1747-1752.

51.   Krüger, E., Wannier states of fcc symmetry qualifying paramagnetic NiO to be a Mott insulator. *Symmetry* **2020**, *12* (5), 687.

52.   Sun, C.; Li, Y.; Song, P.; Ma, F., An experimental and theoretical investigation of the electronic structures and photoelectrical properties of ethyl red and carminic acid for DSSC application. *Materials* **2016**, *9* (10), 813.

53.   Yang, D.; Jang, W. D.; Lee, S. Y., Production of carminic acid by metabolically engineered Escherichia coli. *J. Am. Chem. Soc.* **2021**, *143* (14), 5364-5377.

54.   Altikatoglu, M.; Celebi, M., Enhanced stability and decolorization of Coomassie Brilliant Blue R-250 by dextran aldehyde-modified horseradish peroxidase. *ARTIF. CELL BLOOD SUB.* **2011**, *39* (3), 185-190.

55.   Choi, S.; Yun, J.-I., Stability constants and spectroscopic properties of thorium (IV)-arsenazo III complexes in perchloric acid. *J. Radioanal. Nucl. Chem.* **2019**, *319*, 401-407.

56.   Choi, S.; Lee, J.-Y.; Yun, J.-I., Stability constants and spectroscopic properties of Thorium (IV)–Arsenazo III complexes in aqueous hydrochloric medium. *J Solution Chem.* **2017**, *46*, 1272-1283.

57.   Palade, P.; Vergara, J., Arsenazo III and antipyrylazo III calcium transients in single skeletal muscle fibers. *J. Gen. Physiol.* **1982**, *79* (4), 679-707.

58.   Qiu, L.; Xu, Q.; Lee, W. H.; Wang, X.; Kang, B.; Lv, G.; Cho, K., Organic thin-film transistors with a photo-patternable semiconducting polymer blend. *J. Mater. Chem. C* **2011**, *21* (39), 15637-15642.

59.   Jo, S. B.; Lee, W. H.; Qiu, L.; Cho, K., Polymer blends with semiconducting nanowires for organic electronics. *J. Mater. Chem. C* **2012**, *22* (10), 4244-4260.

60.   Gangopadhyay, R.; Das, B.; Molla, M. R., How does PEDOT combine with PSS? Insights from structural studies. *Rsc Advances* **2014**, *4* (83), 43912-43920.

61.   Sun, K.; Zhang, S.; Li, P.; Xia, Y.; Zhang, X.; Du, D.; Isikgor, F. H.; Ouyang, J., Review on application of PEDOTs and PEDOT: PSS in energy conversion and storage devices. *J. Mater. Sci.: Mater. Electron.* **2015**, *26*, 4438-4462.

62.   Padilla, M.; Michl, B.; Thaidigsmann, B.; Warta, W.; Schubert, M., Short-circuit current density mapping for solar cells. *Sol. Energy Mater Sol* **2014**, *120*, 282-288.

63.   Hishikawa, Y.; Takenouchi, T.; Higa, M.; Yamagoe, K.; Ohshima, H.; Yoshita, M., Translation of solar cell performance for irradiance and temperature from a single IV curve without advance information of translation parameters. *IEEE J. Photovolt.* **2019**, *9* (5), 1195-1201.

64.   Bouzidi, K.; Chegaar, M.; Bouhemadou, A., Solar cells parameters evaluation considering the series and shunt resistance. *Sol. Energy Mater Sol. Cells.* **2007**, *91* (18), 1647-1651.

65.   Babar, F.; Mehmood, U.; Asghar, H.; Mehdi, M. H.; Khan, A. U. H.; Khalid, H.; ul Huda, N.; Fatima, Z., Nanostructured photoanode materials and their deposition methods for efficient and economical third generation dye-sensitized solar cells: A comprehensive review. *Renew. Sust. Energ. Rev.* **2020**, *129*, 109919.

66.   Aslam, A.; Mehmood, U.; Arshad, M. H.; Ishfaq, A.; Zaheer, J.; Khan, A. U. H.; Sufyan, M., Dye-sensitized solar cells (DSSCs) as a potential photovoltaic technology for the self-powered internet of things (IoTs) applications. *Sol. Energy* **2020**, *207*, 874-892.

67.   Nandy, S.; Maiti, U.; Ghosh, C.; Chattopadhyay, K., Enhanced p-type conductivity and band gap narrowing in heavily Al doped NiO thin films deposited by RF magnetron sputtering. *J. Phys. Condens. Matter* **2009**, *21* (11), 115804.

68.   Goel, R.; Jha, R.; Ravikant, C., Investigating the structural, electrochemical, and optical properties of p-type spherical nickel oxide (NiO) nanoparticles. *J. Phys. Chem. Solids.* **2020**, *144*, 109488.

69.   Zhang, K. H.; Wu, R.; Tang, F.; Li, W.; Oropeza, F. E.; Qiao, L.; Lazarov, V. K.; Du, Y.; Payne, D. J.; MacManus-Driscoll, J. L., Electronic structure and band alignment at the NiO and SrTiO$_3$ p–n heterojunctions. *ACS Appl. Mater. Interfaces* **2017**, *9* (31), 26549-26555.

70.   Kumar, M. V.; Muthulakshmi, S.; Paulfrit, A. A.; Pandiarajan, J.; Jeyakumaran, N.; Prithivikumaran, N., Structural and optical behaviour of thermally evaporated p-type nickel oxide thin film for solar cell applications. *Int. J. Chem. Tech. Res* **2014**, *6*, 5174-7.

71.   Sharma, R.; Acharya, A.; Moghe, S.; Shrivastava, S.; Gangrade, M.; Shripathi, T.; Ganesan, V., Effect of cobalt doping on microstructural and optical properties of nickel oxide thin films. *Mater. Sci. Semicond.* **2014**, *23*, 42-49.

72.   Warnan, J.; Gardner, J.; Le Pleux, L.; Petersson, J.; Pellegrin, Y.; Blart, E.; Hammarstrom, L.; Odobel, F., Multichromophoric sensitizers based on squaraine for NiO based dye-sensitized solar cells. *J. Phys. Chem. C* **2014**, *118* (1), 103-113.

73.   Farooq, M.; Mujtaba Shah, S., Fabrication and Characterization of NiO Nanoparticle–Porphyrin-Based Organic–Inorganic Nanohybrid Assembly: a Sustainable Redox Mediator in Dye-Sensitized Solar Cell Construction. *J. Electron. Mater.* **2021**, *50* (8), 4827-4833.

74.   Fomekong, R. L.; Kamta, H. T.; Lambi, J. N.; Lahem, D.; Eloy, P.; Debliquy, M.; Delcorte, A., A sub-ppm level formaldehyde gas sensor based on Zn-doped NiO prepared by a co-precipitation route. *J. Alloys Compd.* **2018**, *731*, 1188-1196.

75.   Al Boukhari, J.; Zeidan, L.; Khalaf, A.; Awad, R., Synthesis, characterization, optical and magnetic properties of pure and Mn, Fe and Zn doped NiO nanoparticles. *Chem. Phys.* **2019**, *516*, 116-124.

76.   Solanki, K.; Sharma, S.; Yadav, S.; Kaushik, B.; Rana, P.; Dixit, R.; Sharma, R., Hierarchical 3D Flower-like Metal Oxides Micro/Nanostructures: Fabrication, Surface Modification, Their Crucial Role in Environmental Decontamination, Mechanistic Insights, and Future Perspectives. *Small* **2023**, 2300394.

77.   Cahen, D.; Hodes, G.; Grätzel, M.; Guillemoles, J. F.; Riess, I., Nature of photovoltaic action in dye-sensitized solar cells. *J. Phys. Chem. B* **2000**, *104* (9), 2053-2059.

78.   Mishra, A.; Bandyopadhyay, S.; Das, D., Structural and magnetic properties of pristine and Fe-doped NiO nanoparticles synthesized by the co-precipitation method. *Mater. Res. Bull.* **2012**, *47* (9), 2288-2293.

79.   Shalini, S.; Balasundaraprabhu, R.; Kumar, T. S.; Prabavathy, N.; Senthilarasu, S.; Prasanna, S., Status and outlook of sensitizers/dyes used in dye sensitized solar cells (DSSC): a review. *Int. J. Energy Res.* **2016,** *40* (10), 1303-1320.

80.   Kamil, A. F.; Abdullah, H. I.; Rheima, A. M., Fabrication of dye-sensitized solar cells and synthesis of $CuNiO_2$ nanostructures using a photo-irradiation technique. *J Nanostruct.* **2022,** *12* (1), 144-159.

81.   Mahmood, A.; Khan, S. U.-D.; Rana, U. A., Theoretical designing of novel heterocyclic azo dyes for dye sensitized solar cells. *J. Comput. Electron.* **2014,** *13,* 1033-1041.

82.   Ansir, R.; Shah, S. M.; Ullah, N.; Hussain, M. N., Performance of pyrocatechol violet and carminic acid sensitized ZnO/CdS nanostructured photoactive materials for dye sensitized solar cell. *Solid State Electron.* **2020,** *172,* 107886.

83.   Aram, E.; Shaki, H.; Ehsani, M., Highly efficient and stable quasi-solid-state dye-sensitized solar cells with PEO/PMMA/single-layered graphene oxide composite electrolytes. *Ionics* **2023,** 1-15.

84.   Yue, G.; Wu, J.; Xiao, Y.; Ye, H.; Lin, J.; Huang, M., Flexible dye-sensitized solar cell based on PCBM/P3HT heterojunction. *Chin. Sci. Bull.* **2011,** *56,* 325-330.

85.   Song, L.; Wang, W.; Körstgens, V.; González, D. M.; Yao, Y.; Minar, N. K.; Feckl, J. M.; Peters, K.; Bein, T.; Fattakhova-Rohlfing, D., Spray deposition of titania films with incorporated crystalline nanoparticles for all-solid-state dye-sensitized solar cells using P3HT. *Adv. Funct. Mater.* **2016,** *26* (10), 1498-1506.

86.   Zhang, M.; Höfle, S.; Czolk, J.; Mertens, A.; Colsmann, A., All-solution processed transparent organic light emitting diodes. *Nanoscale* **2015,** *7* (47), 20009-20014.

87.   Zhang, L.; Yang, K.; Chen, R.; Zhou, Y.; Chen, S.; Zheng, Y.; Li, M.; Xu, C.; Tang, X.; Zang, Z., The role of mineral acid doping of PEDOT: PSS and its application in organic photovoltaics. *Adv. Electron. Mater.* **2020,** *6* (1), 1900648.

88.   Mohd-Nasir, S.; Sulaiman, M.; Ahmad-Ludin, N.; Ibrahim, M.; Sopian, K.; Mat-Teridi, M., Review of polymer, dye-sensitized, and hybrid solar cells. *Int. J. Photoenergy* **2014,** *2014.*

89.   Björström, C. M.; Nilsson, S.; Bernasik, A.; Budkowski, A.; Andersson, M.; Magnusson, K. O.; Moons, E., Vertical phase separation in spin-coated films of a low

bandgap polyfluorene/PCBM blend—effects of specific substrate interaction. *Appl. Surf. Sci.* **2007,** *253* (8), 3906-3912.

90.   Murakami, T. N.; Grätzel, M., Counter electrodes for DSC: application of functional materials as catalysts. *Inorganica Chim. Acta* **2008,** *361* (3), 572-580.

91.   Karuppuchamy, S.; Nonomura, K.; Yoshida, T.; Sugiura, T.; Minoura, H., Cathodic electrodeposition of oxide semiconductor thin films and their application to dye-sensitized solar cells. *Solid State Ion.* **2002,** *151* (1-4), 19-27.

92.   Bunaciu, A. A.; UdriŞTioiu, E. G.; Aboul-Enein, H. Y., X-ray diffraction: instrumentation and applications. *Crit. Rev. Anal. Chem.* **2015,** *45* (4), 289-299.

93.   Feidenhans, R., Surface structure determination by X-ray diffraction. *Surf. Sci. Rep.* **1989,** *10* (3), 105-188.

94.   Griffiths, P. R., Fourier transform infrared spectrometry. *Science* **1983,** *222* (4621), 297-302.

95.   Bates, J., Fourier Transform Infrared Spectroscopy: The basic principles and current applications of a rapidly expanding technique are reviewed. *Science* **1976,** *191* (4222), 31-37.

96.   Schindler, R.; Lendl, B., FTIR spectroscopy as detection principle in aqueous flow analysis. *Anal. Commun.* **1999,** *36* (4), 123-126.

97.   Limniou, M.; Papadopoulos, N.; Roberts, D., An integrated lecture, virtual instrumentation lab approach to teaching UV-Vis spectroscopy. *Educ. Inf. Technol.* **2007,** *12*, 229-244.

98.   Penner, M. H., Basic principles of spectroscopy. *Food anal.* **2017,** 79-88.

99.   Wohletz, K. H., Mechanisms of hydrovolcanic pyroclast formation: grain-size, scanning electron microscopy, and experimental studies. *J. Volcanol. Geotherm. Res.* **1983,** *17* (1-4), 31-63.

100.   Nuspl, M.; Wegscheider, W.; Angeli, J.; Posch, W.; Mayr, M., Qualitative and quantitative determination of micro-inclusions by automated SEM/EDX analysis. *Anal. Bioanal. Chem.* **2004,** *379*, 640-645.

101.   Liu, J.; Maaroof, A. I.; Wieczorek, L.; Cortie, M. B., Fabrication of hollow metal "nanocaps" and their red-shifted optical absorption spectra. *Adv Mater.* **2005,** *17* (10), 1276-1281.

102.   Raj, I. L. P.; Valanarasu, S.; Isaac, R. R.; Ramudu, M.; Bitla, Y.; Ganesh, V.; Yahia, I., The role of silver doping in tuning the optical absorption, energy gap, photoluminescence properties of NiO thin films for UV photosensor applications. *Optik* **2022**, *254*, 168634.

103.   Liu, Z.; Wang, H.; Li, H.; Wang, X., Red shift of plasmon resonance frequency due to the interacting Ag nanoparticles embedded in single crystal SiO 2 by implantation. *Appl. Phys. Lett* **1998**, *72* (15), 1823-1825.

104.   Sharma, R.; Acharya, A.; Shrivastava, S.; Patidar, M. M.; Gangrade, M.; Shripathi, T.; Ganesan, V., Studies on the structure optical and electrical properties of Zn-doped NiO thin films grown by spray pyrolysis. *Optik* **2016**, *127* (11), 4661-4668.

105.   Shaker, A.; Zekry, A., A new and simple model for plasma-and doping-induced band gap narrowing. *J. Electron Devices* **2010**, *8*, 293-299.

106.   Kaur, N.; Singh, J.; Kaur, G.; Kumar, S.; Kukkar, D.; Rawat, M., CTAB assisted co-precipitation synthesis of NiO nanoparticles and their efficient potential towards the removal of industrial dyes. *Micro Nano Lett.* **2019**, *14* (8), 856-859.

107.   Sivakumar, S.; Mala, N. A.; Batoo, K. M.; Raslan, E. H., Efficient, highly stable Zn2+ doped NiO nanoparticles with enhanced magnetic and supercapacitor applications. *Mater. Technol.* **2022**, *37* (10), 1375-1387.

108.   Varunkumar, K.; Hussain, R.; Hegde, G.; Ethiraj, A. S., Effect of calcination temperature on Cu doped NiO nanoparticles prepared via wet-chemical method: structural, optical and morphological studies. *Mater. Sci. Semicond* **2017**, *66*, 149-156.

109.   Ghazal, S.; Akbari, A.; Hosseini, H. A.; Sabouri, Z.; Forouzanfar, F.; Khatami, M.; Darroudi, M., Biosynthesis of silver-doped nickel oxide nanoparticles and evaluation of their photocatalytic and cytotoxicity properties. *Appl. Phys. A* **2020**, *126*, 1-8.

110.   Alam, M. W.; BaQais, A.; Mir, T. A.; Nahvi, I.; Zaidi, N.; Yasin, A., Effect of Mo doping in NiO nanoparticles for structural modification and its efficiency for antioxidant, antibacterial applications. *Sci. Rep.* **2023**, *13* (1), 1328.